Interfacial Properties of Binary Mixtures of Simple Fluids and their Relation to the Phase Diagram

Simon Stephan[1, a)] and Hans Hasse[1]

Laboratory of Engineering Thermodynamics (LTD), TU Kaiserslautern, Kaiserslautern 67663, Germany

(Dated: Sunday 24th May, 2020)

Interfacial properties of binary fluid mixtures were studied using both molecular dynamics (MD) simulations and density gradient theory (DGT). The focus of the study is on the relation of the interfacial properties to the phase diagram of the mixture. Two binary Lennard-Jones mixtures were investigated in a wide range of states: a highly asymmetric mixture (type III), which exhibits vapour-liquid equilibria (VL_1E and VL_2E), liquid-liquid equilibria (L_1L_2E), a three-phase equilibrium (VL_1L_2E), and supercritical fluid-fluid equilibria (F_1F_2E), and, as a reference, an ideal mixture (type I). The studied interfacial properties are: the surface tension, the relative adsorption, the width of the interfacial region, and the enrichment of the low-boiling component, on which we set a focus. Enrichment was observed at VL_1 interfaces; and, to a small extent, also at L_1L_2 interfaces; but not at the supercritical F_1F_2 interfaces. The large enrichment found at VL_1 interfaces of the type III mixture can be interpreted as a wetting transition: approaching the VL_1L_2E three-phase line from the VL_1 side, the enrichment gets stronger and can be interpreted as precursor of the second liquid phase L_2. However, the actual existence of a three-phase line in the phase diagram is no prerequisite for an enrichment. The enrichment is found to be highly temperature-dependent and increases with decreasing temperature.

Keywords: interfacial properties, Lennard-Jones truncated & shifted, molecular dynamics, density gradient theory, wetting transition

a)Electronic mail: Simon.Stephan@mv.uni-kl.de

I. INTRODUCTION

Phase equilibria and interfacial properties of fluid mixtures are of practical importance in many fields such as chemical engineering, environmental science, and energy technology. Information on these properties is, e.g. needed for the design and optimization of fluid separation process like distillation and absorption. Understanding interfacial and phase equilibrium properties is also interesting from a fundamental physical standpoint. Interfacial properties are intrinsically tied to the corresponding phase equilibria. These equilibria are often represented in phase diagrams, which may have complex topologies. Establishing relations between the interfacial properties and the phase diagram requires systematic studies of the different types of equilibria and the corresponding interfaces for a given system. Such work is surprisingly scarce in the literature. We have therefore carried out such a study for a simple model system: a binary mixture of Lennard-Jones truncated and shifted (LJTS) fluids, and have chosen the parameters such that the phase diagram of the mixture is of type III according to the classification of van Konyenburg and Scott[1]. I.e. the mixture has two critical lines and a three-phase line. Hence, the isothermal phase diagram shows vapour-liquid equilibria (VL_1E and VL_2E), liquid-liquid equilibria (L_1L_2E), and a vapour-liquid-liquid equilibrium (VL_1L_2E); furthermore, at very high pressures, also fluid-fluid equilibria (F_1F_2E) exist. For comparison, also an almost ideal mixture (in the sense of Raoult's law) was studied (type I). For both mixtures, the two components have the same size parameter. The mixture types I and III are obtained by appropriate choices for the self and cross interaction energy parameters in the two mixtures (details are given below). The two studied LJTS mixtures were selected based on the experience from our previous study[2]: the strongly non-ideal mixtures of type III are known to have not only a complex phase behavior, but exhibit also interesting interfacial effects. The almost ideal mixture of type I was studied as a reference. The phase equilibria and interfacial properties of these two systems were investigated in the present work in a wide range of temperatures and pressures.

The study was carried out with both molecular dynamics (MD) simulation and density gradient theory (DGT) in combination with the PeTS equation of state (EOS), which describes LJTS fluids excellently[2–5]. The following interfacial properties were investigated with these methods: surface tension, density profiles of the components in the nanoscopic interfacial region, relative adsorption at the interface, interfacial thickness, and the enrichment

of the components.

The enrichment describes a special feature of the adsorption at the interface: while the total density usually changes monotonously across the interface, the density profiles of individual components may exhibit a maximum in the interfacial region, i.e. the density of a component at the interface may be significantly higher than in either of the two bulk phases. At *VL* interfaces enrichment is usually only found for the low-boiling component. Interfacial adsorption and enrichment are related, but have different features. In particular, interfacial adsorption may be present without the presence of an enrichment.

Non-monotonic density profiles of components at interfaces have been reported since the early days of computational work on vapour-liquid interfacial properties of mixtures[6–8]. The enrichment at vapour-liquid interfaces has attracted much attention in the past decades[2,4,8–49], also because it is suspected to influence the mass transfer through the interface[4,20,34,50,51]. Asymmetric mixtures have attracted special interest[27,29–31,33,35,37,44,47] since a particularly high enrichment is found in these types of mixtures. However, there are only few studies in the literature in which the link between the enrichment at vapour-liquid interfaces and the corresponding bulk phase equilibria was explicitly discussed[44], whereas the link between the relative adsorption, the phase behaviour, and the wetting behaviour has been studied more systematically for vapour-liquid-liquid equilibria[52–58].

A further interesting phenomenon observed at fluid interfaces is a non-monotonic behaviour of the total density at liquid-liquid interfaces[51,59–63]. This has been investigated in only few studies compared to the large body of available work on the enrichment at vapour-liquid interfaces.

We have recently carried out two studies[2,4] in which the influence of molecular interactions on both the phase diagram and interfacial properties of binary fluid mixtures were investigated systematically for LJTS mixtures. In Ref.[2] we have demonstrated that the interfacial properties are directly linked to bulk phase equilibrium properties and have established a conformal solution theory for this. The present work is complementary to these studies: while in the previous work[2,4] many different mixtures were studied at basically only one condition, and only *VLE* were considered, a different approach is taken here: two mixtures are studied in full detail for a wide range of conditions and different types of equilibria are considered. The studied mixtures were selected based on the experience from the previous work[2,4] in such a way that important interfacial effects, namely a high enrichment,

are expected in one of them, while the other is an ideal binary mixture that is studied as a reference. To the best of our knowledge, this is the first study in which, for a given mixture, interfacial properties of different types of phase equilibria were systematically investigated and characterized regarding the structure of the interface and its properties.

In systematic studies of interfacial properties and phase equilibria, also the temperature must be varied. The present study therefore also extends the knowledge on the temperature dependency of interfacial phenomena, which is known to be important, especially for the enrichment[10,12,14].

This paper is organised as follows: The employed methods and the studied mixtures are described in Section II, the results are presented in section III, and conclusions are drawn in Section IV.

II. MODELING AND SIMULATION

A. Binary Mixtures of Lennard-Jones Truncated Shifted Fluids

The Lennard-Jones (LJ) fluid in its different versions[64,65] is one of the most frequently used model fluids in the literature[66] as it is computationally cheap but still gives a reasonable picture of the behaviour of simple fluids[67]. The Lennard-Jones truncated and shifted (LJTS) fluid is particularly attractive, especially for studies of interfacial phenomena, as, due to the truncation, no long-range corrections are required. It has been frequently used for studying physical phenomena as well as for developing simulation methods.[13,68–72].

The LJTS potential u_{LJTS} is

$$u_{\mathrm{LJ}}(r) = 4\varepsilon \left[\left(\frac{\sigma}{r}\right)^{12} - \left(\frac{\sigma}{r}\right)^{6} \right] \quad \text{and} \tag{1}$$

$$u_{\mathrm{LJTS}}(r) = \begin{cases} u_{\mathrm{LJ}}(r) - u_{\mathrm{LJ}}(r_{\mathrm{c}}) & r \leq r_{\mathrm{c}} \\ 0 & r > r_{\mathrm{c}}, \end{cases} \tag{2}$$

with u_{LJ} being the full Lennard-Jones potential, ε and σ being the energy and size parameter, respectively. The distance between two particles is denoted by r. The truncation radius r_{c} of the potential is set to $2.5\,\sigma$ throughout the present work, and 'LJTS' always refers to that cut-off radius. The truncation of the potential is crucial for the fluids thermodynamic bulk[64,73–75] and interfacial properties[5,76–82].

Two binary LJTS mixtures are studied in the present work; they are labelled as mixture A and B in the following. Both contain a high-boiling component, denoted as component 1 and a low-boiling component, denoted as 2. The high-boiling component is the same in both mixtures and can be considered as the reference fluid. The low-boiling character of the component 2 is obtained by decreasing its dispersion energy with respect to component 1. The size parameter is not varied and is σ for all components. Also the mass of the LJTS particles M is the same for both components.

The modified Lorentz-Berthelot combination rules are employed[83,84] for the modelling of the interaction between unlike LJTS particles:

$$\sigma_{ij} = \frac{\sigma_i + \sigma_j}{2}\,, \tag{3}$$

$$\varepsilon_{ij} = \xi\sqrt{\varepsilon_i \varepsilon_j}\,. \tag{4}$$

Here, indices i and j stand for the interaction of two particles of the same component and ij for the cross interaction between the different components and ξ is a state-independent interaction parameter.

The studied mixtures are:

- mixture A: asymmetric wide boiling mixture with $\varepsilon_2/\varepsilon_1 = 0.6$ and $\xi = 0.85$
- mixture B: ideal mixture with $\varepsilon_2/\varepsilon_1 = 0.9$ and $\xi = 1$

Mixture A is the mixture for which the highest enrichment was found in a recent study on LJTS mixtures[2], which is due to the underlying bulk densities; see the Supplementary Material for details. The vapour pressure curves of the three pure components are shown in Fig. 1. They were computed with the PeTS EOS, which reproduces both stable and metastable states as well as the vapour-liquid equilibrium of the LJTS fluid very well[3].

The fluid interfaces of the binary mixtures A and B were studied in the present work at five temperatures, which are indicated by the vertical dashed lines in Fig. 1: $T/\varepsilon k_\mathrm{B}^{-1} = 0.66,\ 0.715,\ 0.77,\ 0.825,\ 0.88$. Using the results of Vrabec et al.[85] for the critical point of the LJTS fluid with $r_\mathrm{c} = 2.5\,\sigma$ ($T_\mathrm{c} = 1.0779\,\varepsilon k_\mathrm{B}^{-1}$; $\rho_\mathrm{c} = 0.319\,\sigma^{-3}$) the reduced temperatures with respect to the critical point of the reference component 1 are approximately: $T_\mathrm{red} = T/T_{\mathrm{c},1} = 0.6,\ 0.65,\ 0.7,\ 0.75,\ 0.8$. The lowest temperature $T = 0.66\,\varepsilon k_\mathrm{B}^{-1}$ is slightly above the triple point temperature ($T_\mathrm{trip} = 0.62\,\varepsilon k_\mathrm{B}^{-1}$) of the component 1[86,87]. The low-boiling

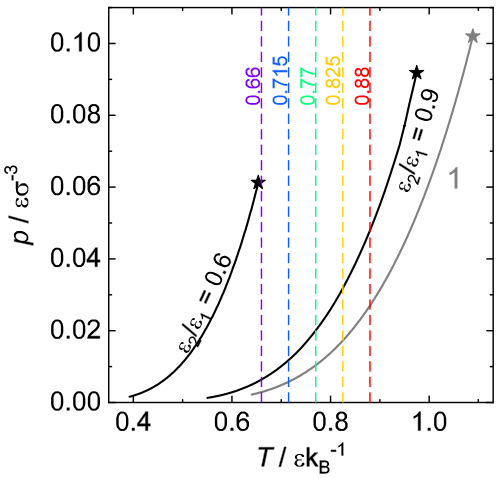

FIG. 1. Vapour pressure curves for the three pure LJTS fluids employed in the present work. The high-boiling component 1 is the grey solid curve. The two low-boiling components 2 are the black solid curves. The critical points are indicated as stars. The temperatures that were investigated in the present study are indicated as coloured vertical dashed lines.

component 2 with only slightly decreased dispersion energy ($\varepsilon_2/\varepsilon_1 = 0.9$) is subcritical at all investigated temperatures, whereas the component 2 with $\varepsilon_2/\varepsilon_1 = 0.6$ is supercritical at all investigated temperatures.

The binary interaction parameter ξ and the ratio of the dispersion energies $\varepsilon_2/\varepsilon_1$ as specified above are used both in MD and DGT. Throughout the present work, all physical properties are reduced using the Lennard-Jones potential parameters of the high-boiling component ε_1, σ_1 and the mass M_1, as well as the Boltzmann constant k_B.

B. PeTS EOS and Density Gradient Theory

PeTS EOS

The perturbed truncated and shifted (PeTS) EOS describes the behaviour of the LJTS fluid[3]. It is based on the perturbation theory of Barker and Henderson[88], which splits the free energy a into an ideal gas part a_id, the free energy of a hard sphere potential a_hs, and a perturbation a_pert part due to dispersion:

$$a = a_\mathrm{id} + a_\mathrm{hs} + a_\mathrm{pert}. \tag{5}$$

The perturbation contribution is modelled as a sum of first- and second-order contributions, i.e. $a_\mathrm{pert} = a_1 + a_2$. As proposed by Gross and Sadowski[3,4,89], they were developed in a Taylor

series as functions of the packing fraction η. The PeTS EOS was fitted to vapour-liquid equilibrium simulation data of the pure LJTS fluid[3] and has been extended to mixtures[4] using van der Waals one-fluid theory[90], which is known to perform well as long as the size parameters σ_1 and σ_2 of the components are similar[91–93]. It was also shown that the one-fluid theory can be extended to interfacial properties using the PeTS EOS[2]. The modified combination rules of Lorentz and Berthelot, cf. Eq. (3) and (4), were also employed for the calculation of the cross interaction parameters σ_{ij} and ε_{ij} in the EOS. The numerical values of the molecular parameters used for the MD simulations and those of the EOS were identical.

For similar mixtures, as those studied here, it was shown that results from the PeTS EOS are in excellent agreement with computer experiment data for isothermal $p-x$ and $\rho-x$ phase diagrams, as well as Henry's law constants[2,4,82]; in most cases the EOS and computer experiment data agree within their statistical uncertainties. For the pure LJTS fluid, the PeTS EOS was also compared with homogeneous pvT data at stable and metastable states from computer experiments and good agreement was found[3]. It is also known that the PeTS EOS gives a realistic description of the region between the binodals, i.e. a single van der Waals loop[3].

Density Gradient Theory

Density gradient theory (DGT) can be applied for the calculation of interfacial properties of pure components[8,94–97] and mixtures[11,45,98–103]. It only requires a free energy model of the fluid and the numbers for the binary influence parameters κ_{ij}, which describe the influence of the density gradients on the free energy. For an introduction into DGT we refer the reader to Refs.[94,104,105].

In DGT, the free energy of the heterogeneous system is expanded in a Taylor series in the density derivative with respect to the spatial coordinate normal to the interface $\nabla^m \underline{\rho},\ m = 1, 2, ..$ and usually truncated after the square gradient term. The free energy density $\hat{a} = A/V$ can thereby be written for a planar interface of a binary mixture with the components i and j as:

$$\hat{a}(\underline{\rho}, \nabla\underline{\rho}) = \hat{a}_0(\underline{\rho}) + \sum_{i=1}^{2}\sum_{j=1}^{2} 1/2\ \kappa_{ij}\nabla\rho_i\nabla\rho_j \tag{6}$$

where $\hat{a}_0(\underline{\rho})$ is the free energy per volume of the homogeneous system at the local density and $\underline{\rho}$ indicates the vector of the number densities ρ_i and $\nabla\underline{\rho}$ the vector of the cor-

responding gradients. The influence parameters κ_{ij} generally depend on the density and temperature[95,104,106]. However, in many applications they are treated as state-independent parameters[14,101], which is also done in the present work.

In the remainder of this paper, we use the following notation: κ_1 and κ_2 stand for the pure component influence parameters and κ_{12} stands for the cross-interaction influence parameter. The influence parameter of the pure LJTS fluid has been determined in Ref.[3] and was adopted here. This leads to: $\kappa_1 = 2.7334\,\sigma^5\varepsilon$ as well as to $\kappa_2 = \kappa_1 \frac{\varepsilon_2}{\varepsilon_1}$. It was shown in Refs.[3,5] that this leads to an excellent description of the pure component interfacial tension of the LJTS fluid, but a slight systematic underestimation of the interfacial thickness predicted from molecular simulation[5,82]. The cross-interaction influence parameter was calculated in the present work from

$$\kappa_{ij} = \sqrt{\kappa_i \kappa_j}\,. \tag{7}$$

It was shown in previous works of our group[2,4,82] that this leads to almost perfect predictions of the interfacial properties of LJTS mixtures as determined in computer experiments, both for ideal and highly non-ideal mixtures, with the exception of slight systematic deviations for the interfacial thickness. In the literature, often an additional adjustable parameter is used in Eq. (7) to handle particularly complex and asymmetric mixtures[27,107]. This was not done in the present work.

The equilibrium density profiles $\rho_i(z)$ in the planar interface were computed by minimizing Eq. (6) in the entire interfacial domain. For solving the DGT equation for both components in the entire interfacial domain, the numerically robust stabilized DGT (sDGT) algorithm proposed by Mu et al.[45] as well as the classical reference density method[8] were employed. The results from both methods were found to agree perfectly. The domain length was at least $30\,\sigma$ and a spatial discretisation of $0.02\,\sigma$ was used.

The surface tension γ was calculated from[8,104]

$$\gamma = \int \sum_{i=1}^{2} \sum_{j=1}^{2} \kappa_{ij} \nabla\rho_i \nabla\rho_j \,\mathrm{d}z\,. \tag{8}$$

Results obtained by DGT in combination with the PeTS EOS are referred to in the following as 'results from DGT' for brevity.

C. Molecular Simulations

The molecular simulations were performed with the MD code *ls1 mardyn*[108] in the NVT ensemble with $N = 16{,}000$ particles. The simulation volume contained two phases, a slab of a first phase in the middle, surrounded by two slabs of a second phase. Periodic boundary conditions were applied, such that two fluid interfaces were obtained, which are planar, if the fluctuations are neglected. The interfaces were perpendicular to the z-axis. The elongation of the simulation box normal to the interface was $80\,\sigma$ and the thickness of the phase in the centre of the simulation box was about $40\,\sigma$, which is large enough to exclude finite size effects[76]. The elongation in the directions parallel to the interface was at least $20\,\sigma$. For the initialization, the bulk phase compositions were estimated with the PeTS EOS to ensure a stable simulation and fast equilibration, see Ref.[2] for details. The equilibration was carried out for 2,500,000 time steps. The production was executed for 7,500,000 time steps to reduce statistical uncertainties. Density and pressure profiles were computed in block averages of 500,000 time steps during the production phase, resulting in 15 sampling points for each state point. The pressure and density profiles were calculated at $N = 1200$ bins, each with a width of $\Delta z = 0.0667\,\sigma$. The equation of motion was solved by a leapfrog integrator[109] with a time step of $\Delta t = 0.001\ \sigma\sqrt{M/\varepsilon}$. The statistical error was estimated to be twice the standard deviation of all block averages. The equilibrium densities and pressures were calculated as an average over the respective phases excluding the area close to the interface, i.e. the area where the first derivative of the density with respect to the z-coordinate deviates from zero significantly.

The position of the phase in the middle of the simulation box fluctuates. This fluctuation would result in a smearing of the averaged density profiles. To avoid this, the individual density profiles from one block average were shifted before the averaging. The shift was carried out such that the z-axis origin was set to the position, where $\rho_{\mathrm{tot}} = \rho''_{\mathrm{tot}} + 0.5(\rho'_{\mathrm{tot}} - \rho''_{\mathrm{tot}})$, where ρ_{tot} is the total number density $\rho_{\mathrm{tot}} = \rho_1 + \rho_2$.

The surface tension was computed from the deviation between the normal and the tangential diagonal components of the overall pressure tensor[110,111], i.e. the mechanical route

$$\gamma = \frac{1}{2}\int_{-\infty}^{\infty} (p_{\mathrm{N}} - p_{\mathrm{T}})\ \mathrm{d}z. \tag{9}$$

The normal pressure p_{N} is thereby given by the z-component of the diagonal of the pressure tensor, and the tangential pressure p_{T} was determined by averaging over x- and y-

components of the diagonal of the pressure tensor. The interfacial area S of each planar fluid interface is given by the cross section of the simulation volume normal to the z-axis.

D. Interfacial Properties

Both the MD simulations and the DGT yield the component density profiles $\rho_i(z)$ for both the high-boiling and low-boiling component $i = 1, 2$ at the planar interfaces. On the basis of the density profiles of both components, the relative adsorption defined by Gibbs[112] was computed by the symmetric interface segregation according to Telo da Gama and Evans[113,114]

$$\Gamma_2^{(1)} = -\left(\rho_2' - \rho_2''\right) \int_{-\infty}^{\infty} \left[\frac{\rho_1(z) - \rho_1'}{\rho_1' - \rho_1''} - \frac{\rho_2(z) - \rho_2'}{\rho_2' - \rho_2''} \right] \mathrm{d}z \ , \tag{10}$$

where ρ_1', ρ_1'' and ρ_2', ρ_2'' are the component densities at saturation in the two coexisting bulk phases $'$ and $''$, respectively. $\Gamma_2^{(1)}$ is the relative adsorption of component 2 at the interface with respect to component 1.

A further property for describing the interfacial excess is the interfacial enrichment E_2 of the low-boiling component 2, which was introduced by Becker et al.[14] as the ratio between the maximum local density of component 2 in the interfacial region and the larger of the component densities in the two bulk phases ρ_2', ρ_2'',

$$E_2 = \frac{\max\left(\rho_2(z)\right)}{\max\left(\rho_2', \rho_2''\right)} \, . \tag{11}$$

The numerator and denominator from Eq. (11) were computed for each block averaged density profile. The bulk densities in the denominator were obtained from a spatial averaging in the corresponding regions, while the maximum value in the denominator is simply the maximal ρ_2 value of the bins in the interfacial region. This can cause artefacts for the evaluation of molecular simulations density profiles, which are superimposed by a random noise: consider the extreme case that the density is uniform in both phases as well as in the interface, i.e. $\rho_2(z) = \text{const}$. Then, obviously $E_2 = 1$. But, due to the fluctuations, the evaluation of Eq. (11) in the way that we have just described will always yield $E_2 > 1$ as the maximal value of the bins in the interface is selected, which will be larger than the averaged values for the bulk phases ρ_2', ρ_2''. The results from the previous studies[2,4,82], indicate that values below $E_2 = 1.1$ cannot be discerned for $E_2 = 1$ in the case of molecular simulations data.

Both the enrichment E_2 and the relative adsorption $\Gamma_2^{(1)}$ quantify the interfacial excess, but they do not contain the same information. The relative adsorption $\Gamma_2^{(1)}$ quantifies the interfacial excess in the sense of Gibbs[112]. It can not only be obtained from the interfacial density profiles but also from data on the concentration-dependence of the surface tension, i.e. from macroscopic data. The relation is given by the Gibbs adsorption equation $\Gamma_2^{(1)} = -(\partial\gamma/\partial\mu_2)_T$. It has been shown many times[7,10,14,21,23,33,37,39,114–120] that $\Gamma_2^{(1)}$ computed via Eq. (10) from the interfacial density profiles $\rho_i(z)$ is in good agreement with data obtained from the interfacial tension using the Gibbs adsorption equation. While $\Gamma_2^{(1)}$ is an integral measure of the interfacial excess, the enrichment E_2 simply quantifies the non-monotonicity of the interfacial density profile, i.e. the relative peak height of $\rho_2(z)$. E_2 is therefore dimensionless, whereas $\Gamma_2^{(1)}$ has the dimension number of particles per unit area. Furthermore, a relative adsorption $\Gamma_2^{(1)} > 0$ may be present when there is no enrichment ($E_2 = 1$), e.g. if the two component density profiles are shifted relative to each other[2,4,14]. But an enrichment $E_2 > 1$ will in general result in an adsorption $\Gamma_2^{(1)} > 0$.

To describe and compare the thickness of fluid interfaces, the 90-10% definition for the effective interfacial thickness L_{10}^{90} according to Lekner and Henderson[121] was used, which is the distance between the points where the total number density $\rho^{\mathrm{tot}}(z) = \rho_1(z) + \rho_2(z)$ reaches 10% and 90% of the total bulk densities respectively:

$$\begin{aligned} L_{10}^{90} &= z(\rho_{90}^{\mathrm{tot}}) - z(\rho_{10}^{\mathrm{tot}})\,, \\ \rho_{10}^{\mathrm{tot}} &= \rho_{\mathrm{tot}}'' + 0.1(\rho_{\mathrm{tot}}' - \rho_{\mathrm{tot}}'')\,, \\ \rho_{90}^{\mathrm{tot}} &= \rho_{\mathrm{tot}}'' + 0.9(\rho_{\mathrm{tot}}' - \rho_{\mathrm{tot}}'')\,. \end{aligned} \tag{12}$$

The origin on the z-axis of the interfacial profiles from both MD and DGT shown in the following was arbitrarily chosen such that $\rho_{\mathrm{tot}}(z) = 0$ at $\rho_{\mathrm{tot}} = \rho_{\mathrm{tot}}'' + 0.5(\rho_{\mathrm{tot}}' - \rho_{\mathrm{tot}}'')$.

III. RESULTS AND DISCUSSION

In the main body of this work, the focus lies on the highly non-ideal mixture A. The corresponding results for the ideal mixture are reported in the Appendix. In Section III A, the phase diagrams are introduced and the results for the bulk phase equilibria are presented. The following Sections report on interfacial properties for different types of phase equilibria: Section III B on VL_1 interfaces, Section III C contains a discussion of the different types of

equilibria adjacent to the three-phase VL_1L_2E, Section III D reports on the results for the F_1F_2E and its' interfacial properties. Finally, in Section III F the results for the interfacial properties of the different types of equilibria are summarised and put into context with each other. The results for both the phase equilibria and the interfacial properties are shown graphically here, the corresponding numeric values of the results are reported in the Supplementary Material.

It was shown in earlier works of our group[2,4] that the interfacial density profiles of LJTS mixtures obtained from MD and DGT+PeTS EOS agree very well. Hence, only the DGT density profiles are discussed here for brevity; the corresponding MD results are provided in the Supplementary Material. The good agreement of the results for the interfacial properties derived from the density profiles obtained from MD and DGT affirms this procedure.

A. Phase Equilibria

Fig. 2 shows the pressure - temperature diagrams with the characteristic curves for the binary mixtures A and B. Besides the vapour pressure curves of the pure components, also the critical lines are shown, and for mixture A the three-phase line. The results were obtained from the PeTS EOS. The phase equilibria were computed with the method and algorithm described in Ref.[122].

Mixture B is almost ideal and shows a type I phase behaviour in the classification of van Konynenburg and Scott[1]. The pure component critical points are connected by a single critical line of the binary mixture. Real mixtures that have qualitatively the same phase behaviour are for example methane + krypton, krypton + xenon, and krypton + argon. Mixture A is strongly non-ideal and has a type III phase behaviour according to Ref.[1]. Real mixtures that have qualitatively the same phase behaviour are for example water + carbon dioxide, different alkanes + carbon dioxide, neon + argon, nitrogen + ammonia, and neon + krypton. Mixtures of type III have attracted much attention in the past[33,44,123,124] as they exhibit an interesting and complex phase behaviour.

For mixture A, the critical line that starts at the critical point of component 2 ends in an upper critical end point (UCEP), where also the three-phase VL_1L_2E line ends. The critical line that starts at the critical point of component 1 exhibits a temperature minimum, i.e. a bicritical end point (BICEP) in which two critical points merge. The branch of the

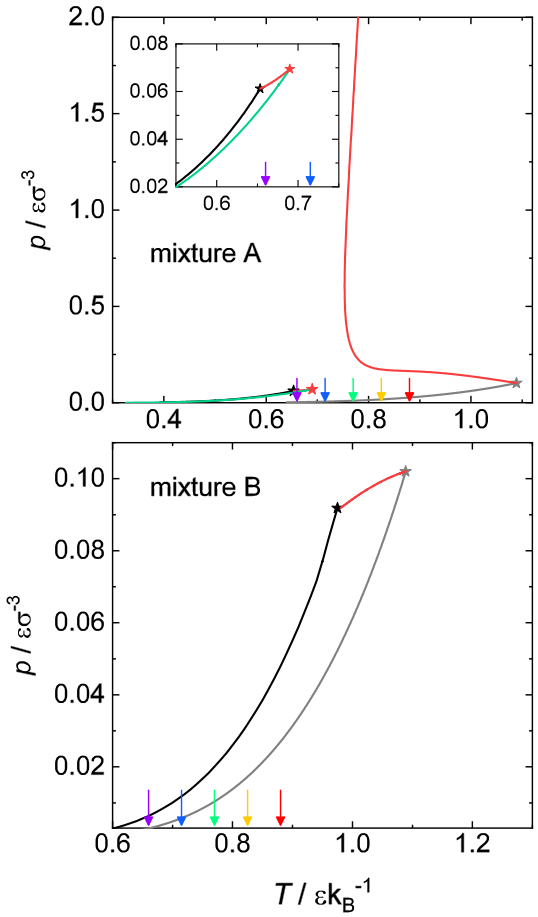

FIG. 2. Pressure-temperature diagrams with characteristic curves for the mixtures A and B. Pure component vapour pressure curves and critical points are grey lines and stars (high-boiling component 1) and black lines and stars (low-boiling component 2). Red lines are critical lines of the mixture; the red star is the upper critical end point of mixture A (UCEP). The green line depicts the VL_1L_2E three-phase line of mixture A. Arrows indicate the five temperatures investigated in this work, cf. Fig. 1 for the colour coding.

critical line that is connected to the critical point of component 1 belongs to common binary vapour-liquid phase envelopes. The branch of the critical line that climbs to high pressures belongs to so-called fluid-fluid equilibria[125] (which are sometimes also referred to as 'gas-gas equilibria'). Even though both components are supercritical at such states, a phase split is observed. The fluid-fluid critical line monotonically increases with increasing temperature starting at the BICEP. In the temperature range $T_{\mathrm{UCEP}} < T < T_{\mathrm{BICEP}}$, the phase envelopes starting at the high-boiling pure component vapour pressure have no critical point. The five temperatures that were studied in the present work were chosen such that the corresponding

phase diagrams include all these phenomena, cf. little arrows in Fig. 2.

Fig. 3 shows the isothermal $p-x$ phase diagrams for the mixtures A and B at the five studied temperatures. Results from computer experiments and the EOS are shown.

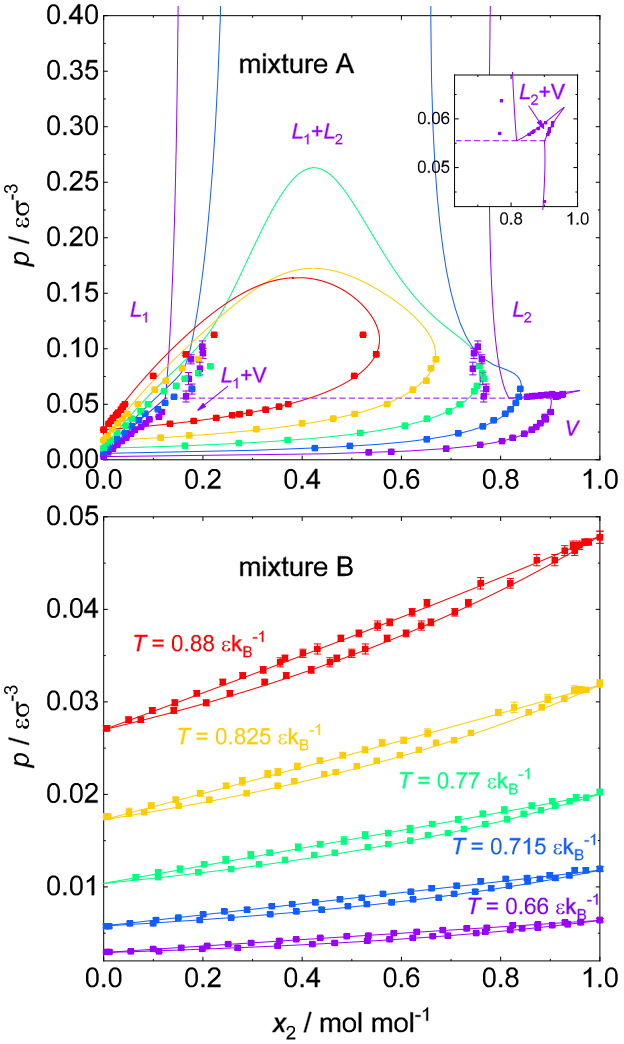

FIG. 3. Isothermal p-x phase diagrams for the mixture A and the mixture B at all five investigated temperatures. The temperatures in the top and bottom plot are colour-coded using the same scale. Symbols are MD results and lines are the PeTS EOS. The one and two phase regions are labelled only for the lowest temperature $T = 0.66\,\varepsilon k_\mathrm{B}^{-1}$. The VL_1L_2 three-phase equilibrium is shown as dashed line.

For mixture A, the low-boiling component 2 is supercritical at all investigated temperatures, whereas the high-boiling component 1 is subcritical at all temperatures. The phase envelope is very wide at low temperatures and gets narrower as the temperature increases. Starting at the critical point of the pure component 1, the critical pressure of the mixture

first increases only slightly with decreasing temperature but then increases dramatically for temperatures below about $T = 0.715\,\varepsilon k_\mathrm{B}^{-1}$, which becomes also clear from the critical line depicted in Fig. 2.

Mixture A exhibits a VL_1L_2 three-phase equilibrium at temperatures below $T = 0.689\,\varepsilon k_\mathrm{B}^{-1}$, cf. Fig. 2. In the phase diagram, there is a VL_1 equilibrium region below the three-phase line, cf. Fig. 3. Above the three-phase line, there is a small region in which VL_2 equilibria exist and a large L_1L_2 equilibrium region.

The isothermal phase diagram at $T = 0.715\,\varepsilon k_\mathrm{B}^{-1}$ is special, as in the single two-phase region that is observed at this temperature, at low pressures equilibria are found that can be classified as vapour-liquid equilibria, while at high pressures, the equilibria resemble liquid-liquid equilibria. The density transition between both types is smooth and can be found at pressures lying approximately on an extension of the three-phase line, cf. Fig. 2. This transition occurs at approximately $x_2^{L1} \approx 0.17\ \mathrm{mol\,mol^{-1}}$ for $T = 0.715\,\varepsilon k_\mathrm{B}^{-1}$. However, no isopycnic point[123] (both phases have the same density) is observed in mixture A.

According to the $p - T$ diagram of mixture A (cf. Fig. 2), with increasing pressure the VL_1 region can either terminate at the three-phase line ($T = 0.66\,\varepsilon k_\mathrm{B}^{-1}$), be open ($T = 0.715\,\varepsilon k_\mathrm{B}^{-1}$), or end in a critical point ($T = 0.77\,\varepsilon k_\mathrm{B}^{-1},\ 0.825\,\varepsilon k_\mathrm{B}^{-1},\ 0.88\,\varepsilon k_\mathrm{B}^{-1}$).

Fig. 3 shows that the agreement between the results from the PeTS EOS with those form the computer experiments are excellent for the ideal mixture B for all temperatures that were studied. Also for the non-ideal mixture A, a good agreement is found in most cases. Exceptions are regions in the vicinity of critical points, and the compositions of the coexisting phases of the L_1L_2 liquid-liquid equilibria, where the EOS yields a miscibility gap which is broader than that obtained from MD. These deviations are probably a result of differences between the force field and the free energy model of the PeTS EOS, which may be due to the simplified expression that is used for the description of the repulsive interactions in the EOS[3,126].

B. VL_1 Interfaces

Fig. 4 shows the VL_1 density profiles of mixture A for all five studied temperatures in the entire composition range. Only DGT results are shown, which agree well in all cases with the MD results (see Supplementary Material). The corresponding results of the vapour-liquid

equilibria of mixture B are reported and discussed in the Appendix, as they are only used as a reference.

In contrast to the ideal mixture B (see Appendix), the VL_1 density profiles of component 2 of mixture A exhibit a distinct maximum at all temperatures, i.e. enrichment is observed. This maximum is most prominent at the lowest investigated temperature and decreases with an increasing temperature. The interfacial thickness increases with increasing temperature, which becomes clear from the density profiles of component 1 and the width of the enrichment peak shown in Fig. 4. The density profiles at the three highest studied temperatures are similar, those for the two lowest show a distinctly different behaviour. This is in line with the differences in the phase diagrams that were obtained for the five temperatures, see Fig. 3 - bottom. For the higher three temperatures, the VL_1E region terminates in a critical point, which is not the case for the lower two temperatures.

For the density profiles at the three higher temperatures ($T = 0.77\,\varepsilon k_\mathrm{B}^{-1}$, $0.825\,\varepsilon k_\mathrm{B}^{-1}$, and $0.88\,\varepsilon k_\mathrm{B}^{-1}$), the enrichment vanishes upon approaching the critical point. Hence, both component density profiles become – as expected at a critical point – horizontally flat. For $T = 0.715\,\varepsilon k_\mathrm{B}^{-1}$, the enrichment vanishes as the pressure increases and the vapour phase density increases significantly. For $T = 0.66\,\varepsilon k_\mathrm{B}^{-1}$, the enrichment is most prominent and furthermore remains present in the entire composition range up to the VL_1L_2E, cf. Fig. 3. The interfacial structure in the vicinity of the VL_1L_2E is discussed in detail in the next section. The enrichment decreases with increasing temperature but does not fully vanish.

For all five temperatures, the enrichment peak is fairly symmetric at low mole fractions of the component 2 in the liquid phase L_1 x_2^{L1}, i.e. for VL_1 equilibria close to the boiling point of the pure component 1. Also, the z-position of the peak does not change for low x_2^{L1}. For high x_2^{L1}, the position of the enrichment peak slightly moves towards the vapour phase. The position of the maximum of the enrichment remains fairly constant upon varying composition and temperature, even when the topology of the phase diagram changes, compare Fig. 4 with Fig. 2. The peak position is approximately at $z(\rho_\mathrm{max}) \simeq -\sigma$ in the coordinates that are used here (cf. Section II). As also reported before, e.g. Refs.[4,14], no enrichment is found for the high-boiling component in the entire investigated temperature and composition range.

For mixture B, no significant non-monotonic behaviour of the density profiles of the two components was found in the entire investigated temperature and composition range. It is noted, however, that at very low temperature and very low concentrations x_2^{L1}, slight maxima

FIG. 4. VL_1 density profiles of component 1 (dashed lines) and component 2 (full lines) for the mixture A obtained by DGT. Results for all studied temperatures. The colour-code indicates the liquid phase composition. Red squares indicate invariant intersection points of density profiles of component 1.

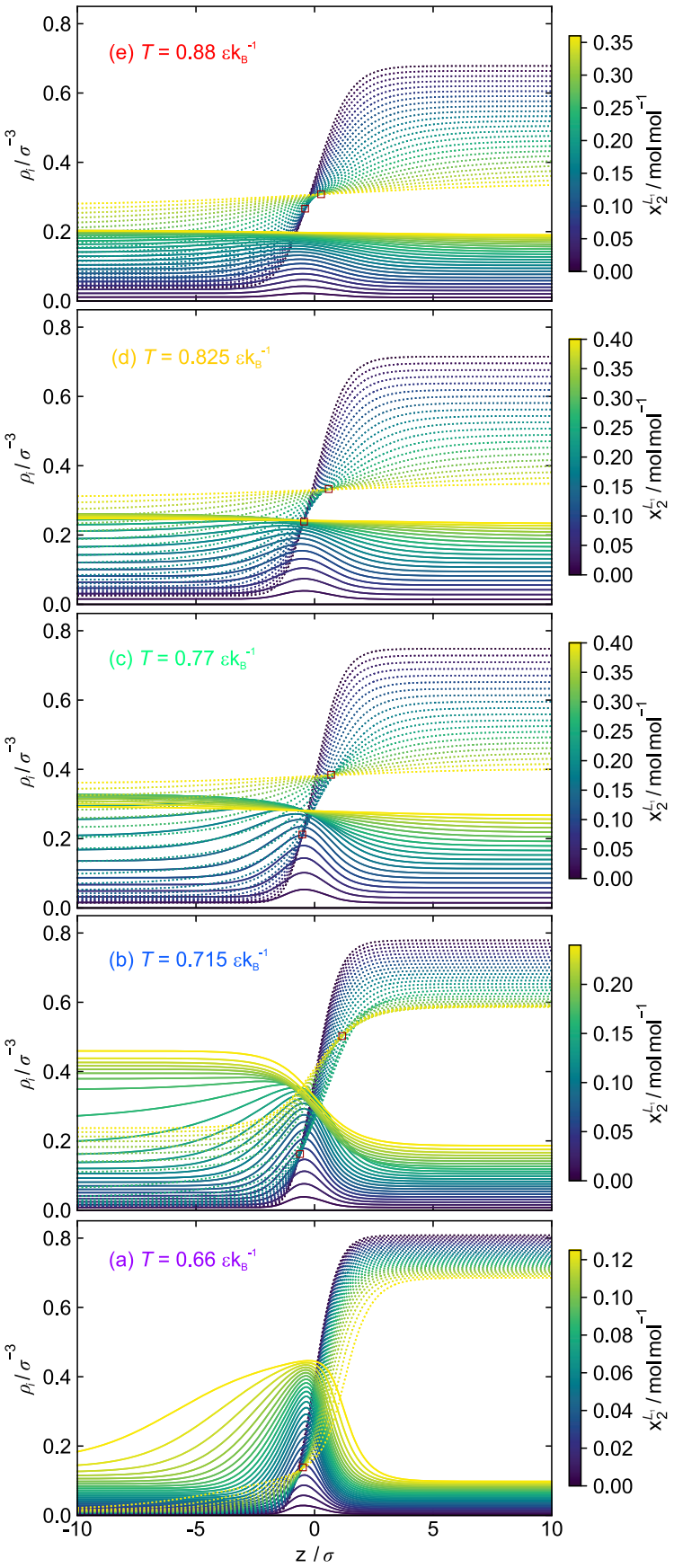

in the density profiles $\rho_2(z)$ of component 2 were observed (see Appendix for details).

For mixture A, some of the density profiles exhibit one or even two invariant common intersection points, which are indicated in Fig. 4. The common intersection points of all studied isothermal sets of density profiles are discussed in section III E.

Fig. 5 (a) - (d) shows the results that were obtained for the surface tension γ, the relative adsorption $\Gamma_2^{(1)}$, and the enrichment of the low-boiling component E_2, as well as the interfacial thickness of the mixture A in the VL_1E region. Results from both MD and DGT are shown. The corresponding plots for mixture B are shown in the Appendix.

The surface tension results from DGT lie within the error bars of the MD results for all but one state point for the ideal mixture B (see Appendix). The agreement is less good for mixture A, cf. Fig. 5 (a), but considering the fact that both methods are independent predictions, the agreement is fair. The deviations increase with decreasing temperature and increasing x_2^{L1}. The DGT results systematically underestimate the molecular simulation surface tensions for such state points. These deviations are probably due to deviations between the PeTS EOS and the LJTS force field since deviations for these state points are also found for the phase behaviour, cf. Fig. 3.

Starting at the pure component 1, the VL_1 surface tension γ of the mixture A first decreases linearly with increasing x_2^{L1} at all investigated temperatures. The slope of the VL_1 surface tension increases with decreasing temperature, which is due to an adsorption of the low-boiling component at the interface following the Gibbs adsorption equation. At $T = 0.66\,\varepsilon k_\mathrm{B}^{-1}$, the surface tension decay remains fairly linear until the three-phase equilibrium is reached (small purple arrow). The results for the isotherm $T = 0.715\,\varepsilon k_\mathrm{B}^{-1}$ are special, as for that isotherm a transition of the phase equilibrium from vapour-liquid-like to liquid-liquid-like occurs, as explained above. For the four higher temperatures, $\gamma(x_2^{L1})$ becomes convex at high x_2^{L1} and falls to zero at the critical point. This is a remainder of the three-phase equilibrium at $T < T_\mathrm{UCEP}$ and the fluid-fluid equilibrium at $T > T_\mathrm{BICEP}$.

The surface tension of the mixture B has a much simpler behaviour: the decay of the surface tension from the pure component 1 to component 2 is practically linear in the entire temperature and composition range (see Appendix).

Fig. 5 (b) shows the adsorption isotherms $\Gamma_2^{(1)}(x_2^{L1})$ for mixture A in the VL_1E region obtained from MD and DGT. The results from both methods agree qualitatively well in all cases. The agreement is excellent for the higher temperatures but less favourable for

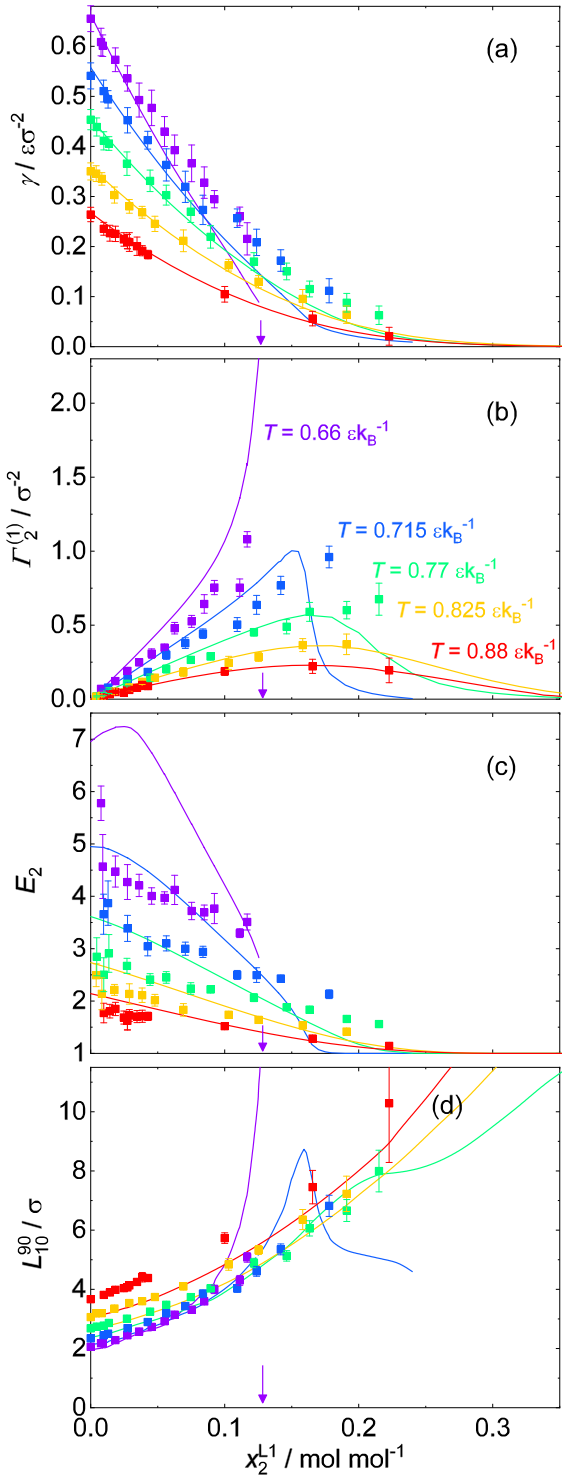

FIG. 5. VL_1 interfacial properties for mixture A: (a) surface tension γ, (b) relative adsorption of component 2 at the interface $\Gamma_2^{(1)}$, (c) enrichment of component 2 E_2, and (d) interfacial thickness L_{10}^{90}. Symbols are MD simulation results, lines are DGT results. Results for all studied temperatures are shown. The colour-code indicates the temperature and is the same for all plots. The arrow indicates the composition of phase L_1 in the three-phase equilibrium.

the lower temperatures. Furthermore, the deviations increase with increasing x_2^{L1}. Also for mixture B, the results for the relative adsorption from MD and DGT agree well, even though the MD results scatter strongly due to numerical uncertainties (see Appendix).

All VL_1 adsorption isotherms for the mixture A have in common that, starting at infinite dilution of the component 2, the relative adsorption $\Gamma_2^{(1)}$ first increases with increasing x_2^{L1}. The adsorption isotherms at $T/\varepsilon k_\mathrm{B}^{-1} = 0.715,\ 0.77,\ 0.825,\ 0.88$ exhibit a maximum; for the three highest temperatures, the mixtures' phase envelope has a critical point, at which the relative adsorption $\Gamma_2^{(1)}$ vanishes. Such adsorption isotherms are usually found in systems with one supercritical component and a single critical point[4,10,14,23,114,117,118]. The adsorption isotherm for $T = 0.715\,\varepsilon k_\mathrm{B}^{-1}$ decreases to zero with increasing x_2^{L1} or p, even though the corresponding phase diagram does not possess a critical point, cf. Fig. 2. This is a result of the transition from the vapour-liquid-like behaviour to liquid-liquid-like behaviour on that isotherm. The adsorption isotherm for $T = 0.66\,\varepsilon k_\mathrm{B}^{-1}$ exhibits a pole at the composition in the liquid phase x_2^{L1} that corresponds to the three-phase equilibrium. Hence, component 2 adsorbs ($\Gamma_2^{(1)} > 0$) at the VL_1 interface in the entire temperature and composition range. The adsorption isotherms in mixture A exhibit values approximately an order of magnitude larger than those in mixture B at low temperatures. However, at high temperatures, both mixtures have similar values for $\Gamma_2^{(1)}$, e.g. for the isotherm $T = 0.88\,\varepsilon k_\mathrm{B}^{-1}$ the relative adsorption is in both cases in the range of $\Gamma_2^{(1)} = 0\ ..\ 0.2\,\sigma^{-2}$.

Fig. 5 (c) depicts the enrichment of the low-boiling component E_2 at VL_1 interfaces of mixture A. Again, the corresponding results for mixture B are given in the Appendix. The enrichment predicted from MD and DGT agrees qualitatively well for both mixtures, but significant deviations are observed. DGT predicts a larger enrichment than MD for mixture A. Such differences have also been reported for other mixtures[4,5,14] and have been explained by fluctuations that are present in MD but not in DGT, but they could also be caused by differences between the PeTS EOS and the LJTS force field. The deviations between E_2 obtained from DGT and MD increase with decreasing temperature (larger E_2). This might be due to the fact that large enrichment at the interface is more sensitive to fluctuations than small enrichment.

For mixture A, values of up to about $E_2 = 7$ are found for the VL_1 interfacial enrichment (cf. Fig. 5 b), which is remarkable considering the fact that it is a simple dispersively interacting system. We have shown in a previous work[2] that the difference of the component

2 bulk density $\Delta\rho_2 = \rho_2^L - \rho_2^V$ has an important influence on the enrichment E_2 (see Supplementary Material for more information). For $\Delta\rho_2 = 0$, any adsorption at a vapour-liquid interface – required to satisfy the Gibbs adsorption equation – contributes to the enrichment for geometric reasons[2]. For all state points studied in the present work, $\Delta\rho_2$ was computed and is shown in the Supplementary Material. For mixture A, $|\Delta\rho_2|$ is small, which favours the large enrichment found at the VL_1 interfaces.

A further interesting finding is that at $T = 0.66\,\varepsilon k_\mathrm{B}^{-1}$, the function $E_2(x_2^{L1})$ shows a non-monotonic behaviour: starting at low x_2^{L1}, it first increases and then, after passing a maximum, decreases. Such a behaviour has to the best of our knowledge not been reported before in the literature. The commonly reported behaviour[4,10,14] of E_2 is a monotonic decay with increasing x_2^{L1}, as observed for all other temperatures for the mixture A.

Mixture B yields much lower values for the enrichment E_2 than mixture A (see Appendix). The enrichment E_2 that is predicted for mixture B by DGT does not exceed E_2 =1.05; values up to about $E_2 = 1.3$ are predicted by MD. The deviations are probably related to the sampling in MD, as discussed above.

Fig. 5 (d) shows the VL_1 interfacial thickness L_{10}^{90}, cf. Eq. (12), for mixture A. The results from DGT and MD agree qualitatively well, but, as discussed in previous works[2,4,5], the interfacial thickness obtained from DGT is systematically smaller than that from MD by about 15%. This has been attributed to fluctuations of the interface present in MD that are not present in DGT[4,5,14]; maybe also differences between the PeTS EOS and the LJTS force field play a role[2,82].

For the upper three temperatures – above the bicritical endpoint – shown in Fig. 5 (d), the interfacial thickness L_{10}^{90} increases monotonously with increasing x_2^{L1}. This increase continues up to the critical point where L_{10}^{90} diverges. The behaviour of L_{10}^{90} that is observed at the lowest temperature $T = 0.66\,\varepsilon k_\mathrm{B}^{-1}$ is highly interesting. Here, L_{10}^{90} diverges upon approaching the VL_1L_2 line, i.e. when x_2^{L1} approaches the composition of the phase L_1 in the three-phase equilibrium. This is discussed and explained in the next section.

Also the maximum of L_{10}^{90} that is observed for $T = 0.715\,\varepsilon k_\mathrm{B}^{-1}$ is directly related to the corresponding phase diagram. The liquid phase composition $x_2^{L1} \approx 0.17$ mol mol^{-1} of the L_{10}^{90} maximum at $T = 0.715\,\varepsilon k_\mathrm{B}^{-1}$ corresponds to the transition of the vapour phase to a 'liquid-like' phase. This goes in hand with a drop of the relative adsorption of component 2 at the interface and a kink in the enrichment $E_2(x_2^{L1})$, cf. Fig. 5 b). This transition is also

observed in the density profiles, cf. Fig. 4 (b).

C. VL_1, VL_2 and L_1L_2 Interfaces Adjacent to the VL_1L_2 Equilibrium

Below the temperature of the upper critical end point (cf. Fig. 2), mixture A exhibits a three-phase VL_1L_2 equilibrium in the phase diagram. Three two-phase equilibrium regions are connected to that VL_1L_2E: VL_1E, VL_2E, and L_1L_2E (cf. Fig. 3). On the three phase line, there are three fluid interfaces VL_1, VL_2, and L_1L_2. Their surface tensions determine the wetting behaviour of the three phases, as discussed in more detail in the literature[52,56,104,127]. The three surface tensions are related by[104]

$$\gamma_{VL1} \leq \gamma_{VL2} + \gamma_{L1L2} \,, \tag{13}$$

where the equality indicates total wetting (plane layer of phase L_2 between L_1 and V) and the inequality indicates partial wetting of the phase L_2 (droplets of phase L_2 on the phase L_1). While interfacial properties and their relation to the wetting behaviour directly on three-phase lines have been discussed in the literature several times[33,52–58], only Falls et al.[44] discuss features of density profiles in the adjacent two phase regions. Therefore, the transitions of the interfacial properties in the two phase regions in the vicinity of the three-phase line in mixture A were systematically studied here. Together with these results we discuss the VL_2 and L_1L_2 interfaces in general.

The vapour pressure and phase compositions of the three-phase equilibrium of mixture A at $T = 0.66\,\varepsilon k_\mathrm{B}^{-1}$ were calculated from the PeTS EOS: $p^s = 0.0555\,\varepsilon\sigma^{-3}$, $x_2^{L1} = 0.124\,\mathrm{mol\,mol^{-1}}$, $x_2^{L2} = 0.817\,\mathrm{mol\,mol^{-1}}$, $x_2^V = 0.901\,\mathrm{mol\,mol^{-1}}$. The three corresponding total number densities are: $\rho^{L1} = 0.78\,\sigma^{-3}$, $\rho^{L2} = 0.51\,\sigma^{-3}$, and $\rho^V = 0.17\,\sigma^{-3}$.

Fig. 6 shows the density profiles at fluid interfaces of VL_1E, VL_2E, and L_1L_2E in the vicinity of the three-phase VL_1L_2 equilibrium at $T = 0.66\,\varepsilon k_\mathrm{B}^{-1}$. As discussed above, a large enrichment is found for VL_1 interfaces. Upon approaching the VL_1L_2E, the enrichment peak of the VL_1 interface changes its shape dramatically: while there are only small changes on the L_1 liquid side of the peak, the vapour side V undergoes a transition upon which the peak becomes much broader. This leads to an extremely high adsorption and interfacial thickness in the vicinity of the VL_1L_2E. This transition can be interpreted as a precursor of the second liquid phase L_2. The second liquid phase L_2 starts growing out of the interface

before the VL_1L_2E is reached, which can be considered as a wetting transition upon which the adsorption $\Gamma_2^{(1)}$ increases drastically. Furthermore, the density profile of the high-boiling component 1 undergoes a transition (cf. Fig. 6 b), which is in line with the interpretation of a new phase growing at the interface upon approaching the VL_1L_2E.

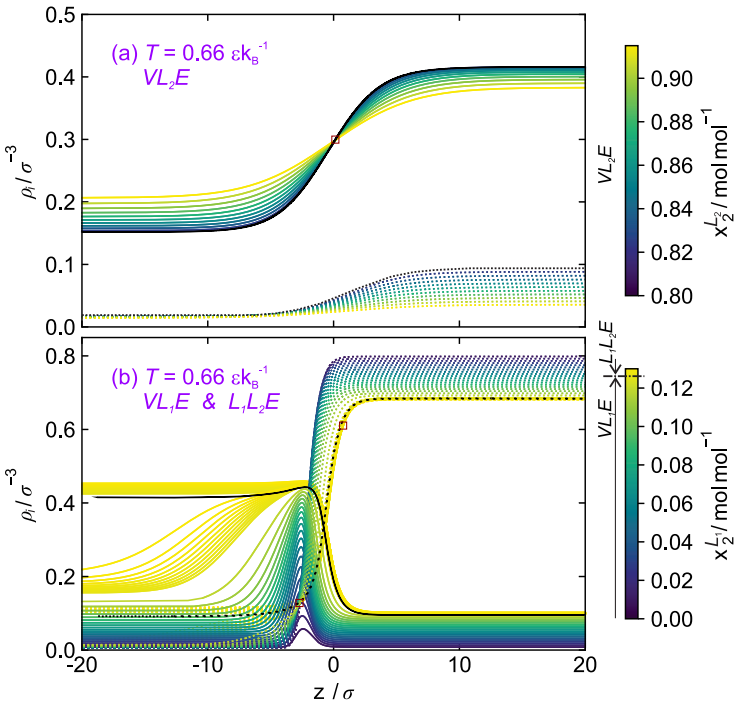

FIG. 6. Density profiles of different fluid interfaces for the binary mixture A at $T = 0.66\,\varepsilon k_\mathrm{B}^{-1}$ in the vicinity of the three-phase equilibrium. (a) shows the VL_2E two phase region (V left, L_2 right); (b) the VL_1E (V left, L_1 right) and L_1L_2E (L_2 left, L_1 right) region. Dashed lines stand for the high-boiling component 1 and solid lines for the low-boiling component 2. The colour-code represents the liquid phase composition. The black lines indicate the density profiles of the three-phase equilibrium. Red squares indicate invariant intersection points of the density profiles.

Interestingly, the enrichment in the VL_1E region is already present at infinite dilution and grows with increasing x_2^{L1} to become eventually the L_2 phase at the three-phase equilibrium. Furthermore, an enrichment in the VL_1E region is also present at temperatures $T > T_\mathrm{UCEP}$, where no VL_1L_2E occur.

From the density profiles at $T = 0.66\,\varepsilon k_\mathrm{B}^{-1}$ close to the three-phase VL_1L_2E, the density and composition of the enrichment peak can be determined roughly as: $\rho^\mathrm{peak} \simeq 0.51\,\sigma^{-3}$ and $x_2^\mathrm{peak} \simeq 0.81\,\mathrm{mol\,mol^{-1}}$. This local composition and total number density at the enrichment peak agrees very well with the composition and density of the second liquid phase L_2 in the

VL_1L_2E at $T = 0.66\,\varepsilon k_B^{-1}$ (see above). Hence, the enrichment of the component 2 at the interfaces in the VL_1 two-phase region can be considered as the nucleation of the L_2 phase – starting already at infinite dilution of component 2. This interpretation is in line with the picture evoked by Falls et al[44].

The fluid interfaces in the three two-phase regions (VL_1E, VL_2E, and L_1L_2E) have strongly differing features, cf. Fig. 6. The interfaces in the VL_1E region exhibit an enrichment of the low-boiling component, whereas the VL_2E region density profiles of both components show a monotonous transition between the bulk phases. Finally, in the L_1L_2E region, a small enrichment is observed in the vicinity of the three-phase equilibrium, cf. Fig. 6.

Fig. 7 shows the interfacial properties (surface tension, relative adsorption, enrichment, and interfacial thickness) of mixture A at $T = 0.66\,\varepsilon k_B^{-1}$ for the VL_1, VL_2, and L_1L_2 interfaces in the vicinity of the VL_1L_2 three-phase equilibrium. The properties of the VL_1 interfaces have already been discussed above.

The VL_2 interfaces show an unexpected behaviour: the surface tension and the relative adsorption are very small, and no enrichment is observed. This may be related to the proximity of the critical point in that small two-phase region. In line with this interpretation, the interfacial thickness is large. As expected, it increases upon approaching the critical point. The predictions of the VL_2 interfacial properties obtained by DGT and MD are in fair agreement.

For the L_1L_2 interfaces, the discrepancies between the predictions of the interfacial properties obtained from the two methods are larger. This is not astonishing, as there were also discrepancies in the predictions of the bulk phase behaviour, cf. Fig. 3. Both methods predict a small surface tension. Again, the enrichment E_2 predicted by DGT is substantially larger than that predicted by MD. However, even for DGT, the maximal enrichment is only about $E_2 = 1.06$. Both methods predict fairly large numbers for the interfacial thickness L_{10}^{90}, but the numbers obtained from MD (about $12\,\sigma$) are again much higher than those obtained from DGT (about $5\,\sigma$). The L_1L_2 surface tension, relative adsorption, and interfacial thickness decrease with increasing pressure.

For all three types of interfaces (VL_1, VL_2, and L_1L_2) in the vicinity of the three-phase equilibrium, the relative adsorption $\Gamma_2^{(1)}$ is highest directly at the three-phase equilibrium and decreases upon moving away from it, cf. Fig. 7 b). The three surface tensions at the

three-phase equilibrium γ_{VL1}, γ_{VL2}, and γ_{L1L2} are directly linked by the wetting behaviour of the phases in direct contact (see above). In the case of mixture A, the phase L_2 wets the VL_1 interface, i.e. $\gamma_{VL1} = \gamma_{VL2} + \gamma_{L1L2}$. Hence, a macroscopic layer of the phase L_2 will form between the phases L_1 and V at the three-phase equilibrium at $T = 0.66\,\varepsilon k_{\mathrm{B}}^{-1}$, which is in line with predictions for simple mixtures of that type[56]. This is completely in line with the picture of a wetting transition discussed for the interfacial structure above.

As mentioned above, at $T = 0.715\,\varepsilon k_{\mathrm{B}}^{-1}$, there is a transition of the vapour phase upon increasing pressure to a high density 'liquid-like' phase in mixture A. Interestingly, also for this transition, the enrichment acts as a precursor, cf. Fig. 4 b). Hence, the 'liquid-like' phase starts forming at the interface in the VL_1 region.

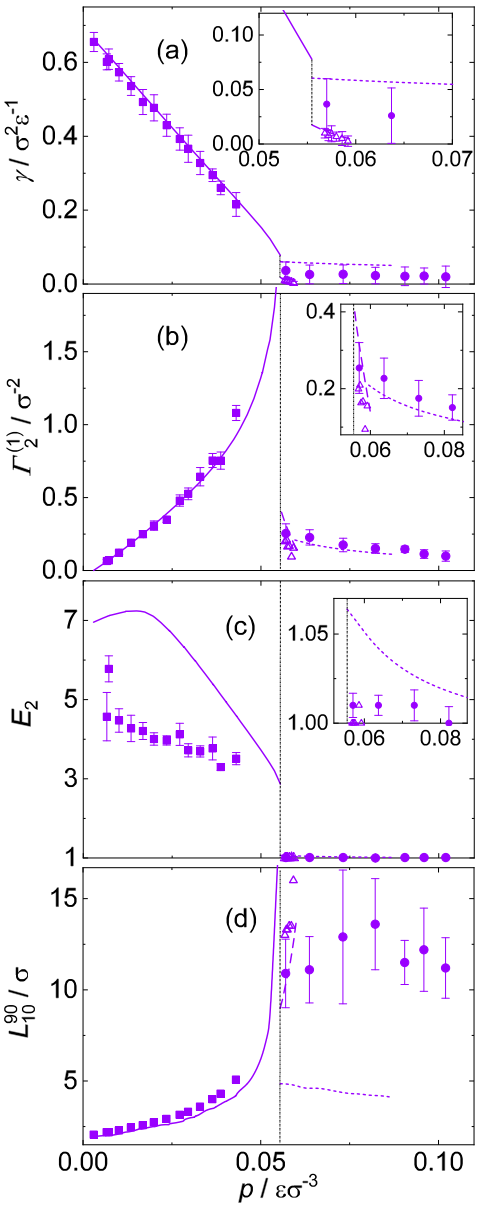

FIG. 7. Interfacial properties of the mixture A at $T = 0.66\,\varepsilon k_{\mathrm{B}}^{-1}$ in the vicinity of the three-phase equilibrium as a function of the pressure. Top to bottom are: surface tension, relative adsorption, enrichment of component 2, and interfacial thickness. Symbols are the MD simulation results, lines are DGT results. Solid lines and squares depict the VL_1E region (left side in the diagrams), dotted lines and circles the L_1L_2E region, and dashed lines and triangles the VL_2E region (right side in the diagrams). The black vertical line indicates the VL_1L_2E three-phase pressure.

D. F_1F_2 Interfaces

Fig. 8 shows the phase behaviour of mixture A at temperatures in the vicinity of the bicritical end point (BICEP) and up to very high pressures. At $T > T_{\mathrm{BICEP}}$, the fluid-fluid equilibrium region F_1F_2 is separated from the VL_1E region. Hence, two critical points are present: the VL_1 region has a pressure maximum critical point, the F_1F_2 region a pressure minimum critical point. In the F_1F_2E two high-density fluid phases F_1 and F_2 coexist. The F_1F_2E is almost symmetric in the phase diagram – especially at high temperatures, cf. Fig. 8.

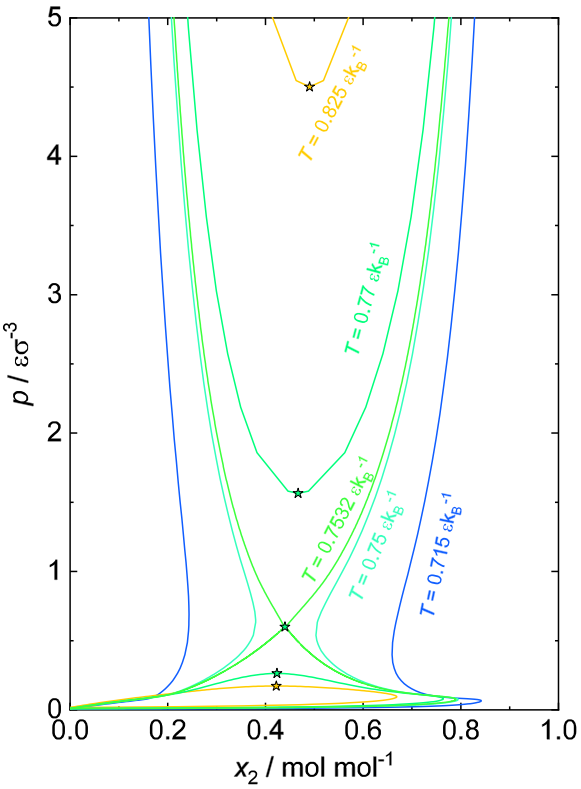

FIG. 8. Isothermal p-x phase diagrams for the mixture A at temperatures close to the bicritical endpoint ($T = 0.7532\,\varepsilon k_{\mathrm{B}}^{-1}$) and up to very high pressures. Results from the EOS. Stars indicate critical points.

We have studied the F_1F_2 interface at $T = 0.77\,\varepsilon k_{\mathrm{B}}^{-1}$ and $T = 0.825\,\varepsilon k_{\mathrm{B}}^{-1}$ with DGT. In preliminary MD simulation runs, stability problems due to the extreme pressures were observed in the employed NVT ensemble. Hence, only DGT results are available for the F_1F_2 interfaces.

The results for the interfacial properties (surface tension, relative adsorption, and interfa-

cial thickness) are shown in Fig. 9. The corresponding density profiles of both components are shown in the Appendix. The enrichment of both components at the interface is unity in the entire F_1F_2E region and is therefore not plotted. Starting at the F_1F_2E critical point, the surface tension is zero and then increases with increasing pressure, cf. Fig. 9 (a). This is opposite to the surface tension dependency in the L_1L_2 equilibrium region, cf. Fig. 7, where the surface tension decreases with increasing pressure. However, the temperature dependency of γ in the L_1L_2 and F_1F_2 equilibrium regions is the same, i.e. the surface tension decreases with increasing temperature. As for the L_1L_2E, the surface tension γ for the F_1F_2E is small and does not exceed $0.06\,\varepsilon\sigma^{-2}$.

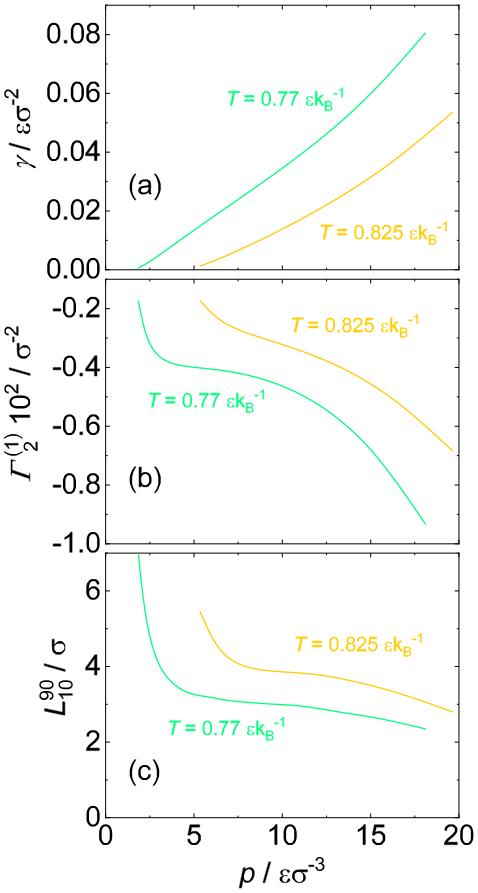

FIG. 9. Interfacial properties of the mixture A at $T = 0.77\,\varepsilon k_{\mathrm{B}}^{-1}$ and $T = 0.825\,\varepsilon k_{\mathrm{B}}^{-1}$ for the high pressure fluid-fluid equilibrium (F_1F_2E) as a function of the pressure. Top to bottom are: surface tension, relative adsorption, and interfacial thickness. Results from DGT. No enrichment was observed for either of the components, i.e. $E_i = 1$.

Interestingly, in contrast to all other types of interfaces that were studied here, the F_1F_2 interfaces are depleted of component 2 (negative values of $\Gamma_2^{(1)}$), cf. Fig. 9 (b). Starting

at the F_1F_2E critical point, the relative adsorption $\Gamma_2^{(1)}$ is zero and then decreases with increasing pressure. The absolute value of $|\Gamma_2^{(1)}|$ is two orders of magnitude smaller than the relative adsorption at the L_1L_2 and VL_1 interfaces. Furthermore, $\Gamma_2^{(1)}(p)$ exhibits an interesting 'S'-shaped behaviour, which is related to the particular structure of the F_1F_2 interface that is described in more detail below.

The interfacial thickness of the F_1F_2 interfaces diverges at the critical pressure and decreases with increasing pressure, cf. Fig. 9 (c). At constant pressure, the interfacial thickness also increases with increasing temperature – as expected. The F_1F_2 and L_1L_2 interfaces have the same qualitative behaviour for the relative adsorption and interfacial thickness – both decrease with increasing pressure.

Fig. 10 shows the density profiles at F_1F_2 interfaces at $T = 0.77\,\varepsilon k_\mathrm{B}^{-1}$. The top plot shows the density profiles of the mixture at $p = 18.1\,\varepsilon\sigma^{-3}$: besides the density profiles of the two individual components, also the total density profile is depicted for a single state point; the bottom plot shows the total density profile for different pressures. The F_1F_2 interfaces are similar to the L_1L_2 interfaces, cf. Fig. 10: also for the F_1F_2 interfaces, the total density of both bulk phases is high and approximately the same. The density profiles of both components $\rho_1(z)$ and $\rho_2(z)$ exhibit a monotonous transition between the bulk phases in both cases. This holds for the entire investigated temperature and pressure range. The density profiles of the two components 1 and 2 are almost symmetric, which is analogous to the symmetry of the underlying $p - x$ phase diagram.

However, the F_1F_2 interfaces reveal an interesting phenomenon, which is not present in the other fluid interfaces examined in the present work. Usually, the total density changes monotonously between the two bulk phases. This is also the case for the F_1F_2 interfaces for moderate pressures. But for very high pressures, an oscillation is observed in the total density profile, cf. Fig. 10 - bottom. A single minimum in the total density profile has been reported before in the literature[51,59–63], but to the best of our knowledge no maximum-minimum structure.

The oscillation structure found at the investigated F_1F_2 interfaces in mixture A formally resembles the oscillatory layering structures[5,59,60,80,128–130] of other types of fluid interfaces. But the single oscillation found here at F_1F_2 interfaces is likely a different phenomenon, since DGT was employed for the calculations, which is not able to predict the common oscillatory layering structures[5]. It should be noted that this oscillation might be an artefact of the

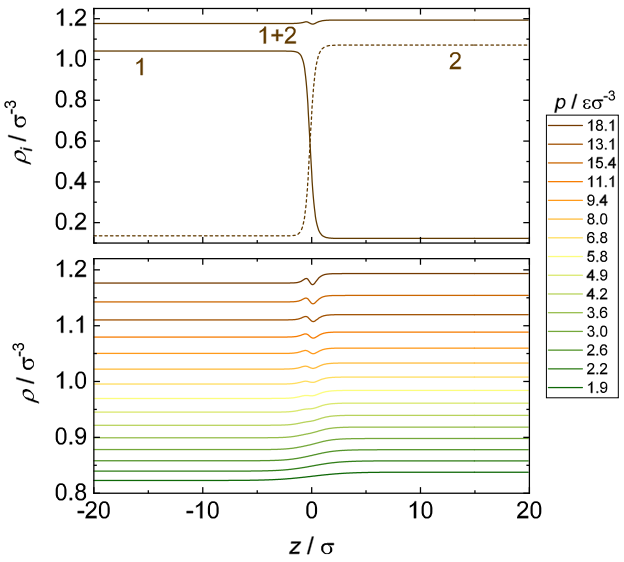

FIG. 10. Density profiles of mixture A at $T = 0.77\,\varepsilon k_{\mathrm{B}}^{-1}$ for the high pressure fluid-fluid equilibrium (F_1F_2E). Results from DGT. Top shows the density profiles of component 1, component 2, and the total density 1+2 at $p = 18.1\,\varepsilon\sigma^{-3}$. Bottom shows the total density 1+2 at different pressures. The colour-code indicates the pressure.

employed EOS type, which is known to exhibit difficulties at extreme pressures due to the simplified repulsive interaction term[3,126]. A detailed investigation would be an interesting topic for future work.

E. Invariant Intersection Points in Density Profiles

Invariant intersection points in the density profiles are observed for many fluid regions studied in the present work, cf. Figs. 4, 6 and Fig. 13 in the Appendix. The phenomenon of invariant intersection points has already been reported for pure substances[5,131] and also simple binary model mixtures[4] as well as for real mixtures[10]. In these invariant intersection points, density profiles $\rho_i(z)$ of a component i intersect for a given temperature. These intersection points have been suspected to be related to critical points[4,5,131]. In the present work, for VL_1 and L_1L_2 interfaces of mixture A, an intersection point was found for the high-boiling component 1, whereas for VL_2 interfaces, an intersection point was found for the low-boiling component 2. For F_1F_2 interfaces, intersection points are observed for the density profiles of both components (see Appendix C). No intersection points are observed in the density profiles obtained for the ideal mixture B. The observations for the intersection points

were in all cases consistent among the MD and the DGT results (see Supplementary Material for MD density profiles). These invariant intersection points probably have a physical cause, which is, however, presently unknown. Further investigations are needed to elucidate its cause. We limit ourselves to reporting our observations regarding the invariant intersection points and a brief discussion of their relation to the corresponding phase diagram, which is given in Appendix C.

F. Overview of the Findings

Overall, the ideal mixture B shows the expected behaviour: the surface tension γ of the VL interfaces is dominated by the two pure substance values and decreases with increasing temperature; the same holds for the relative adsorption $\Gamma_2^{(1)}$, which is moderate ($\Gamma_2^{(1)} < 0.4\,\sigma^{-2}$). There is no significant enrichment ($E_2 = 1$), i.e. the density profiles in the interfacial regions are monotonous, except very shallow maxima that are observed at low temperatures. The thickness of the interface increases with increasing temperature and is in the range of $L_{10}^{90} = 2..5\,\sigma$. There is a smooth transition of L_{10}^{90} between the pure component values.

For mixture A, the results that were obtained for the different types of phase equilibria differ significantly and important mixture effects are observed. The complex phase behaviour of mixture A causes not only a complex behaviour of the surface tension, but also the density profiles at interfaces have complex structures, with wetting transitions, common intersecting points, maxima, and in some cases even minima.

The phase diagram of mixture A has critical points of three different types. For all critical points, the behaviour is as expected: the surface tension γ and the relative adsorption $\Gamma_2^{(1)}$ decay to zero, the enrichment E_2 goes to unity, and the thickness L_{10}^{90} goes to infinity upon approaching the critical point.

As for mixture B, also for mixture A typical values of the thickness L_{10}^{90} are between 2 and $5\,\sigma$ for state points that are far away from critical points and VL_1L_2E. This holds for all types of phase equilibria of mixture A.

The fluid-fluid interfaces in the F_1F_2 region of mixture A have small surface tension ($\gamma < 0.1\,\varepsilon\sigma^{-2}$) but a negative relative adsorption ($\Gamma_2^{(1)} < 0$). An interesting phenomenon is observed in the density profiles of the F_1F_2 interfaces: Even though the density profiles of

both components 1 and 2 are monotonous (i.e. $E_1 = E_2 = 1$), a non-monotonicity in the total density profile with a minimum and a maximum is observed for several state points. This phenomenon cannot be interpreted as a layering structure of the fluids near surfaces, as it is usually predicted by DFT, as it was found by DGT, which cannot yield these layering structures. Further research is needed to elucidate the cause of this interesting structure.

Also the L_1L_2 liquid-liquid interfaces of mixture A have a small surface tension ($\gamma < 0.1\,\varepsilon\sigma^{-2}$), but in contrast to the F_1F_2 interfaces, they have a small positive relative adsorption ($\Gamma_2^{(1)} < 0.3\,\sigma^{-2}$). The enrichment E_2 is in general close to unity, but near the VL_1L_2E, values up to about $E_2 = 1.06$ were found for L_1L_2 interfaces.

There is a small VL_2E region with a critical point in the phase diagram of mixture A, for which the differences in the composition and the density of the coexisting phases are fairly small throughout. This has the expected consequences: the surface tension γ is very small ($\gamma < 0.02\,\varepsilon\sigma^{-2}$), the interfacial thickness is large ($L_{10}^{90} > 10\,\sigma$), and there is no enrichment E_2. The relative adsorption $\Gamma_2^{(1)}$ is small and positive ($\Gamma_2^{(1)} < 0.3\,\sigma^{-2}$).

The VL_1E region in the isothermal phase diagram of mixture A has varying topologies depending on the temperature: at the lowest studied temperature, it connects the boiling point of the pure component 1 with the VL_1L_2 three-phase equilibrium, whereas at high temperatures it ends in a critical point. One intermediate temperature was studied where the phase envelope is open up to extreme pressures and exhibits a smooth transition of the vapour phase V to a high density 'liquid-like' phase, which acts as the transition between the L_1L_2E at lower temperatures and F_1F_2E at higher temperatures for that type III mixture[123]. All this has important consequences for the interfacial properties.

For VL_1E with low mole fractions x_2^{L1}, i.e. near the boiling point of the pure component 1, simple trends are observed: the surface tension is similar to the pure component value ($\gamma < 0.65\,\varepsilon\sigma^{-2}$) and increases with decreasing temperature. The same holds for the relative adsorption, which is positive ($\Gamma_2^{(1)} < 0.5\,\sigma^{-2}$ for $x_2^{L1} < 0.05\,\mathrm{mol\,mol^{-1}}$). The enrichment E_2 is large and increases with decreasing temperature. Values $E_2 > 7$ were found, which is remarkable for a simple dispersive system. In contrast to the common finding that E_2 decreases as x_2^{L1} decreases, $E_2(x_2^{L1})$ has a maximum for the VL_1 interfaces of mixture A at the lowest studied temperature (where the VL_1L_2E exists).

For higher mole fractions x_2^{L1}, the differences between the different topologies of the VL_1 equilibrium type become important for the interfacial properties. For the cases where the

VL_1E region ends in a critical point, the surface tension γ and the relative adsorption $\Gamma_2^{(1)}$ simply decay to zero. But for the case, in which the VL_1E region ends in the VL_1L_2 three-phase line, interesting phenomena are observed: upon approaching the VL_1L_2 three-phase equilibrium, a precursor of the second liquid phase L_2 forms at the VL_1 interface. This leads to a divergence of the relative absorption $\Gamma_2^{(1)}$ and the interfacial thickness L_{10}^{90} in the vicinity of the VL_1L_2E. The enrichment E_2 can be considered to be a precursor of the wetting present at the three-phase equilibrium. This interpretation is supported by the fact that the composition at the peak of the enrichment is in very good agreement with that of the second liquid phase L_2 even for conditions that are not in the direct vicinity of the VL_1L_2E. Further support comes from the fact that the surface tensions obtained in the three-phase equilibrium are such that the phase L_2 wets the VL_1 interface at the considered T.

Some of the features described above for the VL_1E and L_1L_2E region in the phase diagram with a three-phase equilibrium VL_1L_2E are also observed for the isothermal phase diagram for which the VL_1E region is 'open' up to extreme pressures (no critical point) and the vapour phase eventually becomes 'liquid-like' (and no VL_1L_2 three-phase equilibrium exist). Hence, for such temperatures, the relative adsorption $\Gamma_2^{(1)}$ and the interfacial thickness L_{10}^{90} show strong maxima at intermediate pressures. This is interpreted here as a consequence of the fact that the conditions are close to those of the three-phase equilibrium. The transition of the vapour phase to a dense liquid phase is mediated by the enrichment at the interface, which resembles the wetting precursor found at the VL_1 interface in the vicinity of the VL_1L_2E.

IV. CONCLUSIONS

This paper reports on properties of fluid interfaces of binary mixtures (density profiles, surface tension, relative adsorption, enrichment, and thickness) and their relation to the phase diagram. For this purpose, two Lennard-Jones mixtures were investigated with both molecular dynamics (MD) simulation and density gradient theory (DGT) at five temperatures in the entire range in which fluid phase equilibria exist. The low-boiling component 1 is the same in both mixtures. The high-boiling component 2 and the interaction parameters were chosen such that mixture A is a highly asymmetric non-ideal mixture of type III, in which component 2 is supercritical for all studied temperatures, whereas mixture B is an

almost ideal mixture of type I with a subcritical component 2. For mixture B, only vapour-liquid equilibria (VLE) exist, whereas mixture A has a complex phase diagram with a three-phase equilibrium (VL_1L_2E), two vapour-liquid equilibrium regions (VL_1E and VL_2E), and regions in which liquid-liquid equilibria (L_1L_2E), and fluid-fluid equilibria (F_1F_2E) exist.

The results that were obtained from MD and DGT for the interfaces agree well in most cases. Significant differences were, however, observed for L_1L_2 interfaces and in the vicinity of critical points, which are most likely related to the fact that in these cases also the phase equilibria calculated from MD and from the EOS that was used in DGT show differences.

The results from the present work show that the assumption of a temperature-independent influence parameter in DGT works very well even when a broad temperature range is investigated. Also the employed geometric mixing rule for the influence parameter yields good results even though the investigated mixture A is highly asymmetric.

For mixture A, the obtained phase diagrams at the studied temperatures differ significantly. They give insight into the relation of the phase diagram to the interfacial properties in many ways: regarding the critical points, which do not only lead to the well-known effects in their vicinity such as a decrease of the surface tension and the relative adsorption, but are also related to invariant common intersection points that are found in many of the component density profiles. Further research is needed to reveal the relation of these intersection points and the critical behaviour.

The findings for the interfacial properties of mixture A cannot be understood without considering the corresponding phase diagrams. The most interesting observation from the present study is that, as the conditions get closer to those of the three-phase VL_1L_2E, a precursor of the second liquid phase L_2 forms at the VL_1 interface. This leads to a very strong increase of the relative adsorption $\Gamma_2^{(1)}$ and the interfacial thickness L_{10}^{90}. These findings and interpretations are in line with the results and interpretations of Falls et al.[44] on density profiles in a similar system. We argue that the strong enrichment that is observed at VL_1 interfaces even at conditions that are not close to the three-phase equilibrium can be interpreted as a precursor of the L_2 phase that nucleates under the influence of the gradients at the interface. This does not mean that the existence of a three-phase equilibrium in a given system is a prerequisite for the occurrence of interfacial enrichment; but the presence of a three-phase equilibrium is assumed to strongly favour interfacial enrichment.

Furthermore, we assume that what was observed here for mixture A regarding the relation

of the enrichment at VL_1 interfaces and the three-phase equilibrium can be generalized for different wetting conditions[52,53,56] along the three phase line.

Appendix A: Supplementary Information

Supplementary data can be found at [online DOI-link]. Density profiles from molecular simulations and the numeric values for the bulk and interfacial properties obtained from MD and DGT are listed there.

Appendix B: Ideal Reference Mixture

The interfacial properties of mixture B are reported and discussed in this Appendix. The chosen mixture parameters for the mixture B $\xi = 1$ and $\varepsilon_2/\varepsilon_1 = 0.9$ result in a basically ideal mixture in the sense of Raoult's law (cf. Fig. 3 a). The activity coefficients at infinite dilution are in all cases well below 1.05 in the entire temperature range studied here. This ideal behaviour holds for the entire investigated temperature range. Both components are subcritical at all chosen temperatures.

Fig. 11 shows the density profiles of both components at the VL interface at $T = 0.66\,\varepsilon k_\mathrm{B}^{-1}$. As the density profiles at other temperatures do not provide further insight, they are only shown in the Supplementary Material.

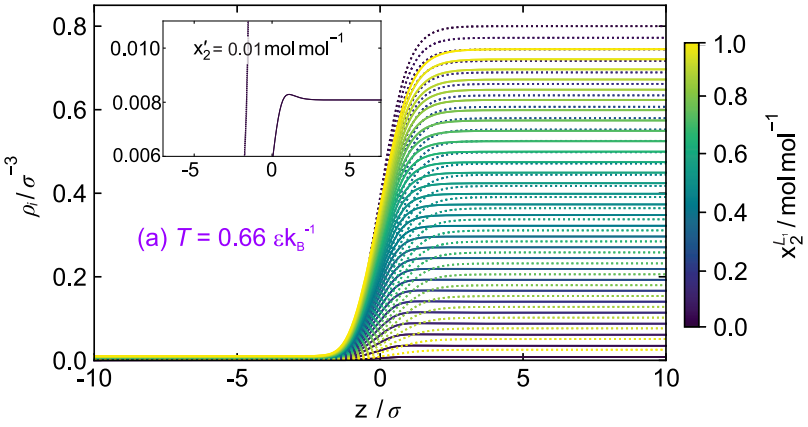

FIG. 11. Density profiles of component 1 (dashed lines) and component 2 (full lines) for the mixture B at $T = 0.66\,\varepsilon k_\mathrm{B}^{-1}$ obtained by DGT. The colour-code indicates the liquid phase composition.

At very low concentrations of component 2, a small but distinct enrichment of component

2 at the interface is found (cf. Fig. 11). This also holds for $T = 0.715\,\varepsilon k_\mathrm{B}^{-1}$ and $T = 0.77\,\varepsilon k_\mathrm{B}^{-1}$ (see Supplementary Material).

Furthermore, a closer look reveals that the density profiles from component 2 are slightly shifted to $-z$ direction with respect to the density profile of the high-boiling component; at all concentrations but especially at high x_2^L. This is an indication that the component 2 adsorbs at the interface – even though no enrichment is present.

Fig. 12 shows the interfacial properties obtained from MD and DGT for the *VL* interface of mixture B. Results for the surface tension, relative adsorption, enrichment, and interfacial thickness are shown. The surface tension of mixture B, starting at the pure component 1, decreases almost linearly with increasing x_2^L. This holds for all five investigated temperatures. The surface tension decreases with an increasing temperature, while the slope of the surface tension $\partial\gamma/\partial x_2^L$ does not depend on the temperature.

The adsorption isotherms (Fig. 12 b) for mixture B are almost linear with a slight concave curvature, which confirms the impressions from the density profiles. Since the relative adsorption and the decay of the surface tension $\partial\gamma/\partial x_2^L$ are linked via the Gibbs adsorption equation, also the temperature dependency of the relative adsorption is faint; the relative adsorption slightly increases with decreasing temperature. This can only be seen in the DGT results, as the scattering of the MD results exceeds this temperature influence on $\Gamma_2^{(1)}$.

For the mixture B the results predicted from DGT lie within the error bars of the MD results, even though the latter scatter intensely and have accordingly large error bars. This is simply due to the fact that the magnitude of the adsorption is relatively small.

As shown in the inset in Fig. 11 also the density profiles of component 2 in mixture B exhibit a slight maximum at the interface, i.e. enrichment $E_2 > 1$. Such an enrichment is only found at low temperatures and low liquid phase concentrations x_2^L, cf. Fig. 12 (c). This is in line with results from a previous study[2], which showed that the enrichment exhibits a continuous transition upon varying mixture parameters ξ and $\varepsilon_2/\varepsilon_1$ at constant temperature and x_2^L. Even though MD seems to overestimate the enrichment in ideal mixtures compared to the theory, the present enrichment is probably not an artefact. The systematic overestimation of the enrichment obtained from MD compared to DGT results in the case of an insignificant enrichment has been attributed to the fact that outliers – in the not perfectly smooth density profiles from MD – will have a strong influence at very small values

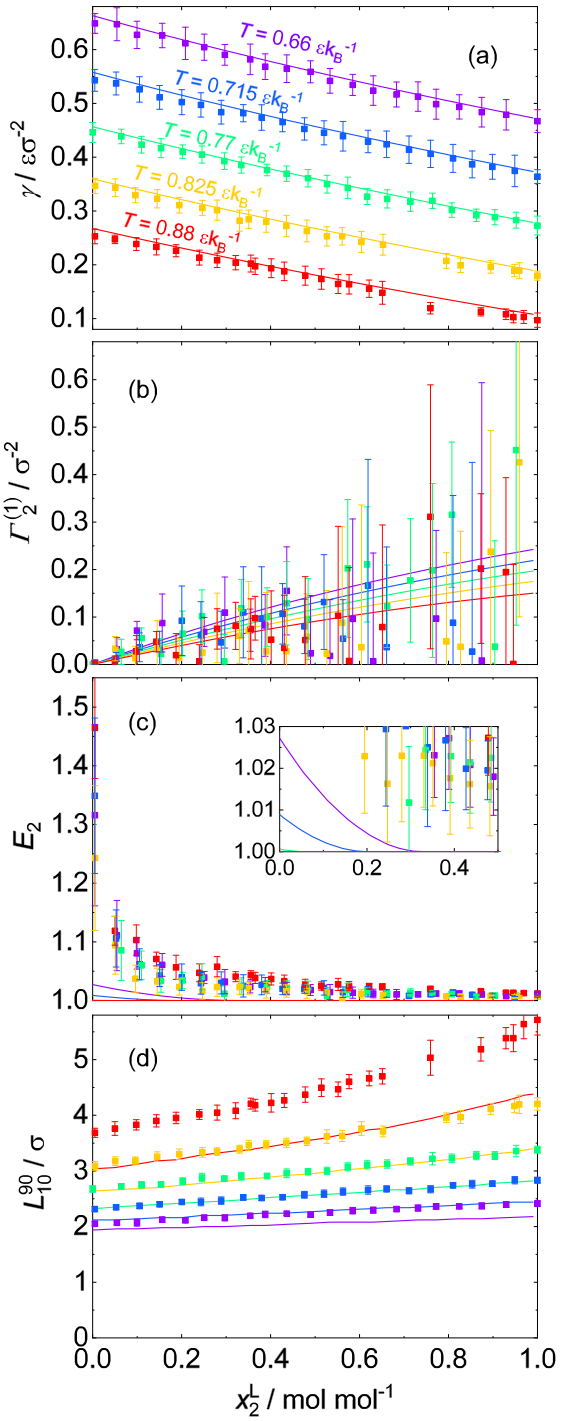

FIG. 12. VL_1 interfacial properties for mixture B: (a) surface tension γ, (b) relative adsorption of component 2 at the interface $\Gamma_2^{(1)}$, (c) enrichment of component 2 E_2, and (d) interfacial thickness L_{10}^{90}. Symbols are MD simulation results, lines are DGT results. Results for all studied temperatures. The colour-code indicates the temperature and is the same for all shown plots.

of E_2[2,4,82]. This can also be seen at the strongly increasing error bars of the E_2 results at low liquid phase concentrations x_2^L in mixture B.

The interfacial thickness of mixture B (cf. Fig. 12 d) increases almost linearly between the two pure component values with varying x_2^L, which is similar to the surface tension behaviour (cf. Fig. 12 a). However, an important difference can be observed: $\partial\gamma/\partial x_2^L$ does not change with varying temperature, whereas $\partial L_{10}^{90}/\partial x_2^L$ depends on the temperature. This is mainly due to differences in the pure component temperature dependency of the surface tension and the interfacial thickness[82]. As found in previous studies[2,4,82] and also for mixture A, the PeTS+DGT results systematically underestimate the MD results of the interfacial thickness.

Appendix C: Overview of Invariant Intersection Points and Their Relation to the Phase Diagram

Table I summarises the findings on the invariant intersection points of the density profiles for mixture A as obtained from DGT. It also gives reference to the figures in which the corresponding profiles can be found. One or two invariant intersection points were observed in the density profiles of component 1 for the VL_1 and L_1L_2 interfaces. For VL_2 interfaces, one invariant intersection point in the density profile of component 2 was found. For F_1F_2 interfaces, an invariant intersection point was observed in the density profiles of both components. For cases with two invariant intersection points in the set of isothermal density profiles of a component (as observed for the VL_1 interfaces of mixture A at four temperatures (cf. Table I) that set can can be split into two subsets. One subset going through the first intersection point and a second one going through the second intersection point. In all cases there is one density profile that belongs to both subsets, i.e. it approximately runs through both intersection points and connects them. That density profile is labelled with an asterisk here. There is a certain pressure p^* and liquid bulk phase composition x_2^* associated with that density profile.

As also noted by Bongiorno and Davis[131], the invariant intersection points are not exact, which might be due to computational reasons, i.e. the discretisation of the density profiles.

Since the MD density profiles exhibit stochastic fluctuations, the intersection points can only be identified approximately in the respective plots (see Supplementary Material). Their

TABLE I. Overview of invariant intersection points and critical point properties in the different fluid regions of mixture A as obtained from DGT and the PeTS EOS. The definitions of the fluid regions are given in the main body of this work, cf. Section III A. The second column refers to the temperature of the respective set of density profiles. The column #IP indicates the number of invariant intersection points and the component profile ρ_i in which they were observed; the following column indicates the corresponding figure. The column #CP indicates the number of critical points present in the given fluid region and for the given T. The column ρ_i^{IP} reports the component density at the invariant intersection points of component i and the last column reports the critical component density $\rho_{\mathrm{c},i} = x_i \rho_{\mathrm{c}}$ computed from the PeTS EOS at a given T. The component-index i in the last two columns corresponds in all cases to the component density indicated in the column #IP.

fluid region	$T \,/\, \varepsilon k_{\mathrm{B}}^{-1}$	#IP	Figure	#CP	$\rho_i^{\mathrm{IP}} \,/\, \sigma^{-3}$	$\rho_{\mathrm{c},i} \,/\, \sigma^{-3}$
VL_1	0.66	1x ρ_1	4 (a)	-	0.11	-
	0.715	2x ρ_1	4 (b)	-	0.16 & 0.5	-
	0.77	2x ρ_1	4 (c)	1	0.21 & 0.38	0.381
	0.825	2x ρ_1	4 (d)	1	0.24 & 0.33	0.330
	0.88	2x ρ_1	4 (e)	1	0.26 & 0.31	0.307
VL_2	0.66	1x ρ_2	6 (a)	1	0.30	0.299
L_1L_2	0.66	1x ρ_1	6 (b)	-	0.62	-
F_1F_2	0.77	1x ρ_1 & 1x ρ_2	13 (a)	1	0.43 & 0.38	0.433 & 0.380
	0.825	1x ρ_1 & 1x ρ_2	13 (b)	1	0.47 & 0.45	0.471 & 0.454

numeric values are not used for the following quantitative evaluation. However, the qualitative features of the invariant intersection points obtained from the DGT and MD results are in all cases consistent.

Bongiorno and Davis[131] found that the invariant intersection point of the density profiles at different temperatures of the pure van der Waals fluid have the same density as the critical point density. The same was reported for the pure LJTS fluid[5]. As discussed below in more detail, similar observations were made in the present work for mixture A.

Table I shows that for phase equilibria in regions that have a critical point, at least one of the component density profiles exhibits an invariant intersection point. The component

density of that intersection point ρ_i^{IP} is in excellent agreement with the corresponding critical component density $\rho_{\mathrm{c}.i} = x_i \rho_{\mathrm{c}}$ computed from the PeTS EOS, cf. Table I. Such common intersection points are labelled here as type i). For the VL_1 component 1 density profiles at $T = 0.77\,\varepsilon k_{\mathrm{B}}^{-1}$, $0.825\,\varepsilon k_{\mathrm{B}}^{-1}$, and $0.88\,\varepsilon k_{\mathrm{B}}^{-1}$, the intersection point at $z > 0$ corresponds to the critical density $\rho_{\mathrm{c}.1}$, i.e. is of type i). For the VL_2 component 2 density profiles, the invariant intersection point corresponds to the critical density $\rho_{\mathrm{c}.2}$, i.e. it is also of type i). For the F_1F_2 interfaces, invariant intersection points are observed in the density profiles of both components and their densities are the same as the respective critical densities, $\rho_{\mathrm{c}.1}$ and $\rho_{\mathrm{c}.2}$, respectively. Also these intersections points are of type i).

The type i) intersection points include the density profile of the critical point. It follows from this, that the component density at the intersection point of type i) must be the critical density. However, nothing can be learnt from this argument about the physical cause for the existence of an intersection point. If this were the sole argument, the component density profiles might as well not intersect in phase equilibrium regions that contain a critical point.

It is noted here that the existence of invariant intersection points is related to the way $z = 0$ is defined for the density profiles, cf. Section II D. The employed definition is based on the averaging of the two bulk densities. This is analogue to the definition of the rectilinear diameter, which is often used to determine the critical point[132–135]. From this one might infer, that the invariant intersection points of type i) that were observed here are related to the so-called 'law of the rectilinear diameter'.

As can be seen from Table I, there are also intersection points that are not of type i), i.e. they do not contain a critical density profile, and the corresponding component density is not a critical density.

Let us first turn to the component density profiles that contain two invariant points (VL_1 at $T/\varepsilon k_{\mathrm{B}}^{-1} = 0.715$, 0.77, 0.825, 0.88, cf. Table I). The invariant point that is not of type i) is labelled type ii) here. The density profiles belonging to the type i) intersection point are in all cases those with the higher pressure; those belonging to the type ii) intersection point are those with the lower pressure. The transition (density profile * going through both points) takes place at the pressure p^*. It is interesting to note that when the pressure p^* is plotted over the temperature T in the p,T-diagram of mixture A, an extension of the VL_1L_2E line is obtained (see Supplementary Material).

The invariant intersection points of type ii) are always found at $z < 0$ whereas those of

type i) are found at $z > 0$. Interestingly, the z-position of the type ii) points in the density profile of component 1 roughly matches the position of the enrichment peak in the density profile of component 2.

All these findings indicate consistently that a relation may exist between the type ii) invariant intersection points, the enrichment, and the precursor of the second liquid phase as discussed in the main body of this paper. This leads to the following tentative classification: type i) invariant points are related to critical points, type ii) invariant points are related to interfacial wetting by a precursor of a second liquid phase.

Following this classification, two of the four invariant points that were not discussed so far can also be assigned. There is a single invariant point in the $\rho_1(z)$ set in the VL_1 region of mixture A at $T = 0.66\,\varepsilon k_\mathrm{B}^{-1}$ (cf. Table I). This invariant point is obviously related to the three-phase equilibrium and, hence, of type ii). This can also be seen from a continuity argument: the density of the invariant points of type ii) in the VL_1 region can be plotted as a function of the temperature. As there is no critical point in the VL_1 region at $T = 0.66\,\varepsilon k_\mathrm{B}^{-1}$, this invariant point is the only one and all profiles $\rho_1(z)$ go through that point.

Furthermore, there are two invariant intersection points in the $\rho_1(z)$ profiles in the VL_1 region of mixture A at $T = 0.715\,\varepsilon k_\mathrm{B}^{-1}$. The one with the lower density is of type ii), as can be deduced from the same continuity argument as given above. The other invariant point has a high density ρ_1. The state point of the * density profile at $T = 0.715\,\varepsilon k_\mathrm{B}^{-1}$ is found to agree well with the transition of the vapour phase to a dense 'liquid-like' phase, cf. Fig. 4 (b) and Section III A for a discussion.

But as there is no upper critical point in the $T = 0.715\,\varepsilon k_\mathrm{B}^{-1}$ phase diagram, the ρ_1 'high density' invariant point cannot be assigned to type i). However, that invariant point resembles the invariant point in the L_1L_2 region at $T = 0.66\,\varepsilon k_\mathrm{B}^{-1}$. Also in that fluid region, there is no upper critical point. We assign the latter two invariant points to a type iii) that, however, has similarities with type i).

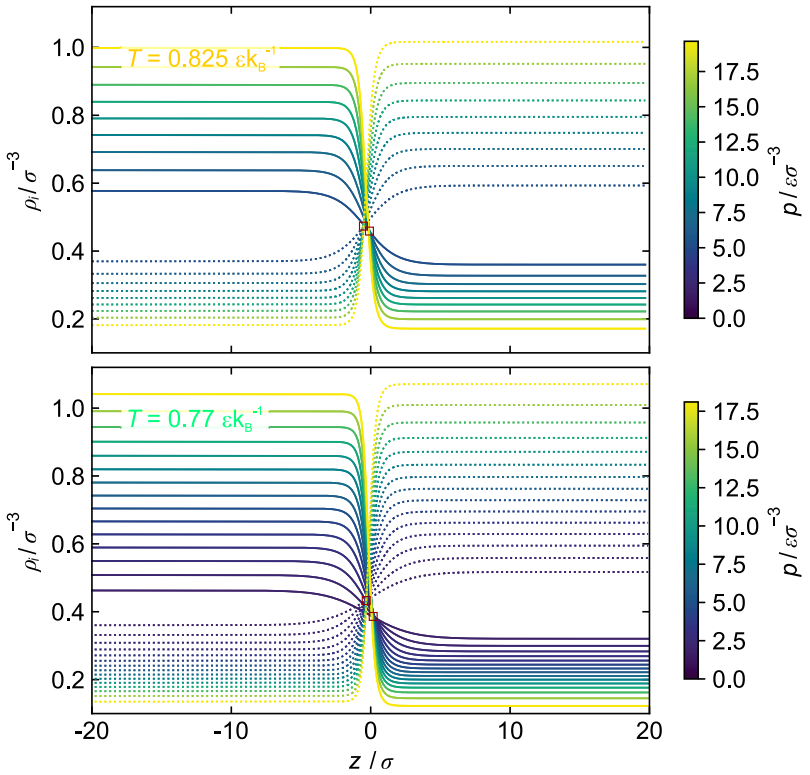

FIG. 13. Density profiles of mixture A at $T = 0.77\,\varepsilon k_\mathrm{B}^{-1}$ (top) and $T = 0.825\,\varepsilon k_\mathrm{B}^{-1}$ (bottom) for the high pressure fluid-fluid F_1F_2 equilibrium obtained from DGT. Dashed lines are the high-boiling component 1 and solid lines are the low-boiling component 2. The colour is coded by the pressure. Red squares indicate invariant intersection points of density profiles.

ACKNOWLEDGMENTS

The authors gratefully acknowledge funding of the present work by the ERC H2020 Advanced Grant ENRICO (grant agreement No. 694807). The simulations were carried out at the Regional University Computing Center Kaiserslautern (RHRK) under the grant TUK-MTD and High Performance Computing Center Stuttgart (HLRS) under the grant MMHBF2. The present research was conducted under the auspices of the Boltzmann-Zuse Society of Computational Molecular Engineering (BZS).

CONFLICTS OF INTEREST

There are no conflicts of interest to declare.

REFERENCES

[1]P. H. van Konynenburg and R. L. Scott, "Critical lines and phase equilibria in binary van der Waals mixtures," Philosophical Transactions of the Royal Society of London A **298**, 495–540 (1980).

[2]S. Stephan and H. Hasse, "Molecular interactions at vapor-liquid interfaces: Binary mixtures of simple fluids," Physical Review E **101**, 012802 (2020).

[3]M. Heier, S. Stephan, J. Liu, W. G. Chapman, H. Hasse, and K. Langenbach, "Equation of state for the Lennard-Jones truncated and shifted fluid with a cut-off radius of 2.5σ based on perturbation theory and its applications to interfacial thermodynamics," Molecular Physics **116**, 2083–2094 (2018).

[4]S. Stephan, K. Langenbach, and H. Hasse, "Interfacial properties of binary Lennard-Jones mixtures by molecular simulations and density gradient theory," The Journal of Chemical Physics **150**, 174704 (2019).

[5]S. Stephan, J. Liu, K. Langenbach, W. G. Chapman, and H. Hasse, "Vapor-liquid interface of the Lennard-Jones truncated and shifted fluid: Comparison of molecular simulation, density gradient theory, and density functional theory," The Journal of Physical Chemistry C **122**, 24705–24715 (2018).

[6]M. M. Telo da Gama and R. Evans, "Theory of the liquid-vapour interface of a binary mixture of Lennard-Jones fluids," Molecular Physics **41**, 1091–1112 (1980).

[7]D. J. Lee, M. M. Telo da Gama, and K. E. Gubbins, "The vapour-liquid interface for a Lennard-Jones model of argon-krypton mixtures," Molecular Physics **53**, 1113–1130 (1984).

[8]B. S. Carey, L. E. Scriven, and H. T. Davis, "Semiempirical theory of surface tension of binary systems," AIChE Journal **26**, 705–711 (1980).

[9]F. J. Martinez-Ruiz and F. J. Blas, "Interfacial properties of binary mixtures of square-well molecules from Monte Carlo simulation," The Journal of Chemical Physics **144**, 154705 (2016).

[10]S. Stephan, S. Becker, K. Langenbach, and H. Hasse, "Vapor-liquid interfacial properties of the binary system cyclohexane + CO2: Experiment, molecular simulation and density gradient theory," Fluid Phase Equilibria (2020), 10.1016/j.fluid.2020.112583.

[11]J. Mairhofer and J. Gross, "Modeling of interfacial properties of multicomponent systems using density dradient theory and PCP-SAFT," Fluid Phase Equilibria **439**, 31 (2017).

[12]D. J. Lee, M. M. Telo da Gama, and K. E. Gubbins, "Adsorption and surface tension reduction at the vapor-liquid interface," The Journal of Physical Chemistry **89**, 1514–1519 (1985).

[13]A. Mejía, J. C. Pàmies, D. Duque, H. Segura, and L. F. Vega, "Phase and interface behaviors in type-I and type-V Lennard-Jones mixtures: Theory and simulations," The Journal of Chemical Physics **123**, 034505 (2005).

[14]S. Becker, S. Werth, M. Horsch, K. Langenbach, and H. Hasse, "Interfacial tension and adsorption in the binary system ethanol and carbon dioxide: Experiments, molecular simulation and density gradient theory," Fluid Phase Equilibria **427**, 476 (2016).

[15]J. C. Neyt, A. Wender, V. Lachet, A. Ghoufi, and P. Malfreyt, "Molecular modeling of the liquid-vapor interfaces of a multi-component mixture: Prediction of the coexisting densities and surface tensions at different pressures and gas compositions," The Journal of Chemical Physics **139**, 024701 (2013).

[16]S. Eckelsbach and J. Vrabec, "Fluid phase interface properties of acetone, oxygen, nitrogen and their binary mixtures by molecular simulation," Physical Chemistry Chemical Physics **17**, 27195–27203 (2015).

[17]M. M. Telo da Gama and R. Evans, "Surface segregation and surface tension at the liquid-vapour interface of a binary mixture of Lennard-Jones fluids," Faraday Symposia of the Chemical Society **16**, 45–58 (1981).

[18]S. P. Protsenko, V. G. Baidakov, and V. M. Bryukhanov, "Binary Lennard-Jones mixtures with highly asymmetric interactions of the components. 2. effect of the particle size on phase equilibria and properties of liquid-gas interfaces," Fluid Phase Equilibria **430**, 67–74 (2016).

[19]S. P. Protsenko and V. G. Baidakov, "Binary Lennard-Jones mixtures with highly asymmetric interactions of the components. 1. effect of the energy parameters on phase equilibria and properties of liquid-gas interfaces," Fluid Phase Equilibria **429**, 242–253 (2016).

[20]C. Klink and J. Gross, "A density functional theory for vapor-liquid interfaces of mixtures using the perturbed-chain polar statistical associating fluid theory equation of state," Industrial & Engineering Chemistry Research **53**, 6169 (2014).

[21]V. G. Baidakov and S. P. Protsenko, "Molecular-dynamics investigation of phase equilibrium and surface tension in argon-neon system," The Journal of Physical Chemistry C **112**, 17231–17234 (2008).

[22]V. G. Baidakov, A. M. Kaverin, and M. N. Khotienkova, "Surface tension of ethane-methane solutions: 1. experiment and thermodynamic analysis of the results," Fluid Phase Equilibria **356**, 90–95 (2013).

[23]V. G. Baidakov and M. N. Khotienkova, "Surface tension of methane-nitrogen solutions: 2. description in the framework of the van der Waals gradient theory," Fluid Phase Equilibria **425**, 402–410 (2016).

[24]F. Llovell, A. Galindo, F. J. Blas, and G. Jackson, "Classical density functional theory for the prediction of the surface tension and interfacial properties of fluids mixtures of chain molecules based on the statistical associating fluid theory for potentials of variable range," The Journal of Chemical Physics **133**, 024704 (2010).

[25]C. I. Poser and I. C. Sanchez, "Interfacial tension theory of low and high molecular weight liquid mixtures," Macromolecules **14**, 361–370 (1981).

[26]O. G. Niño-Amézquita, S. Enders, P. T. Jaeger, and R. Eggers, "Interfacial properties of mixtures containing supercritical gases," The Journal of Supercritical Fluids **55**, 724 (2010).

[27]O. G. Niño-Amézquita, D. van Putten, and S. Enders, "Phase equilibrium and interfacial properties of water+CO_2 mixtures," Fluid Phase Equilibria **332**, 40 (2012).

[28]O. G. Niño-Amézquita, S. Enders, P. T. Jaeger, and R. Eggers, "Measurement and prediction of interfacial tension of binary mixtures," Industrial & Engineering Chemistry Research **49**, 592–601 (2010).

[29]O. G. Niño-Amézquita and S. Enders, "Phase equilibrium and interfacial properties of water+methane mixtures," Fluid Phase Equilibria **407**, 143–151 (2016).

[30]F. Biscay, A. Ghoufi, V. Lachet, and P. Malfreyt, "Monte Carlo simulations of the pressure dependence of the water-acid gas interfacial tensions," The Journal of Physical Chemistry B **113**, 14277–14290 (2009).

[31]M. Sahimi and B. N. Taylor, "Surface tension of binary liquid-vapor mixtures: A comparison of mean-field and scaling theories," The Journal of Chemical Physics **95**, 6749–6761 (1991).

[32]X. Liang, M. L. Michelsen, and G. M. Kontogeorgis, "Pitfalls of using the geometric-mean combining rule in the density gradient theory," Fluid Phase Equilibria **415**, 75–83 (2016).

[33]T. Lafitte, B. Mendiboure, M. M. Piñeiro, D. Bessières, and C. Miqueu, "Interfacial properties of water/CO_2: A comprehensive description through a gradient theory SAFT-VR Mie approach," The Journal of Physical Chemistry B **114**, 11110–11116 (2010).

[34]S. Stephan, K. Langenbach, and H. Hasse, "Enrichment of components at vapour-liquid interfaces: A study by molecular simulation and density gradient theory," Chemical Engineering Transactions **69**, 295–300 (2018).

[35]O. Lobanova, A. Mejía, G. Jackson, and E. A. Müller, "SAFT-i force field for the simulation of molecular fluids 6: Binary and ternary mixtures comprising water, carbon dioxide, and n-alkanes," The Journal of Chemical Thermodynamics **93**, 320–336 (2016).

[36]H. Lin, Y.-Y. Duan, and Q. Min, "Gradient theory modeling of surface tension for pure fluids and binary mixtures," Fluid Phase Equilibria **254**, 75 (2007).

[37]E. A. Müller and A. Mejía, "Interfacial properties of selected binary mixtures containing n-alkanes," Fluid Phase Equilibria **282**, 68–81 (2009).

[38]C. Cumicheo, M. Cartes, H. Segura, E. A. Müller, and A. Mejía, "High-pressure densities and interfacial tensions of binary systems containing carbon dioxide + n-alkanes: (n-dodecane, n-tridecane, n-tetradecane)," Fluid Phase Equilibria **380**, 82 (2014).

[39]L. M. Pereira, A. Chapoy, R. Burgass, and B. Tohidi, "Measurement and modelling of high pressure density and interfacial tension of (gas + n-alkane) binary mixtures," The Journal of Chemical Thermodynamics **97**, 55–69 (2016).

[40]D. Duque, J. C. Pamies, and L. F. Vega, "Interfacial properties of Lennard-Jones chains by direct simulation and density gradient theory," The Journal of Chemical Physics **121**, 11395–11401 (2004).

[41]J. M. Garrido, H. Quinteros-Lama, M. M. Piñeiro, A. Mejía, and H. Segura, "On the phase and interface behavior along the three-phase line of ternary Lennard-Jones mixtures: A collaborative approach based on square gradient theory and molecular dynamics simulations," The Journal of Chemical Physics **141**, 014503 (2014).

[42]E. Salomons and M. Mareschal, "Atomistic simulation of liquid-vapour coexistence: Binary mixtures," Journal of Physics: Condensed Matter **3**, 9215–9228 (1991).

[43]E. Salomons and M. Mareschal, "Surface tension, adsorption and surface entropy of liquid-vapour systems by atomistic simulation," Journal of Physics: Condensed Matter **3**, 3645–3661 (1991).

[44]A. H. Falls, L. E. Scriven, and H. T. Davis, "Adsorption, structure, and stress in binary interfaces," The Journal of Chemical Physics **78**, 7300–7317 (1983).

[45]X. Mu, F. Frank, F. O. Alpak, and W. G. Chapman, "Stabilized density gradient theory algorithm for modeling interfacial properties of pure and mixed systems," Fluid Phase Equilibria **435**, 118–130 (2017).

[46]F. J. Martinez-Ruiz, F. J. Blas, A. I. Moreno-Ventas Bravo, J. M. Miguez, and L. G. MacDowell, "Vapour-liquid interfacial properties of square-well chains from density functional theory and Monte Carlo simulation," Physical Chemistry Chemical Physics **19**, 12296–12309 (2017).

[47]X.-S. Li, J.-M. Liu, and D. Fu, "Investigation of interfacial tensions for carbon dioxide aqueous solutions by perturbed-chain statistical associating fluid theory combined with density-gradient theory," Industrial & Engineering Chemistry Research **47**, 8911–8917 (2008).

[48]P. M. Cornelisse, C. J. Peters, and J. de Swaan Arons, "Application of the Peng-Robinson equation of state to calculate interfacial tensions and profiles at vapour-liquid interfaces," Fluid Phase Equilibria **82**, 119–129 (1993).

[49]P. M. Cornelisse, C. J. Peters, and J. de Swaan Arons, "Interfacial phase transitions at solid-fluid and liquid-vapor interfaces," International Journal of Thermophysics **19**, 1501–1509 (1998).

[50]R. Nagl, P. Zimmermann, and T. Zeiner, "Interfacial mass transfer in water-toluene systems," Journal of Chemical & Engineering Data **65**, 328–336 (2020).

[51]J. M. Garrido, M. M. Piñeiro, A. Mejía, and F. J. Blas, "Understanding the interfacial behavior in isopycnic Lennard-Jones mixtures by computer simulations," Physical Chemistry Chemical Physics **18**, 1114–1124 (2016).

[52]A. Mejía and L. F. Vega, "Perfect wetting along a three-phase line: Theory and molecular dynamics simulations," The Journal of Chemical Physics **124**, 244505 (2006).

[53]P. Tarazona, M. M. Telo da Gama, and R. Evans, "Wetting transitions at fluid-fluid interfaces I. the order of the transition," Molecular Physics **49**, 283–300 (1983).

[54]P. Tarazona, M. M. Telo da Gama, and R. Evans, "Wetting transitions at fluid-fluid interfaces II. the thickness of the wetting layer," Molecular Physics **49**, 301–314 (1983).

[55]M. M. Telo da Gama and R. Evans, "The structure and surface tension of the liquid-vapour interface near the upper critical end point of a binary mixture of Lennard-Jones fluids II. the three phase region and the Cahn wetting transition," Molecular Physics **48**, 251–266 (1983).

[56]M. E. Costas, C. Varea, and A. Robledo, "Global phase diagram for the wetting transition at interfaces in fluid mixtures," Physical Review Letters **51**, 2394–2397 (1983).

[57]E. Díaz-Herrera, J. A. Moreno-Razo, and G. Ramírez-Santiago, "Wetting phenomenon in the liquid-vapor phase coexistence of a partially miscible Lennard-Jones binary mixture," Physical Review E **70**, 051601 (2004).

[58]E. Díaz-Herrera, G. Ramírez-Santiago, and J. A. Moreno-Razo, "Phase and interfacial behavior of partially miscible symmetric Lennard-Jones binary mixtures," The Journal of Chemical Physics **123**, 184507 (2005).

[59]P. Geysermans, N. Elyeznasni, and V. Russier, "Layered interfaces between immiscible liquids studied by density-functional theory and molecular-dynamics simulations," The Journal of Chemical Physics **123**, 204711 (2005).

[60]S. Toxvaerd and J. Stecki, "Density profiles at a planar liquid-liquid interface," The Journal of Chemical Physics **102**, 7163–7168 (1995).

[61]E. Díaz-Herrera, J. Alejandre, G. Ramírez-Santiago, and F. Forstmann, "Interfacial tension behavior of binary and ternary mixtures of partially miscible Lennard-Jones fluids: A molecular dynamics simulation," The Journal of Chemical Physics **110**, 8084–8089 (1999).

[62]I. Napari, A. Laaksonen, V. Talanquer, and D. W. Oxtoby, "A density functional study of liquid-liquid interfaces in partially miscible systems," The Journal of Chemical Physics **110**, 5906–5912 (1999).

[63]F. J. Martinez-Ruiz, A. I. Moreno-Ventas Bravo, and F. J. Blas, "Liquid-liquid interfacial properties of a symmetrical Lennard-Jones binary mixture," The Journal of Chemical Physics **143**, 104706 (2015).

[64]B. Smit, "Phase diagrams of Lennard-Jones fluids," The Journal of Chemical Physics **96**, 8639–8640 (1992).

[65]W. Shi and J. Johnson, "Histogram reweighting and finite-size scaling study of the Lennard-Jones fluids," Fluid Phase Equilibria **187**, 171–191 (2001).

[66]S. Stephan, M. Thol, J. Vrabec, and H. Hasse, "Thermophysical properties of the Lennard-Jones fluid: Database and data assessment," Journal of Chemical Information and Modeling **59**, 4248–4265 (2019).

[67]G. Rutkai, M. Thol, R. Span, and J. Vrabec, "How well does the Lennard-Jones potential represent the thermodynamic properties of noble gases?" Molecular Physics **115**, 1104–1121 (2017).

[68]S. Stephan, M. Dyga, H. Urbassek, and H. Hasse, "The influence of lubrication and the solid-fluid interaction on thermodynamic properties in a nanoscopic scratching process," Langmuir **35**, 16948–16960 (2019).

[69]M. Horsch, H. Hasse, A. K. Shchekin, A. Agarwal, S. Eckelsbach, J. Vrabec, E. A. Müller, and G. Jackson, "Excess equimolar radius of liquid drops," Physical Review E **85**, 031605 (2012).

[70]W. Eckhardt, A. Heinecke, R. Bader, M. Brehm, N. Hammer, H. Huber, H.-G. Kleinhenz, J. Vrabec, H. Hasse, M. Horsch, M. Bernreuther, C. W. Glass, C. Niethammer, A. Bode, and H.-J. Bungartz, "591 tflops multi-trillion particles simulation on SuperMUC," in *Supercomputing* (Springer, Berlin, Heidelberg, 2013) pp. 1–12.

[71]S. Stephan, M. P. Lautenschlaeger, I. A. Alhafez, M. T. Horsch, H. M. Urbassek, and H. Hasse, "Molecular dynamics simulation study of mechanical effects of lubrication on a nanoscale contact process," Tribology Letters **66**, 126 (2018).

[72]S. Stephan, M. Horsch, J. Vrabec, and H. Hasse, "MolMod - an open access database of force fields for molecular simulations of fluids," Molecular Simulation **45**, 806–814 (2019).

[73]A. Lotfi, J. Vrabec, and J. Fischer, "Vapour liquid equilibria of the Lennard-Jones fluid from the NpT plus test particle method," Molecular Physics **76**, 1319–1333 (1992).

[74]A. Trokhymchuk and J. Alejandre, "Computer simulations of liquid/vapor interface in Lennard-Jones fluids: Some questions and answers," The Journal of Chemical Physics **111**, 8510–8523 (1999).

[75]D. O. Dunikov, S. P. Malyshenko, and V. V. Zhakhovskii, "Corresponding states law and molecular dynamics simulations of the Lennard-Jones fluid," The Journal of Chemical Physics **115**, 6623–6631 (2001).

[76]S. Werth, S. V. Lishchuk, M. Horsch, and H. Hasse, "The influence of the liquid slab thickness on the planar vapor-liquid interfacial tension," Physica A **392**, 2359 (2013).

[77]M. Guo, D.-Y. Peng, and B. C.-Y.Lu, "On the long-range corrections to computer simulation results for the Lennard-Jones vapor-liquid interface," Fluid Phase Equilibria **130**, 19–30 (1997).

[78]M. J. P. Nijmeijer, A. F. Bakker, C. Bruin, and J. H. Sikkenk, "A molecular dynamics simulation of the Lennard-Jones liquid-vapor interface," The Journal of Chemical Physics **89**, 3789–3792 (1988).

[79]V. Baidakov, G. Chernykh, and S. Protsenko, "Effect of the cut-off radius of the intermolecular potential on phase equilibrium and surface tension in Lennard-Jones systems," Chemical Physics Letters **321**, 315–320 (2000).

[80]R. Evans, J. R. Henderson, D. C. Hoyle, A. O. Parry, and Z. A. Sabeur, "Asymptotic decay of liquid structure: Oscillatory liquid-vapour density profiles and the Fisher-Widom line," Molecular Physics **80**, 755–775 (1993).

[81]R. Evans, "Oscillatory behaviour of density profiles: Relevance for fluid interfacial phenomena," Berichte der Bunsengesellschaft für physikalische Chemie **98**, 345–352 (1994).

[82]S. Stephan and H. Hasse, "Influence of dispersive long-range interactions on properties of vapour-liquid interfaces of binary Lennard-Jones mixtures," Molecular Physics **187**, 1–14 (2019).

[83]H. A. Lorentz, "Über die Anwendung des Satzes vom Virial in der kinetischen Theorie der Gase," Annalen Der Physik **248**, 127–136 (1881).

[84]D. Berthelot, "Sur le mélange des gaz," Comptes rendus hebdomadaires des séances de l'Académie des Sciences **126**, 1703–1706 (1898).

[85]J. Vrabec, G. K. Kedia, G. Fuchs, and H. Hasse, "Comprehensive study of the vapour-liquid coexistence of the truncated and shifted Lennard-Jones fluid including planar and spherical interface properties," Molecular Physics **104**, 1509 (2006).

[86]J. A. van Meel, A. J. Page, R. P. Sear, and D. Frenkel, "Two-step vapor-crystal nucleation close below triple point," The Journal of Chemical Physics **129**, 204505 (2008).

[87]S. Toxvaerd, "Molecular dynamics simulation of prewetting," The Journal of Physical Chemistry C **111**, 15620–15624 (2007).

[88]J. A. Barker and D. Henderson, "Perturbation theory and equation of state for fluids. II. a successful theory of liquids," The Journal of Chemical Physics **47**, 4714 (1967).

[89]J. Gross and G. Sadowski, "Perturbed-Chain SAFT: An equation of state based on a perturbation theory for chain molecules," Industrial & Engineering Chemistry Research **40**, 1244 (2001).

[90]T. W. Leland, J. S. Rowlinson, G. A. Sather, and I. D. Watson, "Statistical thermodynamics of two-fluid models of mixtures," Transactions of the Faraday Society **65**, 2034–2043 (1969).

[91]J.-P. Hansen and I. McDonald, *Theory of Simple Liquids*, 4th ed. (Academic Press, 2013).

[92]J. Gross and G. Sadowski, "Application of perturbation theory to a hard-chain reference fluid: an equation of state for square-well chains," Fluid Phase Equilibria **168**, 183 (2000).

[93]S. K. Shibata and S. I. Sandler, "Critical evaluation of equation of state mixing rules for the prediction of high-pressure phase equilibria," Industrial & Engineering Chemistry Research **28**, 1893–1898 (1989).

[94]C. Miqueu, B. Mendiboure, A. Graciaa, and J. Lachaise, "Modelling of the surface tension of pure components with the gradient theory of fluid interfaces: a simple and accurate expression for the influence parameters," Fluid Phase Equilibria **207**, 225 (2003).

[95]P. M. Cornelisse, *The Square Gradient Theory Applied Simultaneous Modelling of Interfacial Tension and Phase Behaviour*, Ph.D. thesis, Technische Universiteit Delft (1997).

[96]J. W. Cahn and J. E. Hilliard, "Free energy of a nonuniform system. I. interfacial free energy," The Journal of Chemical Physics **28**, 258 (1958).

[97]J. W. Cahn, "Free energy of a nonuniform system. II. thermodynamic basis," The Journal of Chemical Physics **30**, 1121 (1959).

[98]C. Miqueu, B. Mendiboure, C. Graciaa, and J. Lachaise, "Modelling of the surface tension of binary and ternary mixtures with the gradient theory of fluid interfaces," Fluid Phase Equilibria **218**, 189–203 (2004).

[99]C. Miqueu, B. Mendiboure, A. Graciaa, and J. Lachaise, "Modeling of the surface tension of multicomponent mixtures with the gradient theory of fluid interfaces," Industrial & Engineering Chemistry Research **44**, 3321–3329 (2005).

[100]C. Bühl and S. Enders, "Prediction of interfacial properties of ternary, sulfur-containing mixtures," Journal of Chemical & Engineering Data **61**, 4261–4269 (2016).

[101]H. Kahl and S. Enders, "Interfacial properties of binary mixtures," Physical Chemistry Chemical Physics **4**, 931–936 (2002).

[102]B. S. Carey, L. E. Scriven, and H. T. Davis, "On gradient theories of fluid interfacial stress and structure," The Journal of Chemical Physics **69**, 5040–5049 (1978).

[103]S. Enders and H. Kahl, "Interfacial properties of water + alcohol mixtures," Fluid Phase Equilibria **263**, 160–167 (2008).

[104]J. S. Rowlinson and B. Widom, *Molecular Theory of Capillarity* (Dover Publications, New York, 1982).

[105]P. M. Cornelisse, C. J. Peters, and J. de Swaan Arons, "On the fundamentals of the gradient theory of van der Waals," The Journal of Chemical Physics **106**, 9820–9834 (1997).

[106]V. G. Baidakov, S. P. Protsenko, G. G. Chernykh, and G. S. Boltachev, "Statistical substantiation of the van der Waals theory of inhomogeneous fluids," Physical Review E **65**, 041601 (2002).

[107]X. Liang, M. L. Michelsen, and G. M. Kontogeorgis, "A density gradient theory based method for surface tension calculations," Fluid Phase Equilibria **428**, 153–163 (2016).

[108]C. Niethammer, S. Becker, M. Bernreuther, M. Buchholz, W. Eckhardt, A. Heinecke, S. Werth, H.-J. Bungartz, C. W. Glass, H. Hasse, J. Vrabec, and M. Horsch, "ls1 mardyn: The massively parallel molecular dynamics code for large systems," Journal of Chemical Theory Computation **10**, 4455 (2014).

[109]D. Fincham, "Leapfrog rotational algorithms," Molecular Simulation **8**, 165–178 (1992).

[110]J. Walton, D. J. Tildesley, J. S. Rowlinson, and J. R. Henderson, "The pressure tensor at the planar surface of a liquid," Molecular Physics **48**, 1357–1368 (1983).

[111]J. G. Kirkwood and F. P. Buff, "The statistical mechanical theory of surface tension," The Journal of Chemical Physics **17**, 338–343 (1949).

[112]J. W. Gibbs, *The Scientific Papers of J. W. Gibbs* (Dover Publications, 1961).

[113]M. M. Telo da Gama and R. Evans, "The structure and surface tension of the liquid-vapour interface near the upper critical end point of a binary mixture of Lennard-Jones fluids I. the two phase region," Molecular Physics **48**, 229–250 (1983).

[114]T. Wadewitz and J. Winkelmann, "Density functional theory: Structure and interfacial properties of binary mixtures," Berichte der Bunsengesellschaft für physikalische Chemie **100**, 1825–1832 (1996).

[115]M. Mecke, J. Winkelmann, and J. Fischer, "Molecular dynamics simulation of the liquid-vapor interface: Binary mixtures of Lennard-Jones fluids," The Journal of Chemical

Physics **110**, 1188–1194 (1999).

[116]A. Mejía, M. Cartes, H. Segura, and E. A. Müller, "Use of equations of state and coarse grained simulations to complement experiments: Describing the interfacial properties of carbon dioxide + decane and carbon dioxide + eicosane mixtures," Journal of Chemical & Engineering Data **59**, 2928 (2014).

[117]J. Algaba, M. Cartes, M. A., J. M. Miguez, and F. J. Blas, "Phase equilibria and interfacial properties of the tetrahydrofuran + methane binary mixture from experiment and computer simulation," The Journal of Physical Chemistry C **123**, 20960–20970 (2019).

[118]N. Choudhary, A. K. N. Nair, M. F. A. C. Ruslan, and S. Sun, "Bulk and interfacial properties of decane in the presence of carbon dioxide, methane, and their mixture," Scientific Reports **9**, 1–10 (2019).

[119]P. I. C. Teixeira, B. S. Almeida, M. M. Telo da Gama, J. A. Rueda, and R. G. Rubio, "Interfacial properties of mixtures of molecular fluids: comparison between theory and experiment; methyl iodide + carbon tetrachloride and acetonitrile + carbon tetrachloride," The Journal of Physical Chemistry **96**, 8488–8497 (1992).

[120]J. Aracil, G. Luengo, B. S. Almeida, M. M. Telo da Gama, R. G. Rubio, and M. Diaz Pena, "Surface properties of mixtures of molecular fluids: an experimental and theoretical study of carbon disulfide + dichloromethane and carbon disulfide + carbon tetrachloride," The Journal of Physical Chemistry **93**, 3210–3218 (1989).

[121]J. Lekner and J. R. Henderson, "Surface tension and energy of a classical liquid-vapour interface," Molecular Physics **34**, 333–359 (1977).

[122]U. K. Deiters and T. Kraska, *High-Pressure Fluid Phase Equilibria – Phenomenology and Computation* (Elsevier, Amsterdam, 2012).

[123]S. E. Quiñones-Cisneros, "Phase and critical behavior in type III phase diagrams," Fluid Phase Equilibria **134**, 103–112 (1997).

[124]U. K. Deiters and I. L. Pegg, "Systematic investigation of the phase behavior in binary fluid mixtures. I. calculations based on the Redlich-Kwong equation of state," The Journal of Chemical Physics **90**, 6632–6641 (1989).

[125]J. S. Rowlinson and F. L. Swinton, *Liquids and Liquid Mixtures* (Butterworth, London, 1982).

[126]O. L. Boshkova and U. K. Deiters, "Soft repulsion and the behavior of equations of state at high pressures," International Journal of Thermophysics **31**, 227–252 (2010).

[127]P.-G. De Gennes, F. Brochard-Wyart, and D. Quéré, *Capillarity and wetting phenomena: drops, bubbles, pearls, waves* (Springer Science & Business Media, New York, 2013).

[128]R. Evans, R. J. F. Leote de Carvalho, J. R. Henderson, and D. C. Hoyle, "Asymptotic decay of correlations in liquids and their mixtures," The Journal of Chemical Physics **100**, 591–603 (1994).

[129]A. O. Parry, C. Rascon, and R. Evans, "The local structure factor near an interface; beyond extended capillary-wave models," Journal of Physics: Condensed Matter **28**, 244013 (2016).

[130]M. Dijkstra and R. Evans, "A simulation study of the decay of the pair correlation function in simple fluids," The Journal of Chemical Physics **112**, 1449–1456 (2000).

[131]V. Bongiorno and H. T. Davis, "Modified van der Waals theory of fluid interfaces," Physical Review A **12**, 2213–2224 (1975).

[132]Cailletet, L. and Mathias, E., "Recherches sur les densités des gaz liquéfiés et de leurs vapeurs saturées," J. Phys. Theor. Appl. **5**, 549–564 (1886).

[133]M. R. Moldover and J. S. Gallagher, "Critical points of mixtures: An analogy with pure fluids," AIChE Journal **24**, 267–278 (1978).

[134]K. W. Won and J. M. Prausnitz, "Rectilinear diameter for saturated densities of binary mixtures," AIChE Journal **20**, 200–202 (1974).

[135]J. A. Zollweg and G. W. Mulholland, "On the law of the rectilinear diameter," The Journal of Chemical Physics **57**, 1021–1025 (1972).

Supplementary Material

Interfacial Properties of Binary Mixtures of Simple Fluids and their Relation to the Phase Diagram

Simon Stephan and Hans Hasse

Laboratory of Engineering Thermodynamics (LTD), TU Kaiserslautern, Kaiserslautern, Germany

Simon.Stephan@mv.uni-kl.de

Sunday 24th May, 2020

The Supplementary Material for the publication *Interfacial Properties of Binary Mixtures of Simple Fluids and their Relation to the Phase Diagram* contains the following points:

- the identification of the two investigated mixtures A and B in the map of the enrichment, see Ref.[2], as a function of the mixture parameters ξ and $\varepsilon_2/\varepsilon_1$ (cf. Fig. S1),
- the comparison of the difference of the component 2 bulk density in the VL_1E region $\Delta\rho_2 = \rho_2^{L1} - \rho_2^V$ (cf. Fig. S2) and a discussion of these results,
- two exemplary screenshots of the MD simulation of the mixtures A and B (cf. Fig. S3),
- the plots of the MD VL_1 density profiles from both investigated mixtures A and B at all five temperatures (cf. Fig. S4 and Fig. S5),
- the plots of the DGT VL_1 density profiles for mixture B at all temperatures (cf. Fig. S6),
- the p, T diagram of mixture A; including the state points whose density profiles intersect in two invariant points (see Appendix of the main body of the paper for a discussion),
- and the numeric values for the computed phase equilibria and interfacial properties for both MD and DGT (Table S1-S10 for the phase equilibria and Tables S11-S20 for the interfacial properties).

DISCUSSION OF THE RESULTS FOR THE DENSITY DIFFERENCE $\Delta\rho_2$

We have shown in an earlier work[2], that the difference of the component 2 bulk density in a VLE $\Delta\rho_2 = \rho_2^L - \rho_2^V$ is directly related to the arrangement of the surface excess at the vapour-liquid interface and thereby to the enrichment of the low-boiling component 2 at the interface. It was shown in Ref.[2] that for $\Delta\rho_2 = 0$, all adsorption at a vapour-liquid interface contributes to the enrichment[2]. Fig. S2 shows $\Delta\rho_2$ in the VL_1E region for the mixtures A and B. As for the phase diagrams shown in the main body of the paper, the agreement between the computer experiment and the theory is almost perfect for the mixture B. But significant deviations are observed in the case of the mixture A. The PeTS

EOS predicts $\Delta\rho_2 < 0$ for all temperatures in the entire composition range, whereas the molecular simulations predict small values $\Delta\rho_2 > 0$ for most state points. For mixture A, the function $\Delta\rho_2(x_2^{L1})$ is very different from that for mixture B. For mixtures B, $\Delta\rho_2(x_2^{L1})$ shows an almost linear increase. The slope of $\Delta\rho_2(x_2^{L1})$ decreases with increasing temperature, which is simply due to the decreasing total density difference between both phases with increasing temperature.

In contrast, in mixture A $\Delta\rho_2(x_2^{L1})$ has a highly non-linear behaviour. $\Delta\rho_2$ remains very close to zero at highly diluted mixtures ($x_2^{L1} \to 0$) and then decreases with further increasing concentration x_2^{L1}. This decay increases with decreasing temperature. Close to the VL_1L_2E line, $\Delta\rho_2$ drops almost vertically. The PeTS EOS predicts $\Delta\rho_2$ to exhibit a minimum at the three highest temperatures ($T = 0.77\,\varepsilon k_\mathrm{B}^{-1},\ 0.825\,\varepsilon k_\mathrm{B}^{-1},\ 0.88\,\varepsilon k_\mathrm{B}^{-1}$). By definition of the critical point, the densities and compositions of both phases must equalize upon approaching the very, i.e. $\Delta\rho_2 \to 0$ at the critical point, which is verified from the EOS results.

The poor agreement between MD and the EOS in the case of mixture A is likely due to the deviations observed in the bubble line in the phase diagrams at elevated pressures. Only the convex slope of $\Delta\rho_2(x_2^{L1})$ is captured consistently from both methods.

SIMULATION SCREENSHOTS

Fig. S3 shows screenshots from the molecular dynamics simulation from mixture A and B at $T = 0.66\,\varepsilon k_\mathrm{B}^{-1}$ during the production phase of the simulation. The liquid phase composition is similar in both simulations – just above 10% mole fraction of the low-boiling component. It is evident that the vapour-liquid interface in the case of the asymmetric mixture A shows a strong surface excess of the low-boiling component 2 at the interface which is not present in the mixture B.

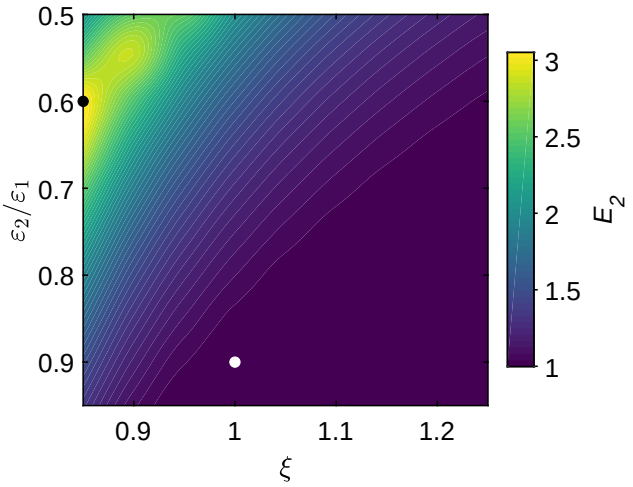

FIG. S1. Interfacial enrichment of the low-boiling component E_2 at vapour-liquid interfaces in binary LJTS mixtures (data from Ref.[2]) as a function of the binary interaction parameter ξ and the ratio of dispersion energies $\varepsilon_2/\varepsilon_1$ at constant temperature ($T = 0.77\,\varepsilon k_\mathrm{B}^{-1}$) and liquid phase composition ($x_2^{L1} = 0.05\,\mathrm{mol\,mol^{-1}}$). The black and the white dot indicates the mixture A and B, that were investigated in the present work.

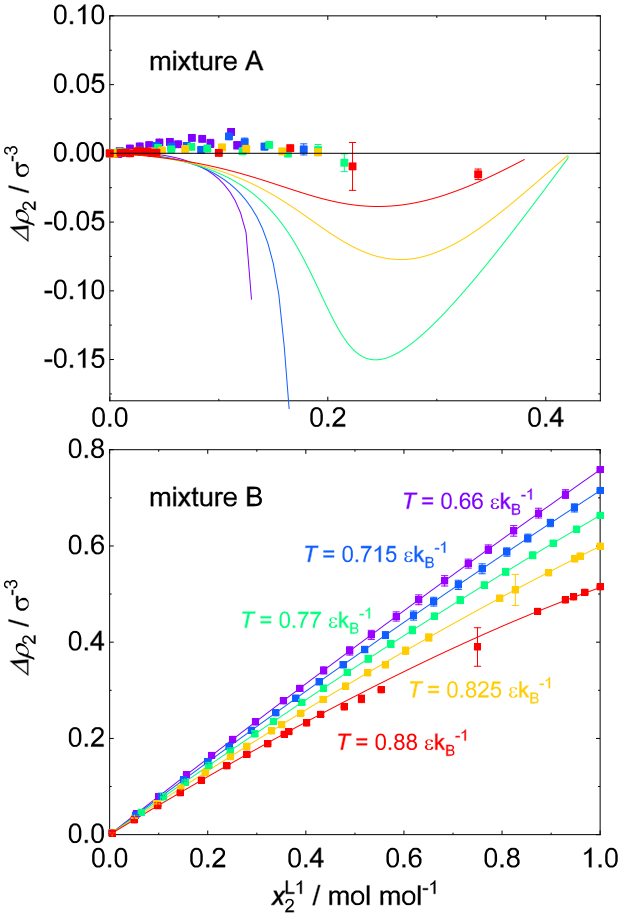

FIG. S2. Difference of the number density of the component 2 $\Delta\rho_2 = \rho_2^{L1} - \rho_2^V$ between both bulk phases. The temperatures in the top and bottom plot are colour-coded using the same scale. Symbols are MD results and lines are the PeTS EOS.

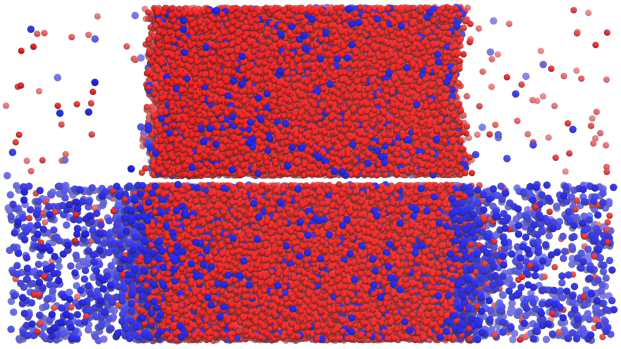

FIG. S3. Screenshots from the molecular simulations of mixture B (top) and mixture A (bottom) at $T = 0.66\,\varepsilon k_B^{-1}$. The liquid phase compositions are $x_2^{L1} = 0.11$ mol mol^{-1} (top) and $x_2^{L1} = 0.12$ mol mol^{-1} (bottom). The high-boiling component 1 is indicated red, the low-boiling component 2 blue.

FIG. S4. Density profiles of component 1 (dashed lines) and component 2 (full lines) for the mixture B obtained by MD. Results for all studied temperatures. The colour-code indicates the liquid phase composition.

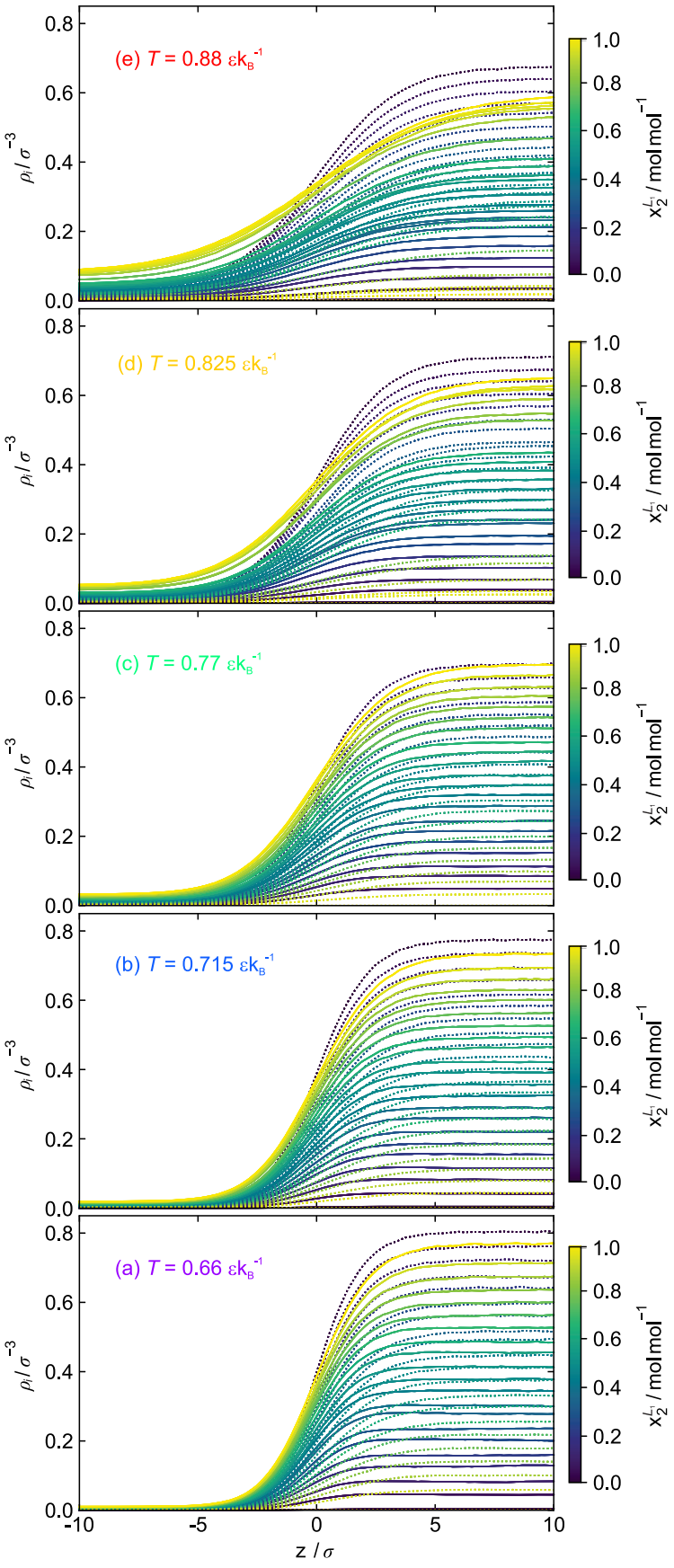

FIG. S5. VL_1 density profiles of component 1 (dashed lines) and component 2 (full lines) for the mixture A obtained by MD. Results for all studied temperatures. The colour-code indicates the liquid phase composition. Red squares indicate invariant intersection points of density profiles.

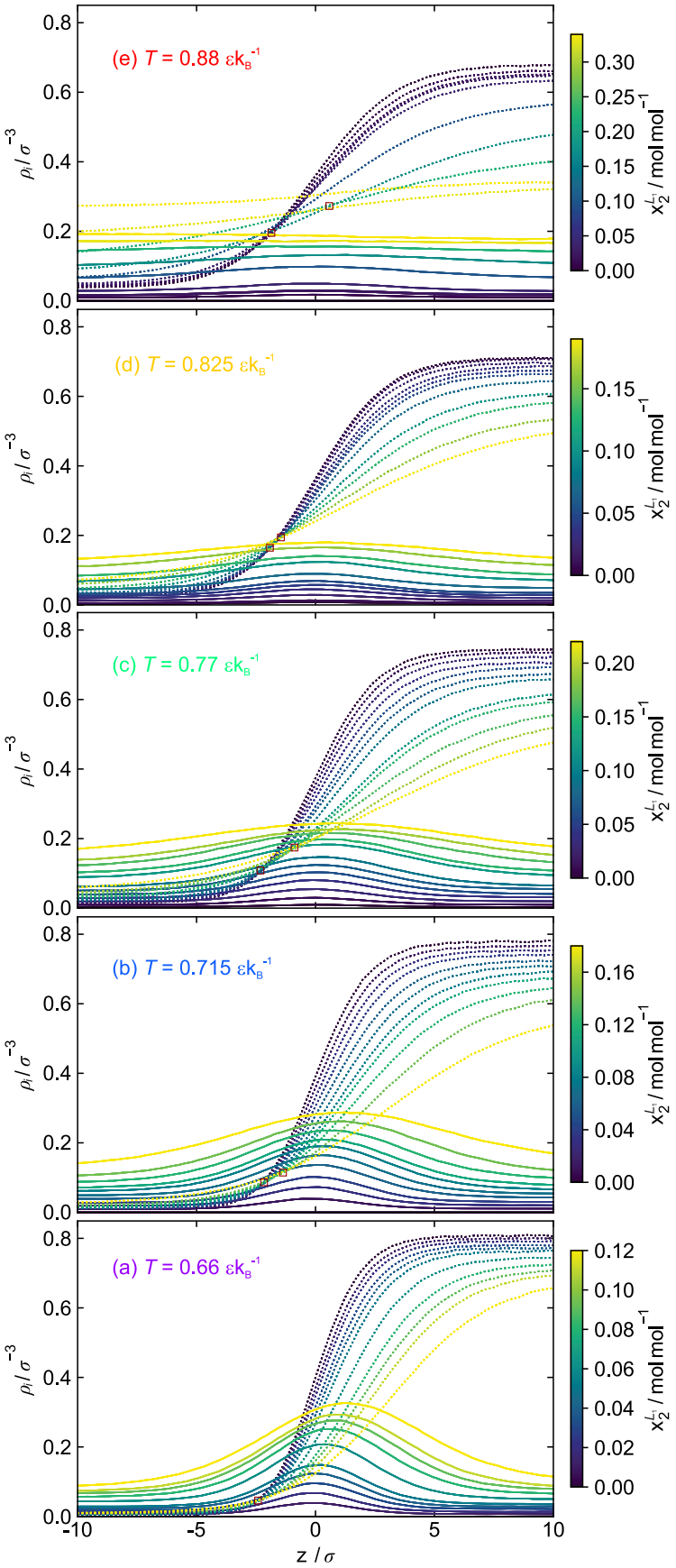

FIG. S6. Density profiles of component 1 (dashed lines) and component 2 (full lines) for the mixture B obtained by DGT. Results for all studied temperatures. The colour-code indicates the liquid phase composition.

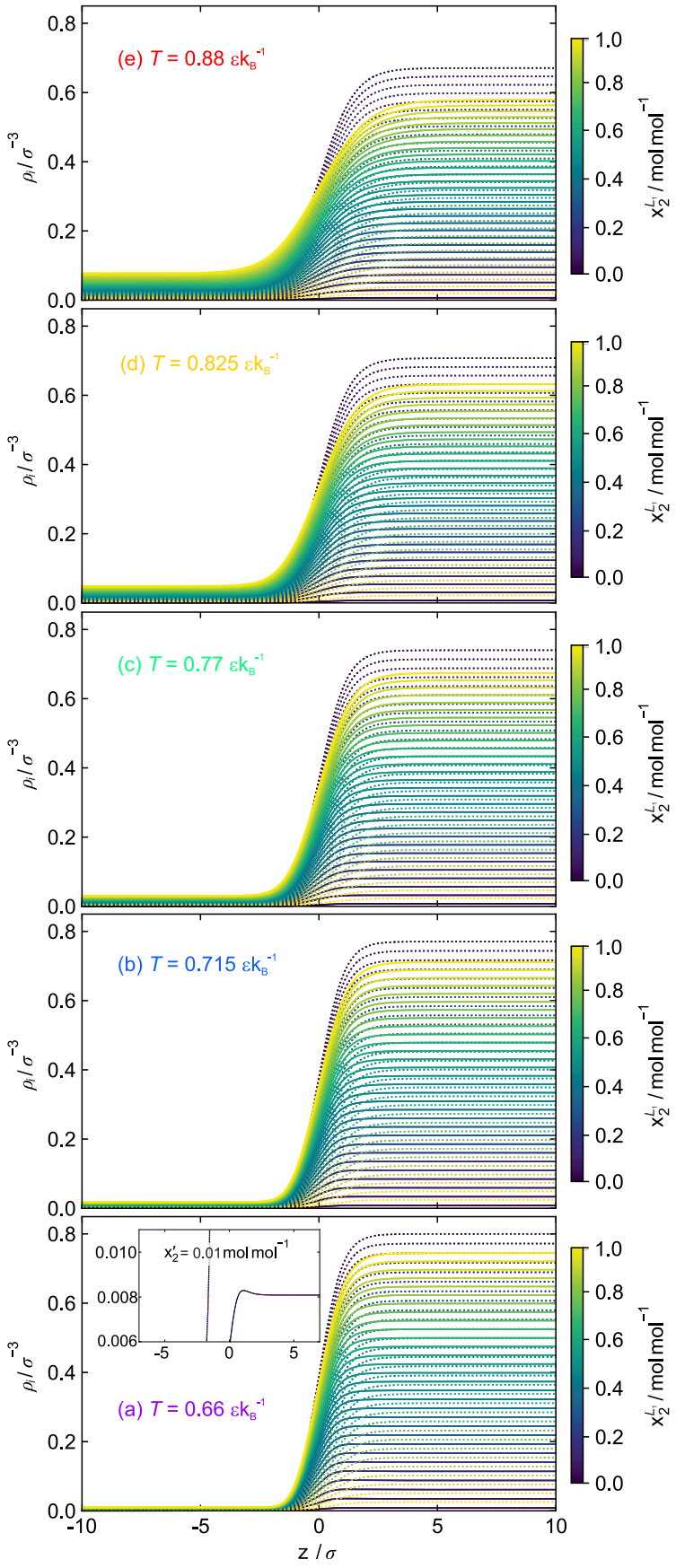

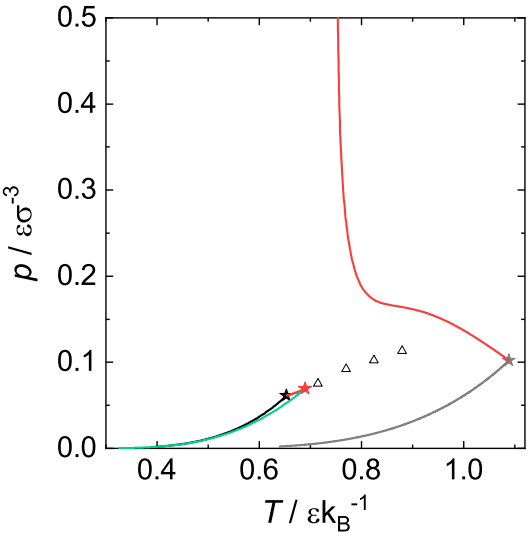

FIG. S7. Pressure-temperature diagram with characteristic curves for the mixture A – including the transition state points observed for the invariant intersection points. Pure component vapour pressure curves and critical points are the grey line and star (high-boiling component 1) and black line and star (low-boiling component 2). Red lines are critical lines of the mixture; the red star is the upper critical end point of mixture A (UCEP). The green line depicts the VL_1L_2E three-phase line. The open triangles indicate the state points p^* of which density profiles intersect multiple invariant points for a given temperature (see Appendix of the main body of the paper for a discussion).

TABLE S1. MD and EOS results for the bulk properties of the binary LJTS mixture B ($\varepsilon_2/\varepsilon_1 = 0.9$ and $\xi_{12} = 1$) at $T = 0.66\,\varepsilon k_\mathrm{B}^{-1}$. Both methods are calculated at the same liquid phase composition x_2^{L1}. The number in the parentheses indicates the statistical uncertainty in the last decimal digit.

x_2^{L1} / mol mol^{-1}	p / $\varepsilon\sigma^{-3}$		x_2^V / mol mol^{-1}		ρ^{L1} / σ^{-3}		ρ^V / σ^{-3}	
	MD	EOS	MD	EOS	MD	EOS	MD	EOS
0.000	0.0030(1)	0.0029	0.00	0.0000	0.808(4)	0.8084	0.0047(3)	0.0046
0.005(1)	0.0030(1)	0.0029	0.01(1)	0.0109	0.808(4)	0.8082	0.0047(3)	0.0046
0.055(1)	0.0030(1)	0.0031	0.11(1)	0.1110	0.806(8)	0.8065	0.0048(4)	0.0049
0.100(1)	0.0033(1)	0.0033	0.20(2)	0.1928	0.804(9)	0.8049	0.0052(5)	0.0052
0.157(2)	0.0034(2)	0.0035	0.27(2)	0.2846	0.80(1)	0.8028	0.0054(5)	0.0055
0.208(1)	0.0036(1)	0.0036	0.35(2)	0.3593	0.80(2)	0.8009	0.0058(5)	0.0058
0.251(1)	0.0038(1)	0.0038	0.42(2)	0.4160	0.80(1)	0.7993	0.0061(5)	0.0061
0.297(1)	0.0039(2)	0.0039	0.47(2)	0.4727	0.80(1)	0.7976	0.0063(5)	0.0063
0.354(1)	0.0042(2)	0.0041	0.53(2)	0.5364	0.80(1)	0.7954	0.0067(6)	0.0067
0.388(2)	0.0043(1)	0.0043	0.58(2)	0.5713	0.79(1)	0.7941	0.0070(6)	0.0068
0.437(2)	0.0045(1)	0.0044	0.62(2)	0.6187	0.79(1)	0.7922	0.0072(6)	0.0071
0.490(1)	0.0047(1)	0.0046	0.66(2)	0.6667	0.79(2)	0.7902	0.0075(6)	0.0074
0.533(1)	0.0047(2)	0.0048	0.69(3)	0.7036	0.79(2)	0.7884	0.0076(6)	0.0077
0.584(1)	0.0050(1)	0.0049	0.75(2)	0.7441	0.79(2)	0.7864	0.0081(6)	0.0080
0.630(2)	0.0051(1)	0.0051	0.77(1)	0.7784	0.78(1)	0.7845	0.0083(6)	0.0083
0.683(1)	0.0053(2)	0.0053	0.82(1)	0.8155	0.78(1)	0.7824	0.0086(6)	0.0086
0.731(1)	0.0055(2)	0.0054	0.84(1)	0.8474	0.78(1)	0.7804	0.0090(6)	0.0089
0.772(1)	0.0056(2)	0.0056	0.88(1)	0.8732	0.78(1)	0.7787	0.0091(6)	0.0091
0.824(2)	0.0059(2)	0.0058	0.90(1)	0.9046	0.78(1)	0.7765	0.0096(6)	0.0094
0.874(1)	0.0059(1)	0.0059	0.94(1)	0.9336	0.77(1)	0.7743	0.0097(6)	0.0097
0.929(1)	0.0062(2)	0.0061	0.96(1)	0.9635	0.77(1)	0.7719	0.0102(8)	0.0101
1.00	0.0064(2)	0.0063	1.00	1.0000	0.769(3)	0.7692	0.0106(5)	0.0104

TABLE S2. MD and EOS results for the bulk properties of the binary LJTS mixture B ($\varepsilon_2/\varepsilon_1 = 0.9$ and $\xi_{12} = 1$) at $T = 0.715\,\varepsilon k_\mathrm{B}^{-1}$. Both methods are calculated at the same liquid phase composition x_2^{L1}. The number in the parentheses indicates the statistical uncertainty in the last decimal digit.

x_2^{L1} / mol mol^{-1}	p / $\varepsilon\sigma^{-3}$		x_2^{V} / mol mol^{-1}		ρ^{L1} / σ^{-3}		ρ^{V} / σ^{-3}	
	MD	EOS	MD	EOS	MD	EOS	MD	EOS
0.000	0.0058(3)	0.0058	0.00	0.0000	0.779(3)	0.7789	0.0087(4)	0.0087
0.0049(2)	0.0057(2)	0.0058	0.011(3)	0.0097	0.779(4)	0.7787	0.0086(5)	0.0087
0.053(1)	0.0061(2)	0.0061	0.10(1)	0.0988	0.777(7)	0.7768	0.0091(6)	0.0092
0.105(2)	0.0064(2)	0.0064	0.19(1)	0.1872	0.775(8)	0.7747	0.0097(6)	0.0097
0.151(1)	0.0067(2)	0.0067	0.26(1)	0.2567	0.773(10)	0.7728	0.0101(7)	0.0101
0.200(1)	0.0070(2)	0.0070	0.34(2)	0.3273	0.771(12)	0.7708	0.0107(7)	0.0106
0.243(1)	0.0073(2)	0.0072	0.39(1)	0.3836	0.769(11)	0.7690	0.0112(7)	0.0110
0.289(2)	0.0075(2)	0.0075	0.44(2)	0.4392	0.767(12)	0.7671	0.0115(7)	0.0115
0.339(1)	0.0079(2)	0.0078	0.49(2)	0.4957	0.765(12)	0.7649	0.0121(7)	0.0120
0.380(2)	0.0081(2)	0.0081	0.53(2)	0.5394	0.764(14)	0.7632	0.0125(8)	0.0124
0.427(2)	0.0083(2)	0.0083	0.58(2)	0.5866	0.761(12)	0.7611	0.0128(8)	0.0128
0.476(1)	0.0087(2)	0.0086	0.62(1)	0.6326	0.759(12)	0.7589	0.0133(8)	0.0133
0.520(1)	0.0088(2)	0.0089	0.68(1)	0.6718	0.757(12)	0.7570	0.0136(8)	0.0138
0.562(1)	0.0092(2)	0.0092	0.71(2)	0.7075	0.755(12)	0.7550	0.0143(8)	0.0142
0.619(2)	0.0095(2)	0.0095	0.75(1)	0.7530	0.753(14)	0.7524	0.0147(8)	0.0148
0.661(3)	0.0099(3)	0.0097	0.78(2)	0.7843	0.751(12)	0.7505	0.0154(8)	0.0152
0.711(1)	0.0101(2)	0.0100	0.82(1)	0.8204	0.749(13)	0.7481	0.0159(8)	0.0157
0.759(2)	0.0106(3)	0.0103	0.85(1)	0.8538	0.746(13)	0.7458	0.0166(8)	0.0162
0.810(1)	0.0109(2)	0.0106	0.88(1)	0.8870	0.744(10)	0.7433	0.0171(8)	0.0168
0.853(1)	0.0110(2)	0.0109	0.91(1)	0.9141	0.741(10)	0.7412	0.0174(12)	0.0172
0.899(1)	0.0112(3)	0.0112	0.94(1)	0.9418	0.739(8)	0.7389	0.0178(8)	0.0177
0.948(1)	0.0118(2)	0.0115	0.97(1)	0.9705	0.736(11)	0.7364	0.019(3)	0.0182
1.000	0.0119(2)	0.0117	1.00	1.0000	0.734(3)	0.7342	0.0190(7)	0.0187

TABLE S3. MD and EOS results for the bulk properties of the binary LJTS mixture B ($\varepsilon_2/\varepsilon_1 = 0.9$ and $\xi_{12} = 1$) at $T = 0.77\,\varepsilon k_\mathrm{B}^{-1}$. Both methods are calculated at the same liquid phase composition x_2^{L1}. The number in the parentheses indicates the statistical uncertainty in the last decimal digit.

x_2^{L1} / mol mol^{-1}	p / $\varepsilon\sigma^{-3}$		x_2^{V} / mol mol^{-1}		ρ^{L1} / σ^{-3}		ρ^{V} / σ^{-3}	
	MD	EOS	MD	EOS	MD	EOS	MD	EOS
0.000	0.0105(3)	0.0104	0.00	0.0000	0.749(3)	0.7480	0.0152(6)	0.0150
0.064(2)	0.0110(3)	0.0110	0.11(1)	0.1102	0.746(7)	0.7451	0.0160(7)	0.0160
0.110(1)	0.0116(1)	0.0114	0.19(2)	0.1812	0.744(9)	0.7430	0.0169(8)	0.0167
0.154(2)	0.0119(3)	0.0118	0.26(1)	0.2450	0.741(9)	0.7410	0.0175(10)	0.0174
0.202(2)	0.0124(2)	0.0123	0.31(1)	0.3111	0.739(9)	0.7387	0.0183(9)	0.0181
0.246(2)	0.0129(4)	0.0127	0.37(2)	0.3662	0.74(1)	0.7366	0.0191(9)	0.0188
0.296(2)	0.0134(4)	0.0132	0.42(1)	0.4263	0.73(1)	0.7342	0.0199(9)	0.0196
0.334(1)	0.0137(3)	0.0136	0.47(2)	0.4691	0.73(1)	0.7323	0.020(1)	0.0202
0.392(2)	0.0143(3)	0.0141	0.53(1)	0.5303	0.73(1)	0.7294	0.021(1)	0.0211
0.436(1)	0.0146(3)	0.0145	0.57(1)	0.5742	0.73(1)	0.7271	0.022(1)	0.0218
0.484(2)	0.0150(4)	0.0150	0.62(1)	0.6199	0.72(1)	0.7247	0.023(1)	0.0226
0.527(2)	0.0156(4)	0.0154	0.65(1)	0.6584	0.723(13)	0.7224	0.024(1)	0.0233
0.574(2)	0.0158(3)	0.0159	0.69(1)	0.6985	0.720(12)	0.7199	0.024(1)	0.0241
0.617(2)	0.0163(4)	0.0163	0.73(1)	0.7345	0.718(12)	0.7176	0.025(1)	0.0248
0.662(1)	0.0168(2)	0.0167	0.77(1)	0.7700	0.715(10)	0.7151	0.026(1)	0.0256
0.714(2)	0.0173(3)	0.0172	0.81(1)	0.8097	0.713(10)	0.7122	0.027(1)	0.0265
0.764(1)	0.0179(3)	0.0177	0.85(1)	0.8457	0.710(9)	0.7093	0.028(1)	0.0273
0.808(2)	0.0183(4)	0.0181	0.88(1)	0.8761	0.707(8)	0.7068	0.028(1)	0.0281
0.863(1)	0.0188(3)	0.0187	0.91(1)	0.9133	0.704(9)	0.7035	0.029(1)	0.0291
0.904(1)	0.0192(2)	0.0191	0.94(1)	0.9404	0.701(7)	0.7010	0.030(1)	0.0298
0.952(1)	0.0197(3)	0.0196	0.973(4)	0.9706	0.698(6)	0.6981	0.031(1)	0.0307
1.00	0.0203(3)	0.0199	1.00	1.0000	0.695(3)	0.6957	0.0320(9)	0.0314

TABLE S4. MD and EOS results for the bulk properties of the binary LJTS mixture B ($\varepsilon_2/\varepsilon_1 = 0.9$ and $\xi_{12} = 1$) at $T = 0.825\,\varepsilon k_\mathrm{B}^{-1}$. Both methods are calculated at the same liquid phase composition x_2^{L1}. The number in the parentheses indicates the statistical uncertainty in the last decimal digit.

x_2^{L1} / mol mol^{-1}	p / $\varepsilon\sigma^{-3}$		x_2^{V} / mol mol^{-1}		ρ^{L1} / σ^{-3}		ρ^{V} / σ^{-3}	
	MD	EOS	MD	EOS	MD	EOS	MD	EOS
0.000	0.0175(3)	0.0173	0.000	0.0000	0.716(3)	0.7149	0.025(1)	0.0246
0.0055(3)	0.0176(3)	0.0173	0.010(3)	0.0092	0.715(4)	0.7146	0.025(1)	0.0247
0.051(1)	0.0181(4)	0.0180	0.082(8)	0.0820	0.713(6)	0.7122	0.026(1)	0.0257
0.096(1)	0.0188(3)	0.0186	0.151(7)	0.1500	0.710(7)	0.7098	0.027(1)	0.0268
0.145(1)	0.0195(2)	0.0193	0.213(9)	0.2189	0.707(9)	0.7072	0.028(1)	0.0279
0.195(2)	0.0201(3)	0.0200	0.29(1)	0.2844	0.705(9)	0.7044	0.029(1)	0.0291
0.246(1)	0.0210(2)	0.0207	0.35(1)	0.3485	0.702(9)	0.7015	0.031(1)	0.0303
0.280(1)	0.0214(4)	0.0212	0.38(1)	0.3878	0.700(10)	0.6996	0.031(1)	0.0311
0.330(1)	0.0222(4)	0.0219	0.44(1)	0.4445	0.697(9)	0.6966	0.033(1)	0.0323
0.351(2)	0.0224(3)	0.0222	0.47(1)	0.4668	0.696(10)	0.6954	0.033(1)	0.0328
0.390(2)	0.0231(3)	0.0228	0.51(1)	0.5078	0.69(1)	0.6931	0.035(3)	0.0338
0.435(2)	0.0236(3)	0.0234	0.55(1)	0.5531	0.69(1)	0.6903	0.035(1)	0.0350
0.481(2)	0.0243(3)	0.0241	0.60(1)	0.5974	0.69(1)	0.6875	0.036(2)	0.0361
0.526(2)	0.0248(3)	0.0247	0.63(1)	0.6389	0.68(1)	0.6846	0.037(1)	0.0373
0.562(4)	0.0253(7)	0.0253	0.66(1)	0.6709	0.68(1)	0.6823	0.043(2)	0.0383
0.604(2)	0.0259(3)	0.0259	0.71(1)	0.7065	0.68(1)	0.6796	0.040(2)	0.0394
0.651(1)	0.0267(4)	0.0266	0.74(1)	0.7458	0.68(1)	0.6764	0.041(2)	0.0407
0.795(2)	0.0289(3)	0.0287	0.86(1)	0.8577	0.667(7)	0.6663	0.045(1)	0.0448
0.83(4)	0.0294(5)	0.0292	0.88(3)	0.8808	0.664(8)	0.6640	0.046(2)	0.0457
0.895(1)	0.0304(4)	0.0302	0.928(4)	0.9289	0.658(8)	0.6589	0.049(3)	0.0478
0.948(1)	0.0313(4)	0.0310	0.965(3)	0.9653	0.655(5)	0.6547	0.050(1)	0.0494
0.959(1)	0.0313(4)	0.0312	0.973(3)	0.9729	0.654(5)	0.6538	0.050(1)	0.0498
1.000	0.0320(4)	0.0317	1.0000	0.9934	0.651(3)	0.6514	0.052(1)	0.0508

TABLE S5. MD and EOS results for the bulk properties of the binary LJTS mixture B ($\varepsilon_2/\varepsilon_1 = 0.9$ and $\xi_{12} = 1$) at $T = 0.88\,\varepsilon k_\mathrm{B}^{-1}$. Both methods are calculated at the same liquid phase composition x_2^{L1}. The number in the parentheses indicates the statistical uncertainty in the last decimal digit.

x_2^{L1} / mol mol^{-1}	p / $\varepsilon\sigma^{-3}$		x_2^{V} / mol mol^{-1}		ρ^{L1} / σ^{-3}		ρ^{V} / σ^{-3}	
	MD	EOS	MD	EOS	MD	EOS	MD	EOS
0.000	0.0271(4)	0.0270	0.000	0.0000	0.679(3)	0.6782	0.039(1)	0.0384
0.0051(3)	0.0272(3)	0.0271	0.007(2)	0.0080	0.679(3)	0.6778	0.039(1)	0.0386
0.050(1)	0.0281(3)	0.0280	0.075(4)	0.0752	0.675(6)	0.6750	0.041(2)	0.0401
0.098(1)	0.0291(3)	0.0289	0.14(1)	0.1434	0.672(6)	0.6719	0.042(1)	0.0418
0.143(1)	0.0299(3)	0.0298	0.21(1)	0.2038	0.669(7)	0.6689	0.044(2)	0.0434
0.187(1)	0.0309(3)	0.0307	0.25(1)	0.2601	0.666(8)	0.6659	0.045(1)	0.0449
0.240(2)	0.0321(3)	0.0318	0.32(1)	0.3235	0.663(8)	0.6623	0.047(1)	0.0468
0.280(2)	0.0328(3)	0.0326	0.37(1)	0.3697	0.660(9)	0.6595	0.049(2)	0.0483
0.322(2)	0.0335(4)	0.0334	0.42(1)	0.4161	0.657(16)	0.6565	0.050(11)	0.0499
0.365(2)	0.0347(3)	0.0343	0.47(1)	0.4626	0.653(8)	0.6540	0.052(2)	0.0512
0.356(2)	0.0344(5)	0.0341	0.46(1)	0.4525	0.653(11)	0.6532	0.051(4)	0.0516
0.401(3)	0.0354(4)	0.0350	0.50(1)	0.4997	0.61(2)	0.6505	0.053(9)	0.0530
0.431(2)	0.0357(5)	0.0356	0.53(1)	0.5292	0.65(1)	0.6483	0.054(3)	0.0542
0.478(4)	0.0364(7)	0.0366	0.56(1)	0.5750	0.645(4)	0.6446	0.057(3)	0.0561
0.514(3)	0.0371(10)	0.0374	0.60(1)	0.6092	0.643(4)	0.6416	0.058(3)	0.0576
0.552(4)	0.0383(9)	0.0381	0.63(1)	0.6435	0.639(4)	0.6386	0.059(4)	0.0592
0.576(6)	0.0386(15)	0.0387	0.66(2)	0.6654	0.637(14)	0.6365	0.060(12)	0.0602
0.622(5)	0.0397(15)	0.0396	0.71(2)	0.7049	0.633(15)	0.6326	0.062(13)	0.0622
0.651(5)	0.0407(13)	0.0402	0.74(1)	0.7303	0.631(13)	0.6300	0.065(11)	0.0636
0.873(1)	0.0453(6)	0.0450	0.909(4)	0.9063	0.61(1)	0.6201	0.076(2)	0.0687
0.76(9)	0.0428(4)	0.0426	0.819(10)	0.8187	0.621(15)	0.6090	0.070(15)	0.0744
0.929(1)	0.0464(5)	0.0463	0.949(4)	0.9483	0.605(5)	0.6030	0.078(2)	0.0775
0.946(1)	0.0469(5)	0.0467	0.959(3)	0.9606	0.603(4)	0.6012	0.079(2)	0.0784
0.969(1)	0.0473(4)	0.0472	0.977(2)	0.9777	0.600(4)	0.5986	0.080(2)	0.0798
1.000	0.0478(7)	0.0477	1.000	1.0000	0.597(3)	0.5963	0.081(2)	0.0810

TABLE S6. MD and EOS results for the bulk properties of the binary LJTS mixture A ($\varepsilon_2/\varepsilon_1 = 0.6$ and $\xi_{12} = 0.85$) at $T = 0.66\,\varepsilon k_\mathrm{B}^{-1}$. Both methods are calculated at the same liquid phase composition x_2^{L1}. The number in the parentheses indicates the statistical uncertainty in the last decimal digit.

x_2^{L1} / mol mol^{-1}	p / $\varepsilon\sigma^{-3}$		x_2^{V} / mol mol^{-1}		ρ^{L1} / σ^{-3}		ρ^{V} / σ^{-3}	
	MD	EOS	MD	EOS	MD	EOS	MD	EOS
0.000	0.0030(1)	0.0029	0.000	0.000	0.808(4)	0.8084	0.0047(3)	0.0046
0.009(1)	0.0066(2)	0.0074	0.534(16)	0.5874	0.806(5)	0.8070	0.0106(8)	0.0108
0.0077(5)	0.0072(2)	0.0067	0.580(18)	0.5503	0.807(5)	0.8067	0.0115(8)	0.0119
0.018(1)	0.0101(2)	0.0119	0.690(15)	0.7337	0.804(6)	0.8049	0.0164(9)	0.0197
0.027(1)	0.0135(3)	0.0161	0.759(9)	0.7953	0.803(7)	0.8032	0.022(1)	0.0274
0.036(1)	0.0168(2)	0.0201	0.803(8)	0.8294	0.801(8)	0.8015	0.029(1)	0.0351
0.045(1)	0.0199(3)	0.0242	0.824(9)	0.8527	0.799(9)	0.7997	0.035(1)	0.0438
0.055(2)	0.0235(3)	0.0283	0.848(8)	0.8687	0.797(11)	0.7978	0.042(1)	0.0532
0.063(3)	0.0271(5)	0.0315	0.863(8)	0.8777	0.796(11)	0.7963	0.050(2)	0.0609
0.075(2)	0.0295(4)	0.0366	0.872(6)	0.8886	0.793(12)	0.7938	0.056(2)	0.0750
0.085(2)	0.0329(4)	0.0403	0.880(8)	0.8941	0.791(14)	0.7919	0.064(2)	0.0865
0.092(5)	0.0364(6)	0.0432	0.891(6)	0.8974	0.789(13)	0.7903	0.074(2)	0.0967
0.111(2)	0.0387(3)	0.0504	0.889(9)	0.9019	0.785(20)	0.7864	0.081(2)	0.1295
0.117(4)	0.0430(4)	0.0525	0.901(5)	0.9020	0.784(18)	0.7853	0.095(3)	0.1429

TABLE S7. MD and EOS results for the bulk properties of the binary LJTS mixture A ($\varepsilon_2/\varepsilon_1 = 0.6$ and $\xi_{12} = 0.85$) at $T = 0.715\,\varepsilon k_\mathrm{B}^{-1}$. Both methods are calculated at the same liquid phase composition x_2^{L1}. The number in the parentheses indicates the statistical uncertainty in the last decimal digit.

x_2^{L1} / mol mol^{-1}	p / $\varepsilon\sigma^{-3}$		x_2^{V} / mol mol^{-1}		ρ^{L1} / σ^{-3}		ρ^{V} / σ^{-3}	
	MD	EOS	MD	EOS	MD	EOS	MD	EOS
0.000	0.0058(3)	0.0058	0.000	0.000	0.779(3)	0.7789	0.0087(4)	0.0087
0.0096(4)	0.0106(3)	0.0110	0.426(10)	0.4476	0.777(5)	0.7769	0.0160(8)	0.0167
0.0129(9)	0.0125(3)	0.0128	0.496(8)	0.5176	0.777(5)	0.7762	0.019(1)	0.0196
0.027(1)	0.0184(4)	0.0203	0.651(10)	0.6775	0.773(6)	0.7732	0.029(1)	0.0322
0.043(2)	0.0238(4)	0.0278	0.715(11)	0.7498	0.770(8)	0.7700	0.038(1)	0.0462
0.056(2)	0.0300(4)	0.0344	0.764(8)	0.7862	0.767(9)	0.7671	0.050(2)	0.0598
0.071(1)	0.0355(4)	0.0409	0.786(8)	0.8092	0.76(1)	0.7640	0.062(2)	0.0746
0.084(3)	0.0415(5)	0.0467	0.809(5)	0.8233	0.76(1)	0.7611	0.076(2)	0.0897
0.109(2)	0.0454(6)	0.0575	0.820(8)	0.8384	0.75(1)	0.7554	0.085(2)	0.1244
0.124(6)	0.0512(8)	0.0635	0.831(8)	0.8416	0.75(2)	0.7521	0.102(3)	0.1497
0.142(5)	0.0568(9)	0.0712	0.836(5)	0.8396	0.74(2)	0.7480	0.121(3)	0.1959
0.178(8)	0.0639(9)	0.1066	0.840(6)	0.7357	0.73(3)	0.7429	0.152(7)	0.5084

TABLE S8. MD and EOS results for the bulk properties of the binary LJTS mixture A ($\varepsilon_2/\varepsilon_1 = 0.6$ and $\xi_{12} = 0.85$) at $T = 0.77\,\varepsilon k_\mathrm{B}^{-1}$. Both methods are calculated at the same liquid phase composition x_2^{L1}. The number in the parentheses indicates the statistical uncertainty in the last decimal digit.

x_2^{L1} / mol mol^{-1}	p / $\varepsilon\sigma^{-3}$		x_2^{V} / mol mol^{-1}		ρ^{L1} / σ^{-3}		ρ^{V} / σ^{-3}	
	MD	EOS	MD	EOS	MD	EOS	MD	EOS
0.000	0.0105(3)	0.0104	0.000	0.000	0.749(3)	0.7480	0.0152(6)	0.0150
0.0045(3)	0.0128(3)	0.0130	0.164(6)	0.1821	0.748(4)	0.7470	0.0185(8)	0.0189
0.0097(6)	0.0151(3)	0.0160	0.272(13)	0.3193	0.746(5)	0.7458	0.022(1)	0.0234
0.0136(9)	0.0178(3)	0.0182	0.371(12)	0.3914	0.745(5)	0.7449	0.026(1)	0.0268
0.0271(9)	0.0242(3)	0.0257	0.517(8)	0.5446	0.742(6)	0.7418	0.036(1)	0.0389
0.044(1)	0.0308(3)	0.0349	0.607(9)	0.6416	0.737(8)	0.7378	0.047(2)	0.0551
0.056(1)	0.0371(4)	0.0411	0.652(9)	0.6810	0.734(8)	0.7349	0.059(2)	0.0670
0.075(2)	0.0435(7)	0.0501	0.696(9)	0.7194	0.729(9)	0.7305	0.071(2)	0.0863
0.089(1)	0.0499(4)	0.0570	0.717(5)	0.7387	0.73(1)	0.7268	0.085(2)	0.1031
0.122(3)	0.0617(6)	0.0715	0.747(6)	0.7607	0.72(1)	0.7186	0.115(3)	0.1464
0.146(3)	0.0666(6)	0.0820	0.753(11)	0.7641	0.71(1)	0.7123	0.129(3)	0.1889
0.163(4)	0.0731(6)	0.0894	0.767(7)	0.7598	0.70(2)	0.7078	0.150(4)	0.2276
0.191(8)	0.078(1)	0.1025	0.763(9)	0.7372	0.69(2)	0.7008	0.170(5)	0.3148
0.215(14)	0.084(1)	0.1165	0.757(15)	0.6988	0.68(3)	0.6953	0.204(8)	0.4069

TABLE S9. MD and EOS results for the bulk properties of the binary LJTS mixture A ($\varepsilon_2/\varepsilon_1 = 0.6$ and $\xi_{12} = 0.85$) at $T = 0.825\,\varepsilon k_\mathrm{B}^{-1}$. Both methods are calculated at the same liquid phase composition x_2^{L1}. The number in the parentheses indicates the statistical uncertainty in the last decimal digit.

x_2^{L1} / mol mol^{-1}	p / $\varepsilon\sigma^{-3}$		x_2^{V} / mol mol^{-1}		ρ^{L1} / σ^{-3}		ρ^{V} / σ^{-3}	
	MD	EOS	MD	EOS	MD	EOS	MD	EOS
0.000	0.0175(3)	0.0173	0.000	0.000	0.716(3)	0.7149	0.025(1)	0.0246
0.0041(3)	0.0200(4)	0.0198	0.114(6)	0.1091	0.714(3)	0.7139	0.029(1)	0.0282
0.0083(9)	0.0219(4)	0.0223	0.173(8)	0.1953	0.713(4)	0.7128	0.031(1)	0.0319
0.0177(6)	0.0275(4)	0.0279	0.308(9)	0.3301	0.711(5)	0.7103	0.040(1)	0.0404
0.029(2)	0.0327(5)	0.0343	0.40(1)	0.4314	0.707(6)	0.7074	0.048(2)	0.0507
0.038(1)	0.0371(5)	0.0397	0.46(1)	0.4906	0.704(6)	0.7049	0.055(2)	0.0598
0.048(1)	0.0413(4)	0.0449	0.51(1)	0.5341	0.701(7)	0.7023	0.062(2)	0.0692
0.069(2)	0.0501(5)	0.0561	0.57(1)	0.5971	0.695(9)	0.6964	0.078(2)	0.0910
0.103(2)	0.0633(5)	0.0727	0.62(1)	0.6477	0.68(1)	0.6868	0.106(3)	0.1297
0.125(3)	0.0713(6)	0.0829	0.65(1)	0.6629	0.68(1)	0.6801	0.125(3)	0.1589
0.158(6)	0.082(1)	0.0973	0.66(1)	0.6686	0.66(1)	0.6700	0.157(4)	0.2098
0.191(5)	0.090(1)	0.1110	0.67(1)	0.6585	0.65(2)	0.6597	0.184(5)	0.2701

TABLE S10. MD and EOS results for the bulk properties of the binary LJTS mixture A ($\varepsilon_2/\varepsilon_1 = 0.6$ and $\xi_{12} = 0.85$) at $T = 0.88\,\varepsilon k_\mathrm{B}^{-1}$. Both methods are calculated at the same liquid phase composition x_2^{L1}. The number in the parentheses indicates the statistical uncertainty in the last decimal digit.

x_2^{L1} / mol mol^{-1}	p / $\varepsilon\sigma^{-3}$		x_2^{V} / mol mol^{-1}		ρ^{L1} / σ^{-3}		ρ^{V} / σ^{-3}	
	MD	EOS	MD	EOS	MD	EOS	MD	EOS
0.000	0.0271(4)	0.0270	0.000	0.000	0.679(3)	0.6782	0.039(1)	0.0384
0.0098(6)	0.0325(4)	0.0331	0.134(5)	0.1479	0.676(4)	0.6752	0.046(1)	0.0475
0.0143(5)	0.0350(3)	0.0359	0.181(6)	0.1993	0.674(4)	0.6739	0.050(2)	0.0517
0.0185(6)	0.0377(4)	0.0384	0.227(6)	0.2391	0.673(5)	0.6726	0.055(2)	0.0556
0.0248(9)	0.0401(4)	0.0421	0.259(8)	0.2902	0.670(4)	0.6707	0.058(2)	0.0616
0.027(2)	0.0411(7)	0.0437	0.274(8)	0.3088	0.669(6)	0.6698	0.060(2)	0.0642
0.029(1)	0.0425(4)	0.0445	0.293(6)	0.3182	0.669(5)	0.6694	0.062(2)	0.0656
0.0345(1)	0.0453(4)	0.0479	0.326(6)	0.3523	0.667(5)	0.6676	0.067(2)	0.0712
0.038(2)	0.0480(6)	0.0501	0.353(9)	0.3726	0.666(6)	0.6663	0.071(2)	0.0751
0.043(1)	0.0501(6)	0.0525	0.372(7)	0.3923	0.664(6)	0.6650	0.075(2)	0.0793
0.100(2)	0.0756(6)	0.0824	0.505(9)	0.5279	0.642(9)	0.6458	0.126(3)	0.1423
0.166(6)	0.0949(11)	0.1116	0.55(1)	0.5554	0.612(15)	0.6214	0.177(5)	0.2320
0.223(11)	0.1126(7)	0.1330	0.52(6)	0.5338	0.583(17)	0.5981	0.27(2)	0.3196

TABLE S11. Interfacial properties of the binary LJTS mixture B ($\varepsilon_2/\varepsilon_1 = 0.9$ and $\xi_{12} = 1$) at $T = 0.66\,\varepsilon k_\mathrm{B}^{-1}$. Results from MD and DGT+PeTS. Both methods are calculated at the same liquid phase composition x_2^{L1}. The number in the parentheses indicates the statistical uncertainty in the last decimal digit.

x_2^{L1} / mol mol^{-1}	γ / $\sigma^2\varepsilon^{-1}$		$\Gamma_2^{(1)}$ / σ^{-2}		E_2		L_{10}^{90} / σ	
	MD	DGT	MD	DGT	MD	DGT	MD	DGT
0.00	0.655(26)	0.6632	-	-	-	-	2.06(5)	1.94
0.005(1)	0.649(18)	0.6620	0.003(10)	0.002	1.32(13)	1.03	2.05(4)	1.94
0.055(1)	0.647(31)	0.6506	0.032(20)	0.019	1.11(5)	1.02	2.07(4)	1.96
0.100(1)	0.627(25)	0.6405	0.07(2)	0.034	1.08(2)	1.01	2.07(6)	1.96
0.157(2)	0.626(23)	0.6280	0.09(5)	0.052	1.06(2)	1.01	2.12(5)	1.98
0.208(1)	0.612(30)	0.6170	-0.11(4)	0.067	0.99(2)	1.00	2.11(5)	1.98
0.251(1)	0.604(24)	0.6080	0.07(3)	0.080	1.04(1)	1.00	2.16(4)	2.00
0.297(1)	0.590(19)	0.5984	0.11(7)	0.093	1.03(2)	1.00	2.16(5)	2.00
0.354(1)	0.582(28)	0.5869	0.08(4)	0.109	1.02(1)	1.00	2.19(3)	2.02
0.388(2)	0.568(24)	0.5803	0.08(7)	0.117	1.03(1)	1.00	2.22(6)	2.02
0.437(2)	0.565(26)	0.5708	0.16(8)	0.130	1.02(1)	1.00	2.23(3)	2.04
0.490(1)	0.559(20)	0.5606	0.01(13)	0.143	1.02(1)	1.00	2.22(4)	2.06
0.533(1)	0.542(23)	0.5523	0.04(12)	0.153	1.01(1)	1.00	2.25(5)	2.08
0.584(1)	0.534(20)	0.5429	0.11(21)	0.165	1.01(1)	1.00	2.28(6)	2.08
0.630(2)	0.524(27)	0.5345	0.03(20)	0.175	1.01(1)	1.00	2.29(5)	2.08
0.683(1)	0.517(23)	0.5251	-0.05(11)	0.186	1.01(1)	1.00	2.31(5)	2.10
0.731(1)	0.513(27)	0.5166	-0.04(12)	0.196	1.01(1)	1.00	2.33(6)	2.12
0.772(1)	0.499(28)	0.5095	0.1(2)	0.204	1.01(0)	1.00	2.36(5)	2.12
0.824(2)	0.494(23)	0.5006	-0.02(36)	0.214	1.01(1)	1.00	2.36(3)	2.14
0.874(1)	0.484(28)	0.4920	0.03(56)	0.223	1.01(1)	1.00	2.37(5)	2.14
0.929(1)	0.479(28)	0.4829	-0.23(84)	0.232	1.01(0)	1.00	2.39(5)	2.16
1.00	0.467(21)	0.4729	-	-	-	-	2.41(5)	2.18

TABLE S12. Interfacial properties of the binary LJTS mixture B ($\varepsilon_2/\varepsilon_1 = 0.9$ and $\xi_{12} = 1$) at $T = 0.715\,\varepsilon k_\mathrm{B}^{-1}$. Results from MD and DGT+PeTS. Both methods are calculated at the same liquid phase composition x_2^{L1}. The number in the parentheses indicates the statistical uncertainty in the last decimal digit.

x_2^{L1} / mol mol^{-1}	γ / $\varepsilon\sigma^{-2}$		$\Gamma_2^{(1)}$ / σ^{-2}		E_2		L_{10}^{90} / σ	
	MD	DGT	MD	DGT	MD	DGT	MD	DGT
0.000	0.541(26)	0.5579	-	-	-	-	2.34(5)	2.12
0.0049(2)	0.543(20)	0.5568	0.004(3)	0.002	1.35(12)	1.01	2.31(5)	2.12
0.053(1)	0.537(21)	0.5463	0.01(2)	0.016	1.11(4)	1.00	2.35(4)	2.12
0.105(2)	0.526(24)	0.5350	0.03(3)	0.031	1.06(3)	1.00	2.37(5)	2.14
0.151(1)	0.511(22)	0.5255	0.03(4)	0.044	1.04(2)	1.00	2.40(4)	2.16
0.200(1)	0.502(23)	0.5152	0.10(7)	0.058	1.04(2)	1.00	2.44(4)	2.16
0.243(1)	0.497(23)	0.5064	0.06(7)	0.069	1.03(2)	1.00	2.44(7)	2.20
0.289(2)	0.484(22)	0.4973	0.03(7)	0.081	1.03(2)	1.00	2.47(7)	2.20
0.339(1)	0.482(16)	0.4876	0.11(10)	0.093	1.03(2)	1.00	2.52(5)	2.22
0.380(2)	0.474(24)	0.4797	0.09(11)	0.103	1.03(2)	1.00	2.51(5)	2.24
0.427(2)	0.465(18)	0.4707	0.10(07)	0.114	1.02(1)	1.00	2.53(5)	2.24
0.476(1)	0.453(21)	0.4616	0.08(5)	0.125	1.02(1)	1.00	2.58(6)	2.26
0.520(1)	0.445(22)	0.4535	0.12(9)	0.134	1.02(1)	1.00	2.59(7)	2.28
0.562(1)	0.439(27)	0.4458	0.05(9)	0.143	1.01(1)	1.00	2.63(7)	2.30
0.619(2)	0.429(21)	0.4356	0.2(3)	0.155	1.02(1)	1.00	2.66(7)	2.32
0.661(3)	0.424(25)	0.4283	0.04(23)	0.163	1.01(1)	1.00	2.68(6)	2.34
0.711(1)	0.414(25)	0.4197	-0.11(18)	0.172	1.01(1)	1.00	2.64(5)	2.34
0.759(2)	0.406(25)	0.4114	-0.04(30)	0.181	1.01(1)	1.00	2.67(6)	2.36
0.810(1)	0.398(26)	0.4028	0.09(27)	0.190	1.013(5)	1.00	2.74(5)	2.38
0.853(1)	0.387(25)	0.3957	0.02(34)	0.197	1.010(4)	1.00	2.76(7)	2.40
0.899(1)	0.382(23)	0.3882	-0.1(4)	0.205	1.009(4)	1.00	2.77(5)	2.42
0.948(1)	0.375(29)	0.3802	-0.8(8)	0.213	1.004(3)	1.00	2.83(7)	2.44
1.000	0.364(13)	0.3734	-	-	-	-	2.83(5)	2.44

TABLE S13. Interfacial properties of the binary LJTS mixture B ($\varepsilon_2/\varepsilon_1 = 0.9$ and $\xi_{12} = 1$) at $T = 0.77\,\varepsilon k_\mathrm{B}^{-1}$. Results from MD and DGT+PeTS. Both methods are calculated at the same liquid phase composition x_2^{L1}. The number in the parentheses indicates the statistical uncertainty in the last decimal digit.

x_2^{L1} / mol mol^{-1}	γ / $\varepsilon\sigma^{-2}$		$\Gamma_2^{(1)}$ / σ^{-2}		E_2		L_{10}^{90} / σ	
	MD	DGT	MD	DGT	MD	DGT	MD	DGT
0.000	0.454(20)	0.4567	-	-	-	-	2.68(4)	2.32
0.064(2)	0.439(13)	0.4433	0.03(3)	0.017	1.09(5)	1.00	2.72(4)	2.36
0.110(1)	0.423(16)	0.4340	0.06(2)	0.029	1.06(2)	1.00	2.75(6)	2.38
0.154(2)	0.417(18)	0.4251	0.02(3)	0.040	1.03(2)	1.00	2.76(4)	2.40
0.202(2)	0.410(12)	0.4155	0.07(5)	0.052	1.03(2)	1.00	2.81(6)	2.42
0.246(2)	0.405(16)	0.4071	0.10(6)	0.062	1.04(2)	1.00	2.88(8)	2.44
0.296(2)	0.393(15)	0.3974	0.01(6)	0.074	1.01(2)	1.00	2.86(5)	2.46
0.334(1)	0.385(15)	0.3902	0.12(6)	0.082	1.024(13)	1.00	2.90(7)	2.48
0.392(2)	0.376(11)	0.3795	0.10(6)	0.094	1.023(10)	1.00	2.91(5)	2.52
0.436(1)	0.369(14)	0.3715	0.13(9)	0.104	1.021(11)	1.00	2.96(8)	2.54
0.484(2)	0.361(16)	0.3628	0.10(9)	0.113	1.023(9)	1.00	2.98(6)	2.56
0.527(2)	0.350(16)	0.3552	-0.02(18)	0.122	1.007(16)	1.00	3.00(7)	2.58
0.574(2)	0.343(20)	0.3471	0.20(15)	0.130	1.018(8)	1.00	3.07(7)	2.60
0.617(2)	0.327(15)	0.3396	0.21(12)	0.138	1.016(6)	1.00	3.11(7)	2.62
0.662(1)	0.323(17)	0.3319	0.12(9)	0.146	1.012(5)	1.00	3.12(7)	2.66
0.714(2)	0.317(18)	0.3231	0.18(13)	0.155	1.013(6)	1.00	3.17(7)	2.66
0.764(1)	0.319(14)	0.3149	0.20(18)	0.163	1.012(4)	1.00	3.22(11)	2.70
0.808(2)	0.302(13)	0.3077	0.32(15)	0.170	1.011(4)	1.00	3.23(7)	2.72
0.863(1)	0.292(11)	0.2988	-0.10(14)	0.179	1.007(4)	1.00	3.27(7)	2.74
0.904(1)	0.288(14)	0.2922	0.04(22)	0.185	1.009(4)	1.00	3.27(7)	2.78
0.952(1)	0.283(15)	0.2846	0.5(4)	0.192	1.008(1)	1.00	3.36(10)	2.80
1.000	0.273(18)	0.2786	-	-	-	-	3.38(6)	2.82

TABLE S14. Interfacial properties of the binary LJTS mixture B ($\varepsilon_2/\varepsilon_1 = 0.9$ and $\xi_{12} = 1$) at $T = 0.825\,\varepsilon k_\mathrm{B}^{-1}$. Results from MD and DGT+PeTS. Both methods are calculated at the same liquid phase composition x_2^{L1}. The number in the parentheses indicates the statistical uncertainty in the last decimal digit.

x_2^{L1} / mol mol^{-1}	γ / $\varepsilon\sigma^{-2}$		$\Gamma_2^{(1)}$ / σ^{-2}		E_2		L_{10}^{90} / σ	
	MD	DGT	MD	DGT	MD	DGT	MD	DGT
0.000	0.350(17)	0.3598	-	-	-	-	3.06(7)	2.62
0.0055(3)	0.347(14)	0.3587	0.00(1)	0.001	1.24(12)	1.00	3.09(8)	2.64
0.051(1)	0.343(16)	0.3497	0.04(2)	0.012	1.09(5)	1.00	3.17(8)	2.66
0.096(1)	0.329(14)	0.3408	0.01(3)	0.023	1.04(2)	1.00	3.18(7)	2.68
0.145(1)	0.323(17)	0.3314	0.04(5)	0.034	1.03(2)	1.00	3.26(9)	2.70
0.195(2)	0.311(15)	0.3221	0.01(4)	0.044	1.02(2)	1.00	3.30(9)	2.74
0.246(1)	0.306(14)	0.3125	0.03(7)	0.055	1.02(2)	1.00	3.33(9)	2.78
0.280(1)	0.302(19)	0.3064	0.08(7)	0.062	1.02(1)	1.00	3.35(7)	2.80
0.330(1)	0.282(20)	0.2973	0.07(5)	0.072	1.02(1)	1.00	3.39(7)	2.84
0.351(2)	0.285(17)	0.2936	0.07(9)	0.076	1.02(1)	1.00	3.47(10)	2.86
0.390(2)	0.280(20)	0.2867	0.03(10)	0.084	1.02(2)	1.00	3.46(6)	2.88
0.435(2)	0.272(20)	0.2788	0.06(7)	0.092	1.02(1)	1.00	3.50(9)	2.92
0.481(2)	0.263(20)	0.2709	0.08(8)	0.100	1.02(1)	1.00	3.53(8)	2.94
0.526(2)	0.253(18)	0.2632	0.05(12)	0.108	1.013(4)	1.00	3.62(12)	2.98
0.562(4)	0.253(16)	0.2572	0.05(10)	0.114	1.002(12)	1.00	3.54(12)	3.02
0.604(2)	0.242(19)	0.2503	0.05(23)	0.121	1.012(7)	1.00	3.75(12)	3.04
0.651(1)	0.237(19)	0.2425	-0.07(17)	0.129	1.008(7)	1.00	3.71(10)	3.08
0.795(2)	0.207(14)	0.2194	0.04(20)	0.150	1.007(3)	1.00	3.96(9)	3.20
0.83(4)	0.199(13)	0.2145	0.03(26)	0.154	1.007(3)	1.00	3.96(12)	3.22
0.895(1)	0.196(12)	0.2040	0.28(18)	0.163	1.008(4)	1.00	4.09(10)	3.30
0.948(1)	0.189(11)	0.1959	-0.08(33)	0.170	1.008(3)	1.00	4.16(12)	3.34
0.959(1)	0.189(15)	0.1942	0.35(31)	0.171	1.008(1)	1.00	4.20(16)	3.36
1.000	0.180(8)	0.1896	-	-	-	-	4.20(11)	3.40

TABLE S15. Interfacial properties of the binary LJTS mixture B ($\varepsilon_2/\varepsilon_1 = 0.9$ and $\xi_{12} = 1$) at $T = 0.88\,\varepsilon k_\mathrm{B}^{-1}$. Results from MD and DGT+PeTS. Both methods are calculated at the same liquid phase composition x_2^{L1}. The number in the parentheses indicates the statistical uncertainty in the last decimal digit.

x_2^{L1} / mol mol^{-1}	γ / $\varepsilon\sigma^{-2}$		$\Gamma_2^{(1)}$ / σ^{-2}		E_2		L_{10}^{90} / σ	
	MD	DGT	MD	DGT	MD	DGT	MD	DGT
0.000	0.264(14)	0.2675	-	-	-	-	3.67(9)	3.04
0.0051(3)	0.253(14)	0.2665	0.002(7)	0.001	1.43(9)	1.00	3.68(8)	3.04
0.050(1)	0.247(8)	0.2582	0.006(13)	0.011	1.11(2)	1.00	3.75(12)	3.06
0.098(1)	0.239(12)	0.2494	0.03(3)	0.020	1.10(2)	1.00	3.83(9)	3.12
0.143(1)	0.233(15)	0.2412	0.05(2)	0.029	1.07(1)	1.00	3.90(11)	3.18
0.187(1)	0.226(11)	0.2334	0.02(4)	0.038	1.05(2)	1.00	3.95(10)	3.20
0.240(2)	0.213(14)	0.2242	0.01(4)	0.047	1.04(1)	1.00	4.01(9)	3.28
0.280(2)	0.208(13)	0.2174	0.07(5)	0.055	1.06(1)	1.00	4.04(13)	3.32
0.322(2)	0.204(13)	0.2102	0.08(4)	0.062	1.04(1)	1.00	4.03(15)	3.36
0.365(2)	0.197(15)	0.2029	0.09(4)	0.069	1.03(1)	1.00	4.17(11)	3.40
0.356(2)	0.202(16)	0.2045	0.08(5)	0.068	1.04(1)	1.00	4.18(12)	3.38
0.401(3)	0.194(17)	0.1970	0.05(7)	0.075	1.03(1)	1.00	4.22(19)	3.44
0.431(2)	0.188(17)	0.1921	0.04(7)	0.080	1.03(1)	1.00	4.26(13)	3.48
0.478(4)	0.180(18)	0.1845	0.05(6)	0.087	1.01(2)	1.00	4.37(16)	3.54
0.514(3)	0.174(19)	0.1787	-0.01(9)	0.093	1.00(3)	1.00	4.49(3)	3.58
0.552(4)	0.164(18)	0.1728	0.10(10)	0.098	1.02(2)	1.00	4.46(19)	3.64
0.576(6)	0.164(18)	0.1689	-0.07(6)	0.102	1.01(3)	1.00	4.6(4)	3.66
0.622(5)	0.156(16)	0.1619	-0.02(8)	0.108	1.01(2)	1.00	4.66(5)	3.74
0.651(5)	0.148(21)	0.1573	-0.08(7)	0.112	1.01(2)	1.00	4.7(3)	3.76
0.873(1)	0.113(8)	0.1245	0.20(19)	0.139	1.010(4)	1.00	5.2(2)	4.16
0.76(9)	0.119(11)	0.1411	0.31(32)	0.126	1.01(6)	1.00	5.03(2)	3.94
0.929(1)	0.108(10)	0.1165	0.19(20)	0.144	1.008(2)	1.00	5.38(19)	4.26
0.946(1)	0.103(11)	0.1141	0.0(3)	0.146	1.007(3)	1.00	5.38(24)	4.30
0.969(1)	0.103(12)	0.1109	-0.2(5)	0.148	1.008(3)	1.00	5.63(26)	4.36
1.000	0.097(13)	0.1080	-	-	-	-	5.70(26)	4.38

TABLE S16. Interfacial properties of the binary LJTS mixture A ($\varepsilon_2/\varepsilon_1 = 0.6$ and $\xi_{12} = 0.85$) at $T = 0.66\,\varepsilon k_\mathrm{B}^{-1}$. Results from MD and DGT+PeTS. Both methods are calculated at the same liquid phase composition x_2^{L1}. The number in the parentheses indicates the statistical uncertainty in the last decimal digit.

x_2^{L1} / mol mol^{-1}	γ / $\varepsilon\sigma^{-2}$		$\Gamma_2^{(1)}$ / σ^{-2}		E_2		L_{10}^{90} / σ	
	MD	DGT	MD	DGT	MD	DGT	MD	DGT
0.000	0.655(26)	0.6632	-	-	-	-	2.06(5)	1.94
0.009(1)	0.601(22)	0.6152	0.07(1)	0.075	4.6(6)	7.12	2.19(6)	2.06
0.0077(5)	0.609(28)	0.6222	0.07(1)	0.064	5.8(3)	7.10	2.18(5)	2.04
0.018(1)	0.573(24)	0.5659	0.12(1)	0.157	4.5(3)	7.22	2.28(5)	2.20
0.027(1)	0.536(25)	0.5201	0.19(2)	0.238	4.3(3)	7.23	2.45(5)	2.34
0.036(1)	0.493(34)	0.4768	0.25(2)	0.318	4.2(2)	7.08	2.58(6)	2.48
0.045(1)	0.477(35)	0.4317	0.31(3)	0.406	4.0(2)	6.74	2.73(3)	2.66
0.055(2)	0.430(30)	0.3871	0.35(2)	0.498	4.0(1)	6.32	2.92(4)	2.88
0.063(3)	0.393(30)	0.3535	0.48(4)	0.573	4.1(3)	5.98	3.15(8)	3.08
0.075(2)	0.366(37)	0.2988	0.53(4)	0.709	3.7(2)	5.38	3.31(10)	3.48
0.085(2)	0.328(31)	0.2594	0.64(6)	0.825	3.7(1)	4.93	3.59(7)	3.88
0.092(5)	0.295(17)	0.2285	0.75(5)	0.933	3.8(3)	4.58	3.00(14)	4.28
0.111(2)	0.260(19)	0.1493	0.75(6)	1.360	3.3(1)	3.67	4.30(17)	6.12
0.117(4)	0.215(32)	0.1253	1.08(5)	1.594	3.5(2)	3.38	5.08(16)	7.22

TABLE S17. Interfacial properties of the binary LJTS mixture A ($\varepsilon_2/\varepsilon_1 = 0.6$ and $\xi_{12} = 0.85$) at $T = 0.715\,\varepsilon k_\mathrm{B}^{-1}$. Results from MD and DGT+PeTS. Both methods are calculated at the same liquid phase composition x_2^{L1}. The number in the parentheses indicates the statistical uncertainty in the last decimal digit.

x_2^{L1} / mol mol^{-1}	γ / $\varepsilon\sigma^{-2}$		$\Gamma_2^{(1)}$ / σ^{-2}		E_2		L_{10}^{90} / σ	
	MD	DGT	MD	DGT	MD	DGT	MD	DGT
0.000	0.541(26)	0.5579	-	-	-	-	2.34(5)	2.12
0.0096(4)	0.511(22)	0.5189	0.05(1)	0.056	3.7(4)	4.93	2.45(5)	2.22
0.0129(9)	0.494(17)	0.5055	0.08(1)	0.076	3.9(4)	4.90	2.50(7)	2.26
0.027(1)	0.452(25)	0.4496	0.14(2)	0.162	3.4(2)	4.73	2.69(5)	2.44
0.043(2)	0.413(18)	0.3944	0.18(2)	0.252	3.0(2)	4.48	2.89(7)	2.68
0.056(2)	0.363(32)	0.3466	0.30(3)	0.336	3.1(1)	4.19	3.19(9)	2.92
0.071(1)	0.319(31)	0.3008	0.38(4)	0.422	3.0(1)	3.87	3.44(8)	3.20
0.084(3)	0.273(29)	0.2608	0.44(3)	0.504	2.9(1)	3.56	3.9(1)	3.52
0.109(2)	0.257(19)	0.1891	0.50(5)	0.675	2.5(1)	2.95	4.0(1)	4.36
0.124(6)	0.208(26)	0.1514	0.64(6)	0.784	2.5(1)	2.59	4.6(2)	5.10
0.142(5)	0.172(22)	0.1061	0.77(6)	0.932	2.43(6)	2.11	5.4(2)	6.52
0.178(8)	0.112(24)	0.0330	0.96(7)	0.180	2.13(8)	1.02	6.8(4)	5.76

TABLE S18. Interfacial properties of the binary LJTS mixture A ($\varepsilon_2/\varepsilon_1 = 0.6$ and $\xi_{12} = 0.85$) at $T = 0.77\,\varepsilon k_\mathrm{B}^{-1}$. Results from MD and DGT+PeTS. Both methods are calculated at the same liquid phase composition x_2^{L1}. The number in the parentheses indicates the statistical uncertainty in the last decimal digit.

x_2^{L1} / mol mol^{-1}	γ / $\varepsilon\sigma^{-2}$		$\Gamma_2^{(1)}$ / σ^{-2}		E_2		L_{10}^{90} / σ	
	MD	DGT	MD	DGT	MD	DGT	MD	DGT
0.000	0.454(20)	0.4567	-	-	-	-	2.68(4)	2.32
0.0045(3)	0.439(28)	0.4423	0.019(4)	0.019	2.8(4)	3.58	2.74(6)	2.38
0.0097(6)	0.411(18)	0.4258	0.03(1)	0.041	2.5(3)	3.53	2.78(7)	2.44
0.0136(9)	0.406(14)	0.4138	0.05(1)	0.057	2.9(4)	3.50	2.87(8)	2.48
0.0271(9)	0.366(23)	0.3734	0.10(1)	0.113	2.7(1)	3.36	3.01(6)	2.64
0.044(1)	0.331(22)	0.3250	0.14(3)	0.184	2.4(1)	3.15	3.2(1)	2.88
0.056(1)	0.303(20)	0.2935	0.20(3)	0.232	2.5(1)	3.00	3.5(1)	3.06
0.075(2)	0.270(22)	0.2485	0.27(2)	0.304	2.2(1)	2.76	3.7(1)	3.38
0.089(1)	0.219(22)	0.2154	0.29(2)	0.360	2.22(6)	2.56	4.0(1)	3.68
0.122(3)	0.170(18)	0.1507	0.45(3)	0.474	2.06(8)	2.12	4.9(2)	4.52
0.146(3)	0.150(17)	0.1090	0.49(5)	0.544	1.88(6)	1.80	5.1(2)	5.40
0.163(4)	0.115(16)	0.0834	0.59(6)	0.566	1.83(6)	1.58	6.1(3)	6.14
0.191(8)	0.088(19)	0.0492	0.60(6)	0.492	1.66(4)	1.26	6.7(4)	7.28
0.215(14)	0.063(18)	0.0282	0.68(11)	0.318	1.56(4)	1.07	8.0(7)	7.72

TABLE S19. Interfacial properties of the binary LJTS mixture A ($\varepsilon_2/\varepsilon_1 = 0.6$ and $\xi_{12} = 0.85$) at $T = 0.825\,\varepsilon k_\mathrm{B}^{-1}$. Results from MD and DGT+PeTS. Both methods are calculated at the same liquid phase composition x_2^{L1}. The number in the parentheses indicates the statistical uncertainty in the last decimal digit.

x_2^{L1} / mol mol^{-1}	γ / $\varepsilon\sigma^{-2}$		$\Gamma_2^{(1)}$ / σ^{-2}		E_2		L_{10}^{90} / σ	
	MD	DGT	MD	DGT	MD	DGT	MD	DGT
0.000	0.350(17)	0.3598	-	-	-	-	3.06(7)	2.62
0.0041(3)	0.346(16)	0.3493	0.02(1)	0.013	2.5(2)	2.70	3.19(5)	2.68
0.0083(9)	0.335(13)	0.3387	0.02(1)	0.026	2.1(3)	2.67	3.19(8)	2.72
0.0177(6)	0.303(16)	0.3159	0.05(2)	0.054	2.2(1)	2.60	3.35(8)	2.82
0.029(2)	0.280(14)	0.2901	0.08(2)	0.087	2.1(2)	2.51	3.5(1)	2.96
0.038(1)	0.268(12)	0.2690	0.12(2)	0.115	2.1(1)	2.43	3.6(1)	3.10
0.048(1)	0.245(15)	0.2487	0.15(2)	0.142	2.0(1)	2.35	3.7(1)	3.24
0.069(2)	0.212(22)	0.2071	0.18(3)	0.198	1.8(1)	2.17	4.1(1)	3.56
0.103(2)	0.163(12)	0.1497	0.25(4)	0.278	1.74(6)	1.88	4.8(2)	4.24
0.125(3)	0.130(12)	0.1177	0.29(3)	0.320	1.64(6)	1.70	5.3(2)	4.78
0.158(6)	0.095(19)	0.0783	0.37(4)	0.358	1.54(7)	1.45	6.4(3)	5.74
0.191(5)	0.064(17)	0.0486	0.37(7)	0.349	1.42(4)	1.25	7.2(6)	6.82

TABLE S20. Interfacial properties of the binary LJTS mixture A ($\varepsilon_2/\varepsilon_1 = 0.6$ and $\xi_{12} = 0.85$) at $T = 0.88\,\varepsilon k_\mathrm{B}^{-1}$. Results from MD and DGT+PeTS. Both methods are calculated at the same liquid phase composition x_2^{L1}. The number in the parentheses indicates the statistical uncertainty in the last decimal digit.

x_2^{L1} / mol mol^{-1}	γ / $\varepsilon\sigma^{-2}$		$\Gamma_2^{(1)}$ / σ^{-2}		E_2		L_{10}^{90} / σ	
	MD	DGT	MD	DGT	MD	DGT	MD	DGT
0.000	0.264(14)	0.2675	-	-	-	-	3.67(9)	3.04
0.0098(6)	0.236(13)	0.2481	0.01(1)	0.022	1.77(19)	2.08	3.81(8)	3.16
0.0143(5)	0.227(16)	0.2394	0.03(1)	0.032	1.81(13)	2.06	3.89(9)	3.20
0.0185(6)	0.225(15)	0.2316	0.05(1)	0.041	1.85(13)	2.03	4.0(1)	3.26
0.0248(9)	0.214(14)	0.2201	0.04(2)	0.055	1.69(12)	1.99	4.0(1)	3.36
0.027(2)	0.210(14)	0.2153	0.06(1)	0.060	1.62(17)	1.98	4.1(1)	3.38
0.029(1)	0.209(19)	0.2128	0.06(1)	0.063	1.72(11)	1.97	4.1(1)	3.40
0.0345(1)	0.201(18)	0.2028	0.08(1)	0.075	1.70(11)	1.93	4.3(1)	3.50
0.038(2)	0.192(10)	0.1961	0.09(3)	0.083	1.71(12)	1.91	4.4(2)	3.56
0.043(1)	0.184(9)	0.1891	0.09(2)	0.091	1.71(8)	1.88	4.4(1)	3.60
0.100(2)	0.105(16)	0.1085	0.19(3)	0.186	1.52(5)	1.55	5.7(2)	4.74
0.166(6)	0.056(14)	0.0476	0.22(5)	0.228	1.28(6)	1.24	7.5(6)	6.66
0.223(11)	0.021(18)	0.0187	0.19(8)	0.185	1.14(3)	1.07	10.3(20)	8.88